UNLIMITED

RSRE
MEMORANDUM No. 4208

ROYAL SIGNALS & RADAR ESTABLISHMENT

UV PHOTO-ENHANCED MOCVD OF CADMIUM AND CADMIUM TELLURIDE

Author: S Haq

PROCUREMENT EXECUTIVE,
MINISTRY OF DEFENCE,
RSRE MALVERN,
WORCS.

RSRE MEMORANDUM No. 4208

UNLIMITED

CONDITIONS OF RELEASE

0050738 BR-111416

********** U

********** Y

Reports quoted are not necessarily available to members of the public or to commercial organisations.

ROYAL SIGNALS AND RADAR ESTABLISHMENT

Memorandum 4208

TITLE: UV PHOTO-ENHANCED MOCVD OF CADMIUM AND CADMIUM TELLURIDE

AUTHOR: Sajad Haq

DATE: April 1988

SUMMARY

This technical memorandum comprises a thesis submitted by the author for the degree of PhD at the University of Birmingham. The research was carried out, both at the Department of Metallurgy and Materials, University of Birmingham, and at RSRE in EM2 Division. The UV photolysis of dimethylcadmium (Me_2Cd) and diethyltelluride (Et_2Te) were investigated using high pressure mercury arc lamps. Metallic Cd films were deposited onto gallium arsenide, silicon and sapphire substrates in order to investigate nucleation mechanisms and film growth models. Cadmium telluride epitaxial layers were grown onto (100) gallium arsenide substrates both with and without UV illumination. Film quality and structure have been studied using transmission electron microscopy, X-ray diffraction, scanning electron microscopy and secondary ion mass spectrometry.

Acknowledgements

I would like to acknowledge Professor R.E. Smallman, FRS for provision of the research facilities at the Department of Metallurgy and Materials, University of Birmingham and the SERC and R.S.R.E. for financial support through the CASE studentship scheme.

Thanks are due to my supervisor, Dr P.S. Dobson for advice, encouragement and many helpful discussions throughout the course of this work. In particular, I am deeply indebted to my external supervisor, Dr S.J.C. Irvine for his continued encouragement and invaluable guidance at every stage of the work, and also for imparting to me at least a modicum of his tremendous enthusiasm and dynamic attitude. His patience and extreme tolerance during my visits to R.S.R.E and his genuine interest are also gratefully acknowledged.

I would also like to thank the following: Mrs J. Clements for substrate preparation at R.S.R.E., Mrs O.D. Dosser for the SEM work at R.S.R.E. and for her expert proof reading, Mr N.G. Chew for the HRTEM and Mr G.W. Blackmore for the SIMS analyses. Thanks are also due to Dr D.C. Rodway (R.S.R.E) and Miss J. Thompson (GEC) for providing specimens for TEM analyses.

I also wish to express my gratitude to the following colleagues, past and present, at Birmingham: Dr D. Loretto and Mr J.D. L'Ecuyer for assistance with the electron microscopy, Mr M.A. Lunn for his vivid explanations of TEM specimen preparation techniques and Mr J.R. Logan, Mr J.N. Shepherd and Mrs P. Church for many useful discussions.

Contents

Chapter 6 Results and discussion: cadmium depositions

Chapter 1: Introduction

Photo-processing is emerging as a technology which holds much promise for future semiconductor production in which photon assisted techniques may be utilised for a wide range of processes pertinent to the electronics industry. Photo-processing encompasses deposition of epitaxial layers, etching, dielectric formation and metallisation and may be pursued with either laser or incoherent lamp radiation sources from wavelengths ranging from the infra-red to the ultra-violet to interact with either the substrate or the precursors.

Its suitability as a production process is emphasised by the potential of pattern generation via non-contact masking or modulation of the radiation source. In addition the compatibility of the individual processes with each other, requiring only a change of precursor in the same system for the separate processing stages is to be favoured.

UV photo-deposition is central to this theme and offers a means of low temperature deposition by photo-dissociation of the precursor molecules in contrast to conventional CVD processes in which deposition is effected thermally. Epitaxial growth, a special case of CVD in which the deposit is single crystal may also benefit from UV photo-deposition in terms of improved surface kinetics induced by the incident radiation and enhanced growth rates. These capabilities attest to the value of photo-deposition for the growth of the new generation of low dimensional devices which require abrupt interfaces, more exact dopant distribution, and minimal impurity diffusion.

II-VI device technology has been inhibited by the lack of availability of large area substrates of sufficiently high crystalline quality for the growth of the ternary semiconductor cadmium mercury telluride, an important infra-red detector material. One approach to circumvent this problem is to employ alternative substrates, over which a buffer layer of cadmium telluride may be deposited to serve as a subsequent nucleating surface for the ternary.

The work undertaken for this thesis is concentrated in two main areas; the UV photo-enhanced deposition of CdTe onto GaAs and an investigation of UV photo-deposition of cadmium metal onto various substrates important in semiconductor device applications, namely silicon, gallium arsenide and sapphire. The aims of the project were to investigate the hetero photo-deposition of both materials with a view to promoting low temperature crystallinity. Deposition of the former was carried out at

RSRE and of the latter in a system constructed at Birmingham. The grown deposits were characterised by a variety of techniques to give structural and chemical information. Transmission electron microscopy (TEM), scanning electron microscopy (SEM), secondary ion mass spectrometry (SIMS) and x-ray diffraction were used.

The remainder of the thesis is laid out as follows. Chapter 2 is a literature review encompassing the MOVPE of II-VI material, the photo-MOVPE of semiconductors, the photodeposition of metals and TEM assessment of some II-VI, III-V heteroepitaxial systems.

Chapter 3 describes the MOCVD equipment designed and constructed at Birmingham for the cadmium depositions and highlights the differences between this equipment and that at R.S.R.E utilised for the compound semiconductor growth.

Chapter 4 discusses the experimental procedures used in this work and includes specimen preparation and the characterisation techniques used.

In chapters 5 and 6 the results of the CdTe and Cd depositions are presented respectively and discussed with reference to earlier relevant work as presented in chapter 2.

In the final chapter the major conclusions which can be drawn from the work are presented along with some suggested further work.

Chapter 2: Literature review

2.1 MOVPE of II-VI compounds

2.1.1 Introduction

Before the advent of metal organic vapour phase epitaxy (MOVPE), conventional thin film growth techniques suffered from lack of control over the growth processes. MOVPE, with the use of a single hot deposition zone and accurate control of the vapour pressures of the entering reactants, has improved versatility and growth control as compared with the earlier VPE techniques which relied on transport of elemental vapours. Although halogen transport VPE also circumvents this latter problem this technique has proved to give rise to doping problems, with the halogens acting as n-type dopants in the II-VI material.

Mullin et al.[1] have pointed out the major advantages of MOVPE over conventional VPE techniques, and have indicated the potential for achieving far higher growth rates at lower temperatures. This is due to the high precursor partial pressures, which may be tolerated because the problem of premature condensation does not exist at temperatures above ambient with MOVPE.

However, in common with VPE, MOVPE does still suffer from the problem of premature reaction or premature pyrolysis of the alkyls. This causes either homogeneous dust formation of II-VI powders (premature reaction) or random deposition of the component elements (premature pyrolysis) and results in degradation of epitaxial quality or non-epitaxial growth.

Although other techniques exist, such as liquid phase epitaxy (LPE) and molecular beam epitaxy (MBE), these also have their drawbacks. The former is essentially a high temperature technique. It is in any case not condusive to the growth of very thin films because layer inter-diffusion, thus rendering this process somewhat limited for the production of the increasingly complex device structures, such as quantum wells, which require sharp interfaces and precise control of composition and uniformity. MBE is a low temperature technique, but suffers from high cost, system complexity and low growth rates. Also, it is not at present a production process.

2.1.2 Alkyls

The alkyls most commonly employed in MOVPE of CdTe are dimethylcadmium

(DMCd) and diethyltelluride (DETe). Therefore for the growth of this material it is essential to have a knowledge of their decomposition characteristics. The linear alkyl molecules decompose by losing an alkyl group, followed rapidly by the loss of the second alkyl group. The decomposition may be either homogeneous or heterogeneous with the latter occurring at a faster rate. Using a statistical mechanical model[1,2] of the decomposition of the DETe, from thermodynamical considerations the data of Mullin et al. was found to be a reasonable fit to experimental values.

Mullin et al.[1] carried out a pyrolysis study of dimethyl- and diethyltelluride (DMTe and DETe) and also of dimethylcadmium (DMCd), using hydrogen as a carrier gas bubbling through a reactant bubbler, and decomposing the alkyls in a silica tube. The authors found that the minimum temperature for maximum of decomposition of the diethyltelluride was between 440 and 460°C, depending on the flow velocity. The pyrolysis curve for the DMTe (figure 2.1(a)) shows it to be more stable than DETe, decomposing to 100% yield at 510°C. The yield curve for DMCd (figure 2.1(b)) shows that Cd is obtained as low as 300°C, with a sharp increase in yield at 370°C; the yield then plateaus at about 400°C, indicating the less stable nature of this alkyl.

Several tellurides less stable than DMTe or DETe are emerging as likely candidates for use in low temperature pyrolytic MOVPE. These include ditelluride[3], ditertiarybutyl telluride[4] and diisopropyl telluride[5]. Kisker et al.[3] have reported growth of CdTe below 300°C using using ditelluride, and ditertiarybutyl telluride has been used by Hoke and Lemonias[4] to deposit at 220°C.

2.1.2.1 Adduct Formation

The decomposition characteristics of the DMCd and the DETe when pyrolysed simultaneously have been investigated by Mullin et al[1]. These authors found that the temperature dependence of the decomposition of DETe in the mixture was substantially lower compared with its decomposition independently. In fact the minimum temperature for 1% decomposition efficiency was reduced by 100°C.

This temperature reduction is evidence for reaction between the major components consistent with adduct formation between DMCd and DETe although direct evidence for an adduct has not been reported.

In addition epitaxial growth of CdTe occurs at 350°C whereas at this temperature the decomposition of DETe is minimal when pyrolysed alone. Other

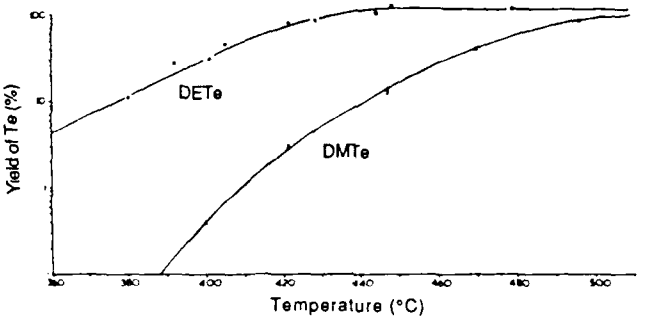

FIG. 2.1 (a). PYROLYSIS CURVES FOR DIMETHYL TELLURIDE AND DIETHYL TELLURIDE (AFTER MULLIN ET AL.[1]).

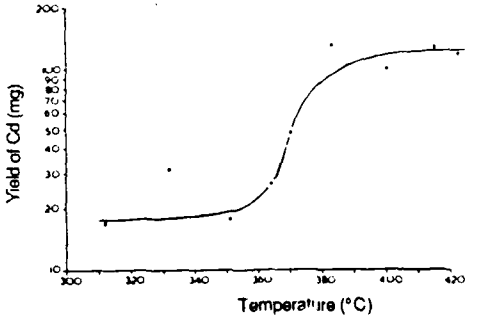

FIG. 2.1 (b). PYROLYSIS CURVE FOR DIMETHYL CADMIUM (AFTER MULLIN ET AL.[1]).

mechanisms for this enhanced DETe pyrolysis may involve free radical reactions with methyl radicals released from DMCd pyrolysis.

Additional evidence for the adduct model was given by Mullin and Irvine.[6] when they deposited cadmium mercury telluride (CMT), and noted that the mercury incorporation decreased rapidly to zero with substrate temperatures below 410°C. This was explained by the adduct formed between the DMCd and the DETe below 410°C not producing free tellurium which is required for reaction with the mercury to enable CMT to be formed. Above 410°C the efficient decomposition of DETe will lead to free tellurium and thus enable the subsequent incorporation of mercury into the growing layer.

Also, Cd and Te yields were found to be 1:1 down to the minimum decomposition temperatures of 310°C. This would not be expected without some type of reaction between the two alkyls and gives further evidence of the adduct model.

However, the adduct model was reconsidered by Mullin et al.[7,8] in the light of evidence from mass spectroscopy studies performed by Czerniak and Easton[9]. These authors identified the presence of MeCdEt and MeTeEt in the reaction products of DMCd and DETe. Mullin et al. pointed out that these reaction products were unlikely to be produced from any straight forward adduct formation. This implies that the adduct model proposed may not be as simple as had been previously thought.

Also noted by Czerniak and Easton was that the separate decomposition of DETe was autocatalytic, resulting in a reduction of decomposition temperature from 410°C down to 350°C in the presence of a deposit of tellurium. This may in part explain the growth of CdTe at lower temperatures than the normal pyrolysis temperature of DETe, as surface adsorbed Te may catalyse the DETe decomposition.

Ghandhi and Bhat[10] have taken an alternative approach towards the growth mechanism of CdTe. They proposed that DETe reacts with elemental Cd, deposited on the substrate surface from the pyrolysis of DMCd. The authors investigated the decomposition of DMCd and concluded that this would decompose above 230°C, and that the reaction was heterogeneous. They found that the CdTe growths gave an activation energy of 22kcal/mol which is closely related to the decomposition rate of DMCd (20.8kcal/mol). Further experiments with the use of elemental Cd vapours instead of DMCd resulted in the growth of CdTe as low as 230°C and led the authors to conclude that the presence of Cd enhances the decomposition of DETe, and also that in

the case of DMCd and DETe it is the Cd adsorbed from the dissociated DMCd that reacts with DETe to give CdTe at temperatures lower than normal DETe pyrolysis temperatures as follows :-

$$(CH_3)_2Cd(g) \rightarrow (CH_3)_2Cd^*$$
$$(CH_3)_2Cd^* \rightarrow (CH_3)Cd^* + \text{hydrocarbons}$$
$$(CH_3)Cd^* \rightarrow Cd^* + \text{hydrocarbons}$$
$$Cd^* + C_2H_5Te^* \rightarrow CdTe(s) + \text{hydrocarbons}$$

where * indicates adsorbed species.

This is in disagreement with the work of Czerniak and Easton[9] in which they detected the mixed alkyl species. Also they found no change in the decomposition of DETe in the presence of Cd, although Bhat et al.[9] claim that the Cd would be converted to CdTe as soon as DETe is introduced into the reactor.

Investigating the dependence of growth rate on the alkyl concentration, Bhat et al.[10] found by increasing the DETe partial pressure at constant DMCd partial pressure (and temperature) that the growth rate was sublinear with respect to DETe pressure. The growth rate continued to increase even at DETe partial pressures greater than that of DMCd. Alternatively, varying the DMCd partial pressure with constant DETe results in the saturation of growth rate once the DMCd partial pressure equals that of DETe.

The reason put forward for the rate limiting effect of DMCd is that DMCd decomposes into Cd and is chemisorbed soon after adsorption, whereas DETe does not react until it comes within the vicinity of the adsorbed Cd molecules. Hence the saturation of growth rate occurs for lower values of DMCd flow compared with the flow of the DETe. This also supports their growth model.

Hoke and Traczewski[11] deposited CdTe from DMCd and DETe using an input ratio of one, and obtained specular surfaces between 370°C and 410°C on (111)A CdTe substrates. A low density of growth pyramids (approx 200 defects/cm^2) was present and capacitance-voltage profiling indicated the films were n-type with free carrier concentrations in the 10^{13} and 10^{14} cm^{-3} range.

Schmit[12] also deposited on the same orientation of CdTe at temperatures between 306°C and 500°C but found the layers to be p-type with a carrier concentration of 10^{15} cm^{-3}. This is at variance with the n-type deposits obtained by Hoke and Trackewski and may be due to differing alkyl ratios employed between the two cases. Schmit however does not state the respective alkyl ratios used.

2.1.3.1 Cadmium Mercury Telluride (CMT) Growth

Irvine and Mullin[13] reported the growth of CMT using DETe, DMCd and elemental mercury with hydrogen as the carrier gas, onto CdTe substrates at a temperature of 410°C. Mercury was chosen in preference to a mercury alkyl because of reduced toxicity and the greater partial pressures needed for growth at these temperatures.

Layers were grown with x values between 0 and 0.5, controlled by regulating the DMCd flow. The grown layers were generally found to be n-type with a carrier concentration of between 10^{16}-$10^{18}cm^{-2}$ due to indium impurities, although a p-type layer was also deposited. Mobilities varied between 10^5 and 2400 $cm^2v^{-1}sec^{-1}$ with x values of 0.14 and 0.25 respectively. Hoke and Traczeweski[11] deposited onto (111) CdTe and obtained n-type layers and this was attributed to gallium and aluminium incorporation into the metal lattice sites. A carrier concentration of $8.9x10^{15}cm^{-2}$ for a layer of x=0.25 and a maximum mobility value of 144 000 $cm^2v^{-1}sec^{-1}$ with an x value of 0.15 were reported. Interdiffusion widths of 0.4μm were reported by Irvine and Mullin[13]. A greater value of ~1μm was reported by Hoke and Traczewski which is greatly improved compared to LPE techniques.

The composition was found by Mullin and Irvine[9] to be highly dependent on the growth temperature below 410°C and relatively insensitive to it above this temperature. This was attributed to the effect of inefficient pyrolysis of DETe below 410°C resulting in little of the free Te which is necessary for the incorporation of Hg in CMT. Above 410°C the more efficient pyrolysis liberates greater concentrations of Te and enables more Hg to be incorporated into the CMT layer.

Further work by Irvine et al.[14] showed that other factors influencing the composition included the alkyl inlet concentrations, the reactor wall heating control of the Hg vapour, boundary layer diffusion effects and the premature pyrolysis of the alkyls on the hot reactor wall.

2.1.3.2 Interdiffused Multilayer Process (IMP)

Tunnicliffe et al.[15] used an interdiffused multi-layer process (IMP) for the growth of CMT, thus avoiding to some degree the tight constraints on the flow and temperature conditions required for the growth of epitaxial CMT by standard MOVPE or direct alloy growth.

The growth takes place by the separate deposition of alternating layers of CdTe and HgTe, each grown under its optimum conditions. Each layer is sufficiently thin ($\sim 0.1\mu m$) for complete interdiffusion of the layers to occur during the growth period (and during a few minutes after the growth period for the interdiffusion of the topmost layers). This resulted in the complete homogenisation of the layer to form CMT.

The films deposited in this manner show better lateral unifomity over conventional MOVPE deposits and, also, accurate control of the layer composition is possible, as this is dependent solely on the thickness ratios of the individual CdTe and HgTe layers.

Thompson et al.[16] used the IMP technique with a di-isopropyltelluride (DIPTe) source, to deposit CMT at the lower temperature of 350°C. Although growth rates are ~50% lower than with DETe, the surface morphology was found to be improved compared to material deposited at ~410°C, and compositional uniformity was also improved with x values of 0.343±0.003 over an area of $1cm^2$. These authors have also reported[17] good uniformity with layers of low x deposited using the same technique; x values of 0.219±0.002 over similar areas were obtained.

2.2 Growth onto alternative substrates

2.2.1 Introduction

A great deal of work has centered on the growth of the II-VI compounds onto alternative substrates. The stimulus for this is the lack of availability of cheap, large area substrates of the II-VI material of sufficiently high crystalline quality.

Mullin et al.[1] deposited CdTe on CdTe, $MgAl_2O$, Al_2O_3, GaAs and InP but were unable to deposit a single crystal layer on the Al_2O_3. For the remaining cases, although epitaxy was obtained the layer surfaces were rough and rippled, especially at and close to grain boundaries on the substrates.

Schmit[12] has also grown on alternative substrates and has demonstrated single crystal growth onto GaAs, InP and InSb. Deposition was also performed onto sapphire, Si, Ge, zirconia, BF_2 and CaF_2 but it was found that the quality of the layers was heavily influenced by the substrate preparation and this was found to be the limiting factor in many cases.

2.2.2 Indium antimonide (InSb) substrates

The first reported growth of CdTe onto (100) InSb by MOVPE was by Ghandhi and Bhat[18]. These authors deposited at 350°C-450°C and obtained good crystallinity below 440°C, with polycrystallinity resulting above this temperature. The authors found however that the surface morphology of the epitaxial layers exhibited four sided pyramidal features consisting of {110} planes with bases aligned in the <100> directions. At higher temperatures these features increased in size as a consequence of greater layer thickness, thus implying that the features originate from the CdTe-InSb interface. Further work was carried out by Taskar et al.[19] to determine the cause of these hillocks. By dissociating the alkyls independently over the heated substrate they discovered that with DMCd an alloy of Cd-Sb-In had formed, which was detected by microanalysis (EDX). However in the case of DETe no reaction on the substrate had occurred and the substrate remained featureless. All further depositions were therefore performed by stabilising the substrate surface with a DETe overpressure prior to introduction of the Cd alkyl to proceed with CdTe growth, and this resulted in featureless morphology at growth temperatures up to 400°C.

Hoke et al.[20] deposited on (110) and (211) oriented InSb and found the best surface morphology was obtained at 440°C, with degradation of surface quality occurring below this temperature. However these authors employed no stabilisation of

Synopsis

An investigation of the low temperature deposition of cadmium telluride and cadmium was carried out by UV photodissociation of dimethylcadmium, (DMCd) and diethyltelluride, (DETe) in an MOCVD system with a horizontal, continuous flow reactor operating at atmospheric pressure.

Cadmium telluride was deposited principally onto (100) gallium arsenide substrates between 230°C and 350°C, and the effects of UV intensity, DMCd:DETe alkyl ratio and temperature on the crystallinity, morphology and purity were investigated by transmission electron microscopy, x-ray diffraction, scanning electron microscopy and secondary ion mass spectrometry.

Epitaxial growth occurs at 350°C with a unity alkyl ratio and a UV beam intensity at 254nm of $1Wcm^{-2}$. At temperatures below this the growth is polycrystalline. However, increase of the alkyl ratio and a reduction of the UV intensity suppresses the polycrystalline growth and epitaxy is achieved with an intensity of $12mWcm^{-2}$ and a DMCd:DETe ratio of 1 and 1.5 at 300°C. The layers deposited with DMCd rich conditions also exhibit improved surface morphology and a much reduced dislocation structure. The degradation of crystallinity at reduced temperatures and increased UV intensities has been correlated with an increase in homogeneous vapour phase nucleation.

The growth rate kinetics have been analysed in terms of the Langmuir-Hinshelwood surface kinetic model and in particular the reduction in growth rate with increasing DMCd concentration has been attributed to a site blocking mechanism.

The nucleation behaviour of cadmium photodeposited onto (100) gallium arsenide, (100) silicon and (0001) sapphire substrates was investigated over a range of temperatures and partial pressures.

Growth occurs in a different manner onto each substrate, showing various degrees of island formation and clustering dependent on the interfacial free energies of the vapour-condensate-substrate system. Deposition onto the gallium arsenide substrates occurs as in the Volmer-Weber growth model and deposition onto the sapphire as in the Stranski-Krastinov model. Deposition onto the silicon ocurred in a layer-by-layer manner.

Although rapid surface diffusion during deposition onto the gallium arsenide substrates promotes non-uniform deposits, continuous films may be deposited by increasing the nucleation density by a reduction of the growth temperature to below room temperature.

The low growth rates encountered with photodeposition may be overcome by a prenucleation process whereby the initial nucleation is carried out photolytically and the subsequent layer thickening is carried out thermally. This technique provides a route for patterned deposition as little growth occurs outside the prenucleated areas.

the substrate surface similar to that of Ghandhi et al.[19] and hence alloy formation may explain the poor morphology for this substrate.

These layers grew with a slight tilt. On the (110) substrates the layers were tilted 0.8° from (110) and for the (211) substrates a tilt of 0.9° from (211) was detected, implying the presence of an interfacial structure.

Investigating the growth rate dependence with temperature, Ghandhi and Bhat[18] found that below 400°C an activation energy of 16 kcal/mol was obtained for deposition onto (100) InSb, and above this temperature the growth rate began to saturate, probably due to mass transport limitation.

Ghandi and Bhat[18] also investigated the effect of using excess DETe or DMCd partial pressures on the electrical properties of the layers. Above 380°C, with excess DETe, n-type behavior was found and was attributed by the authors to the resulting excess Cd vacancies acting as incorporation sites for donor impurities such as Al present in the reactants. With excess DMCd the layers were of high resistivity.

Comparing the photoluminescence (P/L) spectra on the basis of equal band to band intensities these authors found reduced intensity defect peaks for the growths with excess DETe conditions. The near band edge intensity increased rapidly with temperature with DETe rich conditions. This was attributed to the enhanced crystallinity obtained at the higher growth temperatures and it was concluded that the best electrical properties were achieved under these conditions.

Bhat et al.[21] found by DLTS that an increase in the DETe/DMCd partial pressure ratio resulted in an increase in the defect level concentration, thus confirming that the basic defect is either a Te interstitial or a Cd vacancy. They formed Au-CdTe Schottky diodes on these layers and achieved ideality factors of ~1.1 and a barrier height of 0.75 eV, results comparable to the best CdTe to date.

Further study of the same system by Taskar et al.[22] showed that the ratio of the Cd vacancy defect to the band edge P/L intensity decreased rapidly with an increase in the p_{DMCd}/p_{DETe} ratio >0.37. This ratio of the defect associated peak and the near band edge exciton peak is generally accepted as an indicator of CdTe crystalline quality. The defect peak is a broad band occurring at lower energies than the excitonic peak. The authors showed that a wide range of partial pressures (p_{DMCd}/p_{DETe}>0.6) gave low

intensity ratios hence indicating good crystallinity over this range. However it must be pointed out that at the higher ratios the defect level associated with the Te vacancies would also be significant.

2.2.3 GaAs Substrates

Ghandhi et al.[23] also grew CdTe onto GaAs substrates. They achieved parallel epitaxy i.e. (100) layer orientation onto (100) substrate, shown by SEM channelling patterns. Layers were grown between 350°C and 440°C, and specular surfaces obtained at the lower temperatures. However as with the growths on the InSb substrates the morphology degraded at the higher temperatures, probably due to tellurium crystallite formation. Also in accordance with the InSb case the P/L spectra show better crystallinity with increased DMCd partial pressure, and the layers were semi-insulating.

Hoke et al.[20] deposited CdTe onto (100) GaAs and obtained the best surface quality at 440°C. Below this temperature a degradation of surface morphology occurs, in contrast with the growths of Ghandhi and Bhat who obtained superior morphology at lower temperatures. This may be related to the relative alkyl ratios used by both authors, as Ghandhi and Bhat reported that the alkyl ratios had to be optimised for each growth temperature to obtain good morphology, although they do not state which ratios they employed. Hoke et al. employed unity ratios at 440°C but do not state if they attempted to vary this at lower temperatures.

Schmit[12] investigated the morphology of CdTe growth onto (111) and (100) GaAs and found that the smoothest surfaces were obtained on (111) GaAs. Profilometer traces showed the surfaces to be atomically smooth. However the crystallinity as measured by double crystal x-ray diffraction (DCRC) was better in the case of (100) GaAs.

Lu et al.[24] grew CdTe onto (100) GaAs in a low pressure reactor and obtained growth orientations of either (111) or (100) depending on the treatment prior to growth. The former orientation was obtained when annealing of the substrate was carried out at ~585°C and the latter orientation achieved with no such treatment.

The majority of the films were deposited at 370°C as this gave the best surface morphology. The morphology of the two orientations was different. The (111) surfaces were highly specular and essentially featureless as opposed to the (100) surfaces which were pitted and rough. The superior crystallinity of the (111) layers were confirmed by

single crystal x-ray diffraction measurements. Although this appears to be in disagreement with the (111) layers deposited by Schmit[12] the comparison is not a true one as different orientations of substrate were used in the two cases. Also Schmit did not perform a heat clean of his (111) GaAs substrates. The better crystallinity is to be expected in the heat cleaned case as this procedure will remove the surface oxide of the GaAs and possibly allow surface reconstruction of the GaAs. Thus the growth would begin on a clean and ordered surface whereas in the alternative case growth is commencing on a lower quality oxide surface.

Feldman et al.[25] found that for (111) grown layers on GaAs the crystallinity improved with the growth temperature and obtained the best x-ray rocking curve widths of 95 arc seconds at 420°C. The (111) growth was obtained with Te rich conditions and as the conditions were made less Te rich the (100) orientation was obtained.

Anderson[26] specifically approached the growth of CdTe onto GaAs from a large scale commercial viewpoint and deposited CdTe onto two 2" substrates simultaneously. He obtained specular and featureless growth of CdTe films between 220°C and 440°C for the (111) orientation grown under Te rich conditions.

The (100) oriented films were obtained when the growth was initiated with Cd rich conditions. The surface morphology was inferior to the (111) case, with a prismatic appearance, and also required greater attention to the growth conditions, as specular surfaces were obtained only under a narrow range of conditions unlike the (111) films which were more stable. This was confirmed by P/L and x-ray diffraction which indicated the highest quality for the (111) films. Growth onto (111) GaAs resulted in a layer orientation of (111).

Anderson[26] also investigated the temperature dependence of the growth rate and found that up to ~420°C a kinetically limited regime with an activation energy of 16.5 kcal/mole is obtained. Above this temperature there is little temperature dependence and the growth rate is mass transport limited until 470°C, above which a congruent evaporation process becomes important and in fact exceeds the growth rate at above 600°C.

The growth rate dependence at unity mole fraction of DMCd:DETe was found to vary linearly with the metal-organic source partial pressures. At mole fractions ratios other than unity the partial pressure of the least prevalent species becomes rate limiting. However no detailed data about the variation of growth rate with partial pressure is

presented, and it was pointed out that uncertainty exists in the data due to surface morphological effects making growth rate measurements difficult especially at the smaller Te:Cd ratios.

The substrate orientation was investigated by measuring the growth rate onto (111)A and (111)B and also (100) GaAs surfaces. In this temperature regime equal growth rates were obtained, and this is hardly surprising as the author is approaching the mass transport limited region, where the growth is independent of surface kinetic effects such as differences in orientation.

2.2.4 *Silicon substrates*

Growth of CdTe onto silicon substrates has also been reported. Chou et al.[27] carried this out, using a low pressure technique, on (100) substrates at 375°C and pressures of between 20 and 30 torr. The surface was found to be specular although pyramidal features were obtained with an alkyl ratio of one and attributed to the lattice mismatch. Although the alkyl ratio was varied its effect on morphology is not reported.

The authors found increasing the DMCd/DETe ratio from 1 to ~8 led to a degredation of crystallinity as shown by P/L. This is in disagreement with the growth of Ghandhi and Bhat[23] onto GaAs in which they showed improved crystallinity with increasing DMCd/DETe. However these authors were increasing this ratio from DETe rich conditions and did not approach the high levels of excess DMCd achieved by Chou et al.

In further studies by Lin et al.[28] the temperature dependence between 345 and 405°C was investigated again with an alkyl input ratio of one. The pyramidal features reported previously were enhanced at the higher temperatures. The optimum temperature for crystalline quality was found to be 375°C as at lower temperatures the band edge intensity decreases and above 375°C the defect peaks predominate.

2.2.5 Sapphire Substrates

Cole and Woodbury[29] deposited CdTe in a vertical cold wall reactor onto basal plane (0001) sapphire substrates. They obtained a growth rate temperature dependence with a very high value of activation energy. X-ray measurements showed that the CdTe deposited initially as a highly ordered polycrystalline layer. As the layer became thicker there was a gradual transition to a more perfect layer ultimately resulting in a high quality single crystal layer of (111) orientation. The polycrystallinity at the substrate surface and the high value of activation energy suggest that this behaviour is

due to a difficulty in nucleation. Similarly Mullin et al.[1] deposited onto sapphire and obtained an ordered polycrystalline layer with a preferred direction of (111). No homogenisation into single crystal was reported but may due to the layer being too thin for this to have yet occurred.

The surfaces of the deposits obtained by Cole and Woodbury [29] were rough with peaks of 1 micron, which was attributed to turbulence within the reactor. In agreement with these authors Mullin et al.[1] also reported rough surfaces. However it would appear that heat cleaning the substrates in hydrogen results in improved deposits. Cole and Woodbury found the best quality films when the substrates had been heated in hydrogen at 950°C.

Hoke et al.[30] deposited single crystal CdTe on (0001) sapphire which was annealed in hydrogen above 1000°C. The growths were carried out between 400-410°C. These films were specular and very smooth with little background texture. The orientation was (111)A and double crystal rocking curves (DCRC) showed a width of 56 arc secs for an 8.4 micron thick deposit.

Secondary ion mass spectrometry (SIMS) showed little diffusion of aluminium into the CdTe films from the substrate and the authors concluded the material was suitable for the growth of CMT and also demonstrated this.

Thomson et al.[31] investigated the temperature dependence of the crystallinity of CdTe on sapphire. They found that from 360-460°C fully specular surfaces were obtained and the orientation relationship was (111)B CdTe, in contrast to the reports of Hoke et al.[30] who obtained the A surface. DCRC shows that at temperatures below 430°C poor crystalline quality is obtained with typical full widths at half maximum (FWHM) of between 0.31-0.65° being measured. However above this temperature the FWHM improved greatly with a value of 0.07° being obtained at a temperature of 460°C. Although a further increase of temperature improved this value a degradation of the surface morphology was obtained. Also at this higher temperature both (111)A and (111)B CdTe could be grown, with the polarity being dependent on the Cd/Te input ratio. With a ratio of 1:1.2 more than 90% B face material was deposited whereas with 1.5:1 only 60% B face resulted. The A material was of superior crystallinity. Thus below 480°C (111)A is favoured and the O-Te bond is predominant whereas for the (111)B it is the O-Cd, which implies that the nucleation effect is clearly complex.

2.3 Photo-epitaxy of II-VI's, III-V's and silicon

2.3.1 Introduction

The basis of photo-epitaxy is the dissociation of the precursor molecules using radiation, ultraviolet or infrared, in order to deposit at lower temperatures than is possible with conventional MOVPE. Hence the study of the dissociation of the molecular species is central to the theme of photolytic growth.

2.3.2 Absorption spectra

The absorption spectra of some group II and group VI alkyls have been measured by Irvine et al.[32] and the spectrum of DMCd is showr in figure 2.2(a). It can be seen that between 200-300nm the spectrum shows a discrete absorption band, with well resolved vibrational fine structure peaking at around 216nm, together with a broad absorption continuum within this range. There is an electronic transition from a weakly bonding to an anti bonding molecular orbit in the energy range of 43000-47000cm^{-1} which leads to significant weakening of the the C-M-C molecular chain. This excitation can lead to photo-dissociation at room temperature. The mechanism may involve vibrational relaxation to the antisymmetric reaction coordinate of a bound state or it may decay into the underlying continuum which would be dissociative. The spectrum of the DETe (figure 2.2(b)) shows no vibrational fine structural peaking but does however have a strong absorbance in the region of high lamp intensity.

Irvine et al.[32] performed photodissociation of DMCd, DMHg and DETe alkyls in a hydrogen stream at atmospheric pressure onto a silica reactor tube using a 3kW Hg/Xe arc lamp, and investigated the effects of flow velocity, alkyl partial pressure and UV intensity on the deposition rate.

Dissociation of the DMCd resulted in a smooth mirror deposit, forming initially on the high intensity illuminated region and extending subsequently to the lower intensity region. The DETe however resulted in a deposit which appeared downstream in regions of low UV intensity and consisted of a fine powder, in contrast to the Cd. This implies that a more complex process than simple photon absorption and rupture of a C-Te bond is occurring. A possibility is that formation of an intermediate species such as TeEt takes place in the high intensity region which leads to its dissociation in a low intensity region with further photon absorption, or alternatively there may be a problem of adsorption onto the silica.

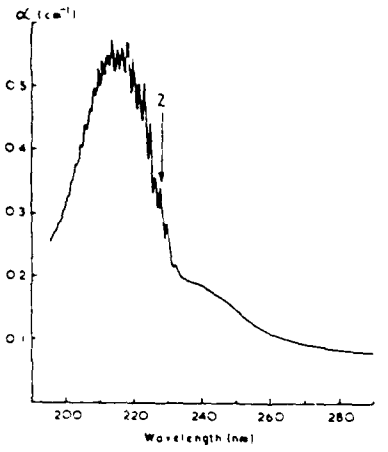

FIG. 2.2 (a). ADSORPTION SPECTRUM FOR DIMETHYL CADMIUM (AFTER IRVINE ET AL.[32]).

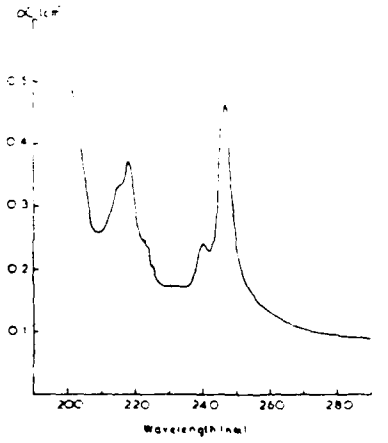

FIG. 2.2 (b). ADSORPTION SPECTRUM FOR DIETHYL TELLURIDE (AFTER IRVINE ET AL.[32]).

2.3.3 Mercury telluride (HgTe)

The first reported photo-epitaxial growth of compound semiconductors was by Irvine et al.[33] who deposited HgTe using a photo-sensitisation method. Growth was onto CdTe and InSb substrates, and epitaxial HgTe was grown as low as 198°C, indicated by x-ray diffraction and SEM channeling.

It was suggested that rupture of the DETe molecules occurred by imparting energy to the alkyl molecules from the excited Hg states. The UV from a high pressure Hg arc lamp causes surface excitation of chemisorbed Hg to a $Hg(^3P_1)$ level which then has sufficient energy to dissociate the DETe molecule.

This proposal was based upon the effect on the growth rate of Hg partial pressure as it was found that a high Hg pressure (3 orders of magnitude higher than the equilibrium value) was required for growth to occur, thus suggesting that the photochemical reaction dissociating the DETe involves the presence of Hg.

The role of surface kinetic factor was also indicated by the sublinear dependence of the growth rate on DETe partial pressure and also by the growth rate dependence on the substrate orientation. Growth of HgTe by Ahlgren et al.[34] showed a similar growth rate dependence on the square root of DETe partial pressure, and this was modelled by an adsorption process with the DETe occupying two surface sites. The growth rate was also seen to vary with the square root of lamp intensity, but this could not be explained in the context of this model.

2.3.4 Cadmium Mercury Telluride (CMT)

CMT was deposited as low as 250°C photo-epitaxially by Irvine et al.[35] using DMCd, DETe and elemental Hg. It was found that the crystalline quality of the deposit was heavily dependent on the carrier gas employed. With a hydrogen carrier a highly porous polycrystalline layer was obtained whereas to achieve epitaxy it was necessary to use a helium carrier.

The effect of the carrier gas was explained by a reduction of the probability of homogeneous gas phase nucleation with the helium. With the hydrogen the concentrations of the active species are increased as the hydrogen plays an active role in the expected reaction mechanisms, by the decomposition of diatomic hydrogen (H_2) which reacts with the photo-excited $Hg(^3p_1)$ thus:

$$Hg^* + H_2 \rightarrow Hg + 2H$$

The monotomic H is then free to react with the alkyls to liberate free Cd and Te atoms, thus increasing the supersaturation.

By changing the carrier gas a small reduction in growth rates was obtained indicating that although the photosensitisation dissociation of H_2 should be competitive with the dissociation of Et_2Te, the surface reaction is not significantly affected by the presence of H_2. This is consistent with the formation of a surface complex between Hg and the DETe before excitation of Hg by the UV. The reduction in growth rate may be due to the photogenerated alkyl radicals, generated in the absence of H_2, inhibiting the surface decomposition of DETe or having an etching effect on the layer.

It was found that the region over which specular single crystal growth occurred was limited to the UV focus region, where the UV is most intense. In the less intense region the growth was vapour phase nucleated and deposited as a dust. This was explained by diffusion of the Cd and Te from the intensely illuminated region into the defocussed region where there are insufficient free radicals, as a result of the quenching of these species to form stable alkanes, resulting in an excess Cd and Te concentration, above the critical value for homogeneous dust formation.

Further work on this system by Irvine et al.[36] led to increased deposition area by the addition of dimethylmercury (DMHg) to the inlet flow. This when photolysed provides an extra source of free radicals, reducing the Cd and Te supersaturations and the vapour phase nucleation. Increasing the DMHg concentration led to increased areas over which epitaxial growth was achieved.

Carbon contamination, a known problem in low temperature photolytic depositions of GaAs due to lower desorption and possible incorporation of organic products, was monitored for the CMT and the HgTe layers on InSb substrates by Irvine et al[35]. No significant difference in the contamination level was found with change of the carrier gas. With the hydrogen carrier less carbon could be expected because of reduced radical lifetimes. Carbon was detected at a level of 20-30 ppm in the layer and peaking at the layer/substrate interface observed. This was attributed to residual contamination on the substrate surface prior to growth.

Morris[37] deposited CMT with high x values (0.8) using an excimer laser operating at 193nm at substrate temperatures of 150°C. The reactor configuration was such that the UV was incident parallel to the inverted CdTe substrate, reducing any temperature effects from the high power density of the laser and also preventing vapour

phase nucleated particles from settling on the substrate. Growth rates in excess of 4μm/hr were achieved and the epitaxial nature over at least small areas was indicated by back-reflection Laue x-ray diffraction.

Ahlgren et al.[34] deposited CMT by growing a CdTe/HgTe layer structure, onto a cadmium zinc telluride (CdZnTe) substrate at 280°C using a Hg/Xe arc lamp, which was interdiffused to form CMT with an x of 0.26. This process is somewhat similar to the IMP process described by Tunnicliffe et al[15]. However poor carrier concentrations and mobilities led the authors to conclude that the interdiffusion of the alternating layers was incomplete.

2.3.5 Cadmium Telluride

Vapour phase nucleation also affected the growth of CdTe. Irvine et al.[35,36] found difficulty in depositing single crystal CdTe with a hydrogen carrier, especially at low temperatures, but overcame this to some degree using helium. At higher temperatures the effect was reduced and epitaxial layers of CdTe were obtained. This was explained by the chemical potential being too low for homogeneous nucleation.

The presence of elemental mercury caused breakdown of the crystallinity once again and this result was significant from the point of view of growing HgTe/CdTe superlattices, where it would be advantageous to have the Hg always present and alternate the layers by switching the organometallics.

Kisker and Feldman[39] deposited CdTe photolytically onto (100) GaAs using a low pressure Hg vapour lamp, and in contrast to the work of Irvine et al. deposited single crystal CdTe with a hydrogen carrier at temperatures as low as 250°C. However in order to do this a DMCd:DETe alkyl ratio of 1.5 was necessary otherwise a polycrystalline deposit was obtained upto 420°C. The authors concluded that this was due to the greater dissociation efficiency of the DETe compared with the DMCd, although this appears to be contrary to the photodissociation study of the alkyls by Irvine et al. However the UV sources used in the two cases were different and the broad band source used by Irvine et al. may dissociate a greater amount of DMCd.

As the UV transparent window of these authors'[40] reactor suffered from window fogging during deposition they were able to measure growth rates for short and long time intervals to obtain an indication of the importance of the photolytic growth rate compared with the thermal growth rate.

Growth rates were measured for layers grown at 250°C and 350°C and it was found that even at the higher temperature there is considerable growth rate enhancement with the UV. At 350°C a threefold increase in growth rate was obtained over the purely thermal case.

Preliminary photoluminescence measurements indicate that the material grown photolytically at 350°C is of better crystallinity than the purely thermally grown layer, giving $I_{exciton}$ to I_{defect} ratios of 20 compared with 5. However in comparing the poorer crystallinity of the thermal growth it must be noted that the alkyl ratios were not optimised for the thermal depositions.

Consideration of the growth rates showed that an anomalously high quantum efficiency was obtained compared with that of Irvine et al. Kisker and Feldman[39,40] tentatively suggested this may be due to a modification of the UV absorbance by the precursor molecules as they are adsorbed onto the substrates or to the effects of photogenerated carriers or thermal effects. Although these effects may cause some change it is unlikely that they will cause the large increase in the efficiency obtained.

Mullin et al.[7] investigating the growth mechanisms of CdTe growth with a hydrogen carrier suggested that the high efficiencies (>1) obtained by Kisker and Feldman[39,40] may result from radical formation and subsequent reactions with the hydrogen.

Ahlgren et al.[34] also deposited CdTe on GaAs. These authors used a 1kW high pressure Hg/Xe arc lamp with a hydrogen carrier and deposition was performed between 182 and 352°C. In contrast to the work of Irvine et al. and Kisker and Feldman all layers deposited were epitaxial using unity DMCd:DETe ratios. However growth rates with the UV showed no increase in the thermal depositions onto GaAs but may be due to UV attenuation effects as the authors did express concern about the difficulty in maintaining a clear window for the UV.

Deposition onto (111) CdTe substrates by the same authors[34] did show a growth rate difference under UV illumination. Also the morphology was affected by the polarity of the substrate, with the A face being smooth and the B face yielding rough layer surfaces at T>350°C and the reverse being true at temperatures below this.

2.3.6 CdTe/HgTe multilayer structures

Irvine et al.[41] investigated the interface abruptness of CdTe/HgTe multilayers and found that the photolytically deposited layers yielded an interface width of 105Å with a growth temperature of 230°C.

Multilayer structures were grown by venting the DMCd as required and always having the elemental Hg present in the reactor; although it was necessary to cool the mercury reservoir during the CdTe cycles to reduce homogeneous vapour phase nucleation.

Predictions of interdiffusion widths of CdTe/HgTe heterostructures were made by the authors using SIMS data of layers grown at temperatures of 230°C and 410°C and it was found that to achieve adequately stable superlattice structures a temperature of below 150°C was desirable.

Gallium diffused from the GaAs substrate into the growing layer can have an adverse effect on its electrical properties. Irvine et al. found that at the low temperatures employed for photodeposition (270°C) the Ga level falls to 0.05ppm within 500Å of the interface. This compares well with values of 0.1 ppma at 4 microns from the interface achieved by Giess et al.[42] with conventional MOVPE.

Ahlgren et al.[43] have demonstrated the growth of 123Å period HgTe-CdTe superlattices at temperatures of 182°C. As with the growth of the multilayer structures by Irvine et al.[41] the alternate layers were grown simply by switching the DMCd flows. However a hydrogen carrier was used and the substrates were CdZnTe.

At the low growth temperatures, growth rates of <0.1 μm/hr were obtained using the high pressure Hg arc lamp. The superlattice consisted of 35 periods and all were visible by SEM after angle etching the specimen. X-ray diffraction measurements showed the lattice period to be 123Å as estimated from the satellite peaks. The measured bandgap was extremely low having a value of 0.118eV at 300K and 0.0532eV at 77K.

2.3.7 Silicon

Deposition of single crystal silicon at temperatures as low as 100°C has been demonstrated by Nishida et al.[44] using a mercury photosensitisation process, with a low pressure Hg vapour lamp, disilane (Si_2H_6) and a hydrogen carrier. This is a reduction of ~800°C compared with normal epitaxial pyrolytic growth of silicon.

Deposition was onto (100) silicon and the substrate was not given a conventional preanneal prior to growth in order to remove surface oxides, etc. The authors found the addition of SiH_2F_2 enabled growth of epitaxial layers instead of polycrystalline material and this may be due to the gettering effect of fluorine on the hydrogen present on the growing surface and also to the removal of the native oxide on the substrate.

Continued investigation of this system by Yamada et al.[45] showed that deposition with monosilane exhibited better crystallinity at 250°C although difluorosilane was still used. SIMS measurements on doped substrates showed negligible autodoping across the interface (500Å), a direct product of the low temperatures used.

2.3.8 Gallium Arsenide

Putz et al.[46] investigated the effect of UV radiation on the growth of GaAs from trimethyl gallium (TMG) and arsine (AsH_3), using a low pressure mercury vapour lamp. They found that irradiation improved topography, and enhanced the growth rate in the low temperature kinetically limited regime. The surface morphology improved from a rough whisker like surface to a smooth and specular surface with UV exposure, at temperatures of 550°C and 600°C. Photoluminescence also indicated improved crystallinity compared with the growths performed by purely thermal means.

Roth et al.[47] stimulated the growth of GaAs with a pulsed Nd-YAG laser operating at a wavelength of 530nm, using similar precursors to Putz et al. These authors found that epitaxial layers could be deposited between 360°C and 540°C in the laser illuminated region. In the non-irradiated area the growth rate decreased rapidly below 480°C. The growth enhancement in this case relies on the local transient temperature increase of the substrate. During the 3ns irradiation the surface temperature rises to 1000°C but falls below 500°C within 1μs.

2.3.9 Germanium (Ge)

Epitaxial films of germanium have been deposited onto (100) NaCl substrates by Eden et al.[48]. The authors photodissociated germane (GeH_4) at 248nm using a KrF laser at a temperature of 120°C.

From film growth rates and spectroscopic measurements the authors concluded that the growth process is initiated by single photon absorption in the vapour phase, and that the Ge is arriving at the surface in atomic form.

2.3.10 Zinc selenide (ZnSe)

Ando et al.[49] deposited epitaxial films of ZnSe onto GaAs by photo enhancement using a low pressure mercury lamp to dissociate dimethyl zinc (DMZn) and diethyl selenide (DESe). Growth at temperatures greater than 450°C was found to be epitaxial and a twofold enhancement over purely thermal deposition was achieved. Deposition, albeit of a polycrystalline nature was observed at temperatures as low as 200°C, whereas no pyrolytic deposition was obtained lower than 350°C.

Deposition onto glass substrates indicated that the UV also influenced the orientation of the ZnSe, which grew with a preferred orientation of (111). This preferential deposition was not obtained in the purely pyrolytic case.

2.3.11 Indium phosphide (InP)

Donnelly et al.[50] deposited epitaxial InP at a base temperature of 320°C on a variety of substrates using the 193nm radiation from an ArF excimer laser. The precursors used were the adduct $(CH_3)_3InP(CH_3)_3$ and phosphine (PH_3). The InP adduct is thermally dissociated into TMIn and TMP on introducing the precursors into the reaction cell prior to their photolysis.

The crystallinity was heavily influenced by the energy density of the laser beam, with an amorphous layer being obtained at the low energy density of ~0.01-0.03 Jcm^{-2}. At levels greater than this, up to ~0.1Jcm^{-2}, polycrystalline deposits with grain sizes ranging from 50Å to 400Å were obtained. Increasing the laser power to above 0.1Jcm^{-2} resulted in epitaxy although the mechanism for this is probably a recrystallisation one. At these energy densities, the InP surface is taken close to the melting point. At even greater laser powers damage to the deposit, causing P depletion and intermixing between the layer and the substrate, was observed at the most intense part of the beam.

2.4 Photodeposition of metals

2.4.1 Introduction

The current interest in the photodeposition of metals stems from its potential for low temperature processing of semiconductor surfaces. Patterning by laser scanning or mask patterning by either laser or incoherent sources removes the need for contact masks. High writing speeds, localised reactions, little or no background heating and the relative ease with which it can be used with present processes or in fact in the future for complete devices made by photo-processes make this an attractive prospect.

A wide variety of metals has been deposited photolytically on differing substrates using both UV lasers and lamps. The precursors normally used are the metal-organics, halides, carbonyls or organic complexes of the parent metal. A selection of the metals deposited in this manner is listed in table 2.1 along with the radiation source, the precursor and the substrate used.

2.4.2 Adsorbed layers

Many of the common metal alkyls can form thick Van der Waals films, with low binding energy, onto surfaces at or below room temperature. Photolysis of these adlayers results in permanent metal deposits on the supporting substrate. Amongst the advantages is that it can result in greater resolution, better uniformity and higher density of the deposits.

By measuring mass changes Ehrlich and Osgood[64] obtained adsorption isotherms of DMCd and trimethyl aluminium (TMAl) (dimerised to $[TMAl]_2$), due to adsorbed molecules, as a function of the gas pressure and the substrate temperature. The isotherms were determined for Ag, Au and Si substrates.

The sets of curves obtained are shown in figure 2.3 and are indicative of gases with a strong surface interaction. The low pressure knee is characteristic and occurs at the coverage of one monolayer. The slight inflections seen in the graph occur at integral multiples of a monolayer and correspond to subsequently adsorbed monolayers.

From the BET theory for multimolecular layer adsorption the amount of adsorbed material at a temperature T, compared with a monolayer coverage θ, is given by

METAL	PRECURSOR	RADIATION SOURCE	SUBSTRATE	REFERENCE
Zn	$Zn(CH_3)_2$	Hg/Xe arc lamp	quartz	(51)
"	"	KrF	Si	(52)
Al	$Al(CH_3)_3$	Low pressure Hg lamp	Si	(53)
Cr	$Cr(CO)_6$	Cu hollow cathode laser	Si quartz	(54)
Mo	$Mo(CO)_6$	Cu hollow cathode laser	Si quartz	(54)
W	$W(CO)_6$	Cu hollow cathode laser	Si quartz	(54)
	WF_6	ArF	Si,sapphire	(55)
	"	"	Si,oxidised Si	(56)
Cd	$Cd(CH_3)_2$	ArF,Ar+	quartz	(57)
Sn	$Sn(CH_3)_4$	KrF	InP	(52)
	"	Ar+	carbon	(58)
Ga	$Ga(CH_3)_3$	Ar+	quartz	(59)
Cu	Cuhf complex	KrF	-	(60)
	Cuhf-ethanol	"	-	(60)
Ni	$Ni(CO)_4$	Ar+	silica	(61)
Fe	$Fe(CO)_5$	ArF	-	(62)
In	$In(CH_3)_3$	Ar+	silica	(63)
Pt	PtCFAcAc	Ar+	silica	(63)

TABLE 2.1

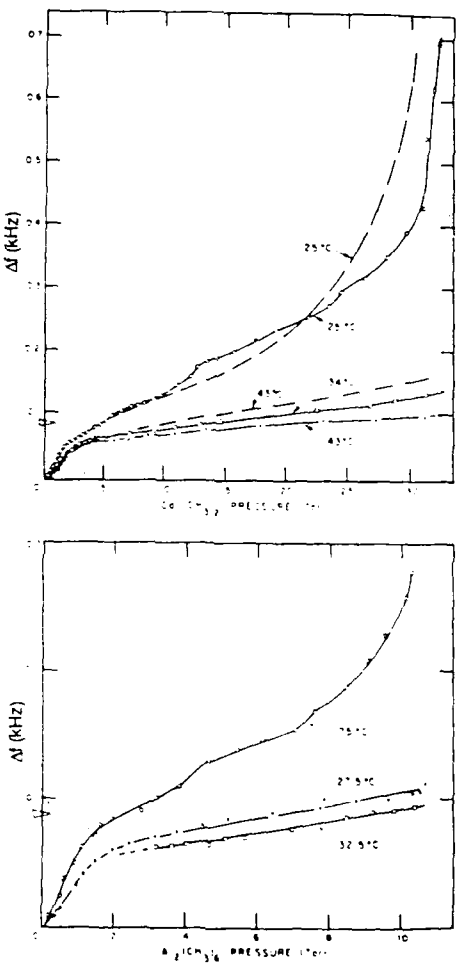

FIG. 2.3. ADSORPTION ISOTHERMS FOR DIMETHYL CADMIUM (TOP) AND TRIMETHYL ALUMINIUM (BOTTOM) (AFTER EHRLICH AND OSGOOD[64]).

$$\theta(T) = \frac{p}{p_o} \frac{p}{\frac{1}{c} + \frac{(c-1)p}{cp_o}}$$

where $c=\exp[(E_1-E_L)]$ and p_0 is the equilibrium vapour pressure, p the partial pressure of the vapour, E_1 the binding energy of the adsorbent and E_L the heat of liquification.

The inflections seen at integral multiples of monomolecular layers are not included in the BET theory and result from slight modifications of the binding energy E_L of the subsequent adlayers. Also apparent from figure 2.3 is the effect of slight increases in the temperature, which lead to desorption of many of the topmost molecular layers.

The binding characteristics of the adsorbed layers were investigated by an evacuation procedure which showed that a rapid desorption of the top layers resulted, indicating the weak binding nature of these physiosorbed layers. The first monolayer however was found to be more stable and strongly bound, and is indicative of a chemisorbed layer.

The absorption spectra of the adsorbed layers were also found to be modified from that obtained from the free vapour of the alkyl and show a distinct shift towards longer wavelengths. Further detailed work on the spectra by Chen and Osgood[65] showed the vibronic structure peaks had been suppressed and an overall broadening of the spectra was observed.

2.4.3 Contamination

Contamination has been a drawback in photodeposits. It can arise from lack of purity of the starting reagents or in some cases as a by-product of the photolytic reactions themselves, especially where organic molecules are dissociated. The low deposition temperatures can also increase the problem due to incomplete desorption of molecular species.

Contamination in the form of oxygen, carbon and fluorine were detected by Johnson and Schlie[51] in their deposits of zinc, and the authors postulated that many of these were created by the broad spectral output of their Hg arc lamp photodissociating contaminant molecular species present in the starting reactants.

Houle et al.[60] measured carbon contents of up to 90% of the total composition of copper photodeposited layers from different CuHF complexes. A slight reduction in

the carbon content was obtained at the higher UV intensities. Carbon levels were found to be lower with the copper ethanol complex and indicate that the alcohol is affecting the surface chemistry.

Attempts at the photodeposition of aluminium by Bouree et al.[53] resulted in deposition of one micron fine alumina powder. Alumina, in contrast to pure aluminium was obtained because of the large specific area presented by the granular aluminium particles and its large chemical activity towards residual oxygen. In photodepositing tungsten from its parent carbonyl Solanki et al.[54] also showed oxygen to be a major contaminant.

2.4.4 Prenucleation

Prenucleation is a technique whereby a substrate is initially nucleated by the photodissociation of an adsorbed molecular monolayer in a sharp characteristic pattern. Further exposure to an atmosphere of the reactant species and a dissociating source with flood illumination results in the original pattern being reproduced with high contrast. Careful selection of the UV conditions can result in considerable enhancement of the prenucleated areas with no nucleation occurring outside this region.

Ehrlich et al.[66] performed the prenucleation of cadmium, using a focussed ArF laser operating at 193nm, and the subsequent growth enhancement effected by this laser defocussed.

An essentially similar process was carried out by Tsao and Ehrlich[67] who created nucleation centres by photolysing tri-isobutyl aluminium (TIBA) onto quartz substrates. However they thickened this layer by pyrolytic means using a CO_2 laser giving a local temperature rise of 400°C.

As with the purely photolytic prenucleation process, careful control of the reactant pressure and the CO_2 laser enhanced temperature resulted in growth on the initially nucleated region, with no background nucleation occurring on the bare substrate. Performing laser transmission experiments to obtain an indication of the film thickness it was found that if the pyrolytically dissociating CO_2 laser beam was switched on before illumination with the photodissociating source, i.e prior to prenucleating, no deposit was obtained. The absence of any deposit is consistent with adsorbed layer formation, whose coverage decreases with increasing temperature.

2.4.5 Substrate Effects

Ehrlich et al.[68] investigated the effect of different substrate materials on the photo-deposition process. It is highly desirable, for deposition of metals and insulators onto integrated circuits, to use a process which is insensitive to local changes in substrate material. In laser thermal deposition the changes in the thermal conductivity or optical absorption cause linewidth variations. These authors[68] photodeposited a zinc line from dimethylzinc (DMZn) written across an aluminium metallisation pattern on a quartz substrate and obtained identical linewidths on each portion. Although sticking coefficients of zinc on the two materials are widely different this similarity is a consequence of the adsorbed layer effect. The DMZn adsorbs strongly onto the substrate and yields a dense coverage of zinc at the substrate on photodissociation.

Conformal deposition was demonstrated on stepped surfaces for feature heights smaller than the confocal parameter of the focussed laser beam, which for f/1 focussing of the 257nm beam is approximately six times the focal spot size. Hence height changes in the substrate of ~2 micron can be tolerated for writing lines of 0.3 micron linewidths.

Solanki et al.[54] demonstrated conformal step coverage of tungsten over a polysilicon step, with no visible evidence of cracking or thinning at the vertical walls. Deutsch[56] also demonstrated conformal coverage of this material over silicon dioxide steps on a silicon substrate although at the higher temperature of 285°C.

2.4.6 Gas Phase Collisional Processes

Radiative and collisional properties of the gas phase are important in controlling the flux of the atoms to the surface. The atomic species, once formed, can recombine by collisions with other photofragments, the parent gases or other species. This results in an increase in the loss rate of the atomic population in the cell, and also reduces the spatial extent of the atomic flux, and subsequently acts to localise the reaction on the substrate.

Ehrlich et al.[57] investigated the gas phase collisional processes by using a cadmium atom resonance lamp at 326.1nm. This was used as a Cd atom probe to measure the absorption at this wavelength of the photodissociatively produced Cd atoms, as a function of the 193nm intensity from an ArF pulsed laser. The cadmium atom density increased linearly and confirmed the single step photodissociation process.

Time dependent measurements showed that the ground state Cd atoms have an extremely long lifetime, of the order of seconds for the typical DMCd operating

pressures used. The lifetime is also heavily influenced by the gas purity, cell wall cleanliness and the buffer gas pressure.

Increasing length of exposure of the cell walls to DMCd results in a longer decay time being measured. Additionally a freshly deposited Cd film resulted in faster gas phase atom decay and this is consistent with the different sticking coefficients, being high on a cadmium surface and low on a DMCd passivated surface.

The effect of an argon buffer added to the gas mixture results in an increase in the diffusion time to the walls resulting in the domination by the gas phase reactions of the Cd decay prior to wall condensation.

2.4.7 Resolution

High resolutions are obtainable with photodeposited films, and although the dominant factor in determining the dimensions of a photodeposit is the size of the UV beam on the substrate surface it is not the only factor to influence available resolution.

Ehrlich et al.[68] deposited zinc lines of 0.7 micron width by scanning a 1 micron diameter 257nm focussed beam from an argon ion laser. The linewidth is less than that of the beam diameter due to the strong non linearities of the surface nucleation process hence confining growth to the most intense, central part of the beam. Buffer gases also increase the resolution by reducing the gas phase nucleation and confining growth to the illuminated region.

Ehrlich et al.[57] used CW and pulsed argon ion lasers to deposit cadmium with spot sizes as small as 3 microns by focussing the beam. These showed interference fringes of 0.2 micron width illustrating the resolution ultimately achievable. The spatial resolution was greater in the case of the CW laser although comparable resolutions were obtainable if the peak power of the pulsed laser was reduced to avoid pyrolysis.

Aylett and Haigh[52] attempted deposition of Sn from tetramethyltin at a wavelength of 193nm by using an ArF excimer laser. Definition was poor probably due to the greater absorbance in the gas phase. Good film definition was achieved using radiation at 249nm from a KrF excimer laser.

Higashi and Fleming[69] demonstrated excimer laser imaging onto substrates by using a masked patterning system and TMAl. Increasing the temperature had an adverse effect on the spatial resolution as it caused poor definition, presumably by increasing the

gas phase reactions. After further work [70], these authors reported that surface diffusion effects may be important and hence may also degrade the resolution.

2.4.8 Microstructure

Preliminary work by Ehrlich et al.[68] on the microstructure of deposited films of Cd and Zn by transmission electron microscopy (TEM) shows that the deposits are fine grained polycrystalline. The initial nucleation is very dense due to the low substrate temperatures and high vapour pressures which promote dense adsorbed layers.

The effect of varying the laser excitation source has also been investigated. Photodeposition of gallium by Rytz-Froidevaux[59] using a pulsed laser showed that the morphology was inferior to CW depositions with re-evaporation of the gallium occurring in the deposit centre, presumably because the high peak powers induced high temperature gradients at the substrate, resulting in the non uniformity. Defocussing the beam resulted in better uniformity with morphologies somewhat similar to the CW deposits. These features were determined to be polycrystalline with an average grain size of 0.13μm.

Solanki et al.[54] deposited chromium, molybdenum and tungsten from their parent carbonyls using focussed and defocussed conditions. Using a focussed beam a cluster of metal crystallites was formed onto the substrates of 0.25μm size whereas defocussing the beam resulted in threads of crystallites appearing nonuniformly on the substrate as a consequence of the low intensity.

Characterisation of photodeposited tin and platinum by Braichotte and van de Bergh[58] shows the structure to be amorphous. Low deposition temperatures and deposition onto amorphous substrates are probably primarily responsible for this.

Bouree and Flickstein[53] investigated the nucleation processes of aluminium by photodepositing onto silicon substrates using a low pressure mercury lamp and noted that at regions of low intensity the deposit was in the form of islands of 10 micron size distributed on the surface. The islands coalesced into a coherent film as the higher intensity region was approached.

Ripple structures have been observed by Brueck and Ehrlich[71] in photodeposited metal thin films, when the UV radiation has been polarised. This has been attributed to randomly scattered waves in the substrate plane, generated by coupling of the roughness of the depositing film with the electric field vector, resulting in a

periodic surface structure. Osgood and Gilgen[72] have reported that this effect has been utilised to grow high quality submicron gratings.

2.4.9 Resistivity

Resistivity measurements by Osgood and Gilgen[72] show that the resistivity is dependent on the precursor pressure used. For the DMCd system studied a minimum resistivity of 7 times the bulk values was obtained. At lower precursor pressures the resistivity increases and this may be explained by the rippled non uniform morphology of the deposit.

At higher precursor pressures, gas phase nucleation is dominant and this results in the deposit being of low density, and therefore of higher resistivity. Also it was found that the addition of a buffer gas improves the conductivity, as it increases the diffusion time of the molecules to the surface thus limiting the hydrocarbon impurities entrained in the film during the growth. A minimum value 4 times the bulk resistivity is achieved with the buffer gas.

The same sort of behaviour was exhibited with the deposition of indium from trimethylindium. However the high resistivities at high pressures were caused by the photolysis from a liquid-like adlayer, thus resulting in a high susceptibility to impurity incorporation.

The variation of the resistivity with the laser power has also been investigated and showed an exponential decrease with an increase in the intensity. This was attributed to more complete photodissociation of the reactant species and also possibly to the effect of substrate heating at the high intensity levels.

Resistivity values between 9μΩcm and 90μΩcm have been obtained for nickel deposits by Adams et al.[61]. The lowest resistivities were obtained with fine grained polycrystalline deposits and the higher resistivities with features of a large spherical nature. This latter microstructure was due to a change in the nucleation mechanism, with the pyrolytic component becoming the more dominant growth process. Again, a change in the microstructure of photodeposited tungsten from ß-phase to an alpha phase between 330°C and 440°C, and a consequent change in crystallite size from 5-10μm to 150-250μm, was thought to be the cause of the minimum resistivity of 17μΩcm (3 times the bulk) being obtained.

Higashi and Fleming[69] measured resistivities of aluminium films deposited at room temperature and achieved values of the order of 100Ωcm, about 30 million times the bulk resistivity of aluminium. However increasing the deposition temperature to 200°C resulted in lower resistivity films being obtained ~50 μΩcm.

This increase in conductivity may be due to (a) a decrease in the carbon contamination because of fewer methyl radicals or (b) the individual crystallites not being in contact with each other or (c) the oxidation of the crystallites. Further work by Blonder et al.[74] demonstrated line resistivities of aluminium interconnects a factor of ten times better at 5 μΩ-cm. However the deposits are extremely rough. The temperature used in this case was an increased one of 250°C using TIBA as the precursor. The mechanism was to induce prenucleation using a laser for the first few minutes or so of the growth run.

2.5 Transmission electron microscopy (TEM) assessment

2.5.1 Cadmium telluride (CdTe) on gallium arsenide (GaAs)

2.5.1.1 Orientation effects

Depositions of CdTe onto (100) GaAs have been shown by a variety of techniques to grow in either the (100) or (111) orientation.

Lu et al.[24] deposited CdTe onto (100) GaAs by a metal organic chemical vapour deposition (MOCVD) process and found that if the substrate was heat treated at 585°C in a stream of hydrogen the deposited layer grew with a (111) orientation, otherwise parallel epitaxy with growth in the (100) orientation was obtained.

Kolodziejski et al.[74] investigated growth of both (100) and (111) CdTe onto GaAs by MBE. They also found that (111) grown layers deposited when the oxide was removed and (100) orientation was achieved with the oxide present. Further investigations by the same authors[75] showed the (100) orientation could be obtained even with the substrate oxide removed. This was carried out by forming either a tellurium interfacial layer or a cadmium zinc telluride interfacial layer. The former technique is somewhat similar to that of Mar et al.[76]

Mar et al.[76] investigated the initial growth stages of CdTe onto thermally cleaned, oxide desorbed GaAs by using Auger and reflection high energy electron diffraction (RHEED) measurements, which indicated the influence of Te. They found exposing the substrate to a Te flux resulted in a monolayer or so being adsorbed onto the substrate even at the low growth temperature of 225°C, whereas a Cd flux resulted in no sticking unless Te atoms were present.

Growth from a congruently evaporating CdTe source led to the authors proposing a Stranski-Krastinov type of growth mechanism in which the first monolayer or two consist of Te deposited in a 2D layer-by-layer fashion followed by the nucleation and growth of 3D CdTe crystallites which subsequently coalesce giving rise to a (111) oriented film, whereas under similar conditions Kolodziejski grew a (100) film.

This anomaly may be related to the amount of Te adsorbed in the two cases and is consistent with the findings of Feldman et al.[77], who also investigated the influence of Te fluxes applied prior to growth, and noted that a flux of Te after desorbing resulted

in an interfacial layer of Ga-As-Te, which deviates from (100) symmetry, is deficient in Te, and will give rise to a (111) film. If this deficiency is relieved by greater exposure to Te prior to Cd adsorption the surface returns to (100) and results in (100) layer growth.

This result also agrees somewhat with the findings of Giess et al.[78] whose investigation of the orientation dependence of MOVPE grown CdTe films on GaAs showed that the orientation was dependent on both the growth conditions and the substrate treatment prior to growth. A (111) layer is obtained if a Cd-As-Te interfacial layer is formed by the adsorption of Te during a heat clean and the epitaxial layer has to be nucleated under Te rich conditions. (111) growth occurs above 400°C as Te rich conditions are expected due to the enhanced efficiency of DETe pyrolysis.

2.5.1.2 Transmission electron microscopy (TEM)

2.5.1.2.1 (100) orientation

Lu et al.[24] showed by TEM cross-sectional characterisation that in the case of the (100) layer a highly dislocated interfacial region beyond 0.1μm of the interface is observed. Many of the dislocations do not propagate beyond this thickness, although those that do generally extend through the entire layer. This type of structure is attributable to the large lattice mismatch. Bicknell et al.[79] characterised (100) GaAs by TEM of chemically stripped films at controlled depths of the MBE deposited layers and also showed a highly complex dislocation structure at the interface region, which decreased towards the surface of the layer. These authors also detected stacking faults throughout the entire layer, which were attributed to the impurities present on the GaAs surface prior to growth. The authors found that the surface preparation could control the dislocation densities observed and obtained better crystallinity with non contact polishing.

Kolodziejski[74] showed that the (100) layers which nucleated by forming either an initial layer of CdZnTe or a monolayer or less of Te onto the GaAs exhibit an array of misfit dislocations of the pure edge type at the interface, with a Burgers vector of a/2[110]. These further generate threading dislocations which propagate perpendicular to the interface. At the interface they have a large density of 10^{12}-10^{11}cm^{-2} and reduce to 10^{6}-10^{5}cm^{-2} at 4μm from the interface.

High resolution transmission electron microscopy (HRTEM) performed on cadmium manganese-cadmium telluride superlattices deposited on GaAs by Kolodziejski[75] showed no misfit dislocations at the interface between the CdTe and the

GaAs substrate. If the deposited layer is sufficiently thin it is more energetically favourable for it to become strained, and dislocations are only introduced into the layer if a certain critical thickness is exceeded.

Cullis et al.[80] have characterised MOVPE grown CdTe on GaAs (100) and also show that there is a high density of dislocations at the interface, falling off as the surface is approached. High resolution lattice imaging of the interface region shows many inclined microtwin lamellae originating from the interface, and an array of misfit dislocations at the interface itself, with Burgers vector of a/2[110] which is consistent with them being undissociated 60° type dislocations. They occur with a separation of 28Å which is in good agreement with that predicted from the lattice mismatch. However this latter observation is contradictory with the high density of dislocations observed under conventional dark field imaging at the interface, as any mismatch strain should be effectively taken up by the misfit dislocations. One explanation may be that the constant density of the misfits occurs only over the very limited region being observed in HRTEM.

An alternative explanation is supplied by Petruzzullo et al.[81] who made a study of the dislocation structure as a function of the layer thickness of CdTe grown by MOVPE onto GaAs, and suggested that there are two distinct regions of dislocation formation. In the early stages of growth an array of misfit dislocations of constant density is formed but does not completely relieve the mismatch strain, and therefore for thin layers (< 0.1μm) the layers are elastically strained. Evidence of strain still being present was given by photoluminescence measurements. If the growth is continued dislocations are created from surface sources and migrate towards the interface, under the influence of the remaining strain, along (111) planes, and form above the interface, thus relieving strain in the layer. After growth of about 1μm the layer is completely relaxed and few dislocations are seen above this thickness.

Kolodziejski[75] has reported that HRTEM also shows that the oxide is present at the GaAs surface in cases where it has not been desorbed, and is seen as a 15Å interfacial layer. In the desorbed case an extremely thin interfacial layer is observed and may indicate the presence of Te.

2.5.1.2.2 (111) Orientation

Generally the dislocation structure differs from that of the (100) orientation in that twinning parallel to the CdTe-GaAs interface is observed. Lu et al.[24] showed that

the dislocation structure of the (111) layer consists of a high density of twin plates, which decreases towards the film surface.

Cross sectional TEM carried out by Brown et al.[82] shows lamellae twins in (111) CdTe deposited on (100) GaAs substrates and also on (i11) CdTe substrates. The authors concluded that the twinning is a phenomenon of the growth of CdTe on a (111) plane rather than being due to the accommodation of mismatch or to a nucleation process occurring at the interface.

Kolodziejski[74] showed by high resolution microscopy that in the [112] projection of the CdTe layer there are no misfit dislocations visible. Observing in conventional dark field imaging however a high density of threading dislocations is seen to have formed and propagated towards the free surface. Cheung and Magee[83] deposited CdTe of a (111) orientation onto (100) GaAs by using a laser assisted deposition process (LADA) and TEM performed by low angle depth sectioning also showed that complex nesting and high dislocation densities were observed close to the interface but decreased rapidly at >2.3μm from the interface.

Cullis et al.[84] observed plan view specimens of (111) MOVPE grown layers and showed that growth had occurred by the nucleation of growth islands of different orientations. These authors observed islands of 20nm diameter and ~15 nm thickness of (100) and (111) orientations joined at triple boundaries.

2.5.2 CMT on GaAs

Cullis et al.[80] carried out high resolution lattice imaging of CMT and showed this was somewhat similar to the CdTe with an array of closely spaced misfit dislocations. However conventional dark field imaging shows a densely packed band of defects extending approximately 250nm into the ternary alloy beyond the interface. At the upper surface of the band a raft of dislocations, cavities and misoriented material is present.

Buffering the GaAs substrates with the CdTe prior to growth of the CMT gives a much improved microstructure, as has been shown by Cullis et al.[83]. However the CMT layer buffered with CdTe on a GaAs substrate shows triangular amorphous features at the II-VI side of the interface which may be related to the diffusion of mercury.

2.5.3 CdTe on InSb

TEM characterisation of CdTe grown onto InSb by MBE has also been reported. Cullis et al.[80] observed few defects and a clean layer under diffraction contrast. In fact the only visible feature is a line of dark contrast at the interface, due to either residual impurity strain or a local change in atomic bonding causing a lattice relaxation. Growth onto a contaminated substrate resulted in the impurities giving rise to dislocations and microtwinning. Wood et al.[85] demonstrated near perfect epitaxial CdTe films on InSb but also found the quality to be critically dependent on the substrate cleaning. Poor cleaning resulted in irregularities at the substrate surface and was shown to lead to the nucleation of microtwins at the interface as did precipitation of indium from the heat treatment.

Chapter 3: Equipment

3.1 Introduction

A Metal Organic Chemical Vapour Deposition (MOCVD) system was constructed, principally to investigate the low temperature deposition of cadmium onto semiconductor substrates by a UV assisted process.

The system must be capable of handling toxic and reactive gases, provide controlled and monitored flows of reactants into the reactor, and be able to dispose of waste products and unreacted gases in a safe and efficient manner. As deposition was to be effected either photolytically using a UV radiation source, or thermally, the reactor was to be transparent to the UV illumination and also capable of being heated if required to ~500°C.

An inert carrier gas is introduced into the system from whence it passes through a bubbler containing the reactants usually in liquid form. The carrier gas is then saturated with the reactants, and the vapour is subsequently directed into the reactor, where it is passed over a substrate. Here the reactants are dissociated by pyrolysis or photolysis and the required material is deposited on the substrate surface. A prime consideration in the design of this type of system is that of safety.

3.2.1 Safety considerations

The importance of safety precautions is due mainly to hazards presented by two different sources. Firstly the reactants being used are by nature toxic, corrosive and potentially pyrophoric. This necessitates a system which is leak tight, has efficient removal of waste gases and unused reactants, and is constructed as far as possible of rugged, highly corrosion resistant materials such as stainless steel, Viton rubber and silica.

The second major source of danger is the high pressure mercury arc lamp, which is the source of the ultraviolet radiation for the photo-assisted growth processes. The main hazard in this case is physical exposure of skin tissues and eyes to the radiation. Also ozone is generated by the arc lamp and must be removed.

3.2.2 Implementation

The problem of removing any toxic gases created as a by-product of the reactions and by the arc lamp has been overcome by installing the MOCVD equipment

and the arc lamp in a high flow rate fume cupboard.

To prevent exposure to the ultra violet radiation the fume cupboard sash was completely blanked off and a microswitch fitted, rendering the arc lamp inoperative if the fume cupboard sash were to be left open or if only partially closed. Any experiments to be performed with the sash open e.g. checking of the lamp focus etc., were carried out wearing full protective clothing comprising goggles, ultraviolet face shield and rubber gloves so that no part of the body remained uncovered and with the micro-switch over-ridden.

Controlling and monitoring of the system, whilst the arc lamp is operating is therefore only possible outside the fume cupboard. Hence all power supplies, gas switching, temperature control and monitoring had to be remotely operated.

The MOCVD equipment can be split into three main categories, namely the evacuating or pumping system, the electronic control console and the gas flow system.

3.3.1 Gas flow system

The flow system was constructed as far as possible out of stainless steel, PTFE or silica. All pipework was 316 stainless steel and of 1/4" gauge.

The 1/4" tubing was fitted together using a compression coupling system. Swagelock fittings were chosen and used throughout the system due to their ease of assembly, reliable leak tightness and all stainless steel construction. These consist of front and rear ferrules which are placed over the 1/4" tube. When inserted into the Swagelock body and tightened with the back nut they form a leak tight seal by pinching and deforming the tubing. All components of the Swagelock fittings, i.e the ferrules, body, nuts etc are manufactured from 316 stainless steel. The various swagelock components used were unions, weld connections, reducers etc.

A schematic diagram of the flow system is shown in figure 3.1, with the main components of the system indicated.

3.3.2 Valves

All on/off type valves on the MOCVD system are of the bellows seal type. These are so engineered as to prevent any leaks along the valve stem, as the bellows provides a metal barrier between the system and atmosphere. This results in far greater reliability than conventional sliding stem seals of ordinary packed valves.

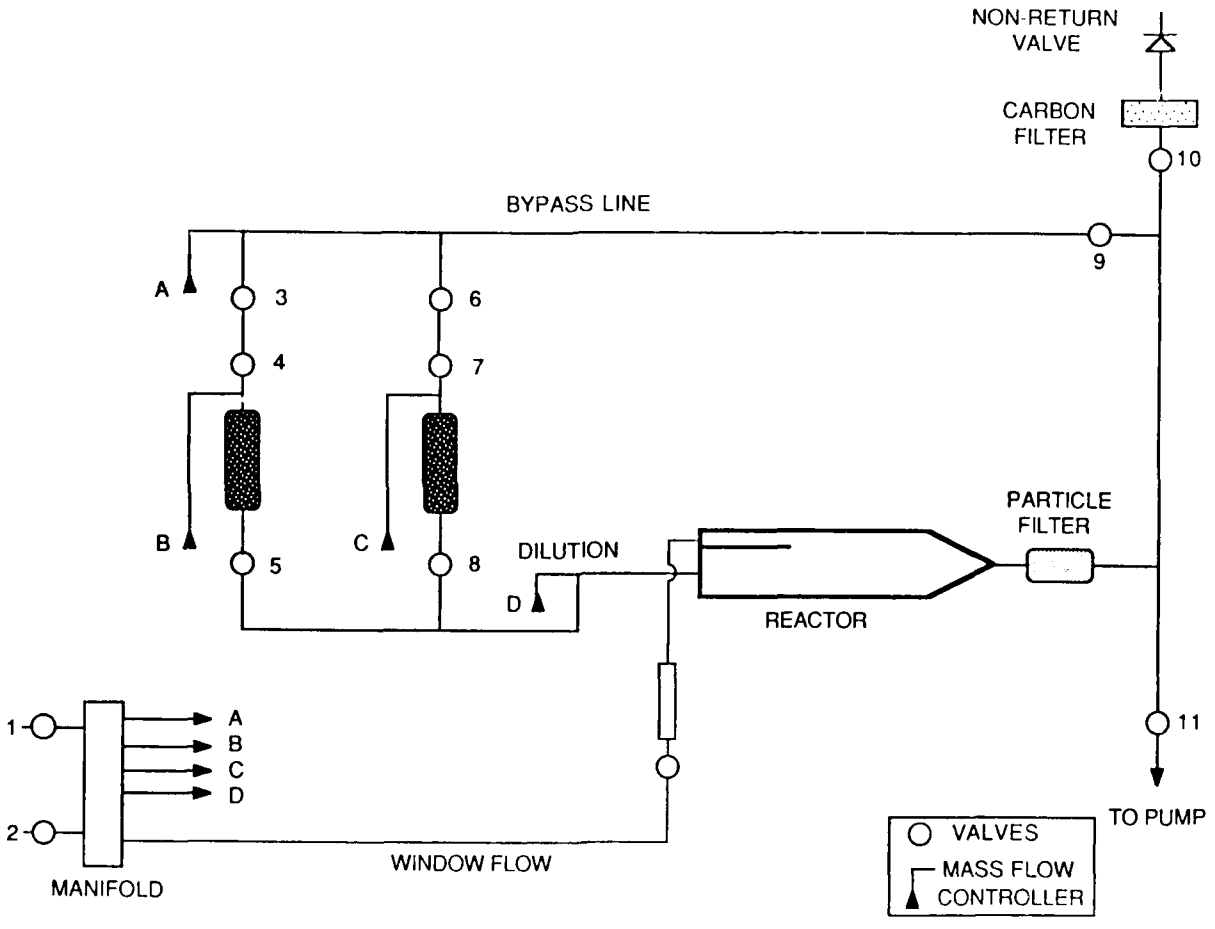

FIG. 3.1. SCHEMATIC DIAGRAM OF FLOW SYSTEM.

The valves purchased were Nupro SS-4BK-1C and -10, which are the normally open and normally closed variants of the same valve. These valves are pneumatically operated, as remote actuation is required when the system is operating with the ultraviolet radiation on. Pneumatic control is to be preferred to electrically activated valves as it does not pose a safety hazard due to coil shorts, chatter noise and seat leakage etc.

The normally closed models require compressed gas to open the valve and close automatically by means of a spring upon loss of air pressure. The reverse is true for the normally open models. A pressure of between 50-100 p.s.i. is required for their operation, and is provided via a gas regulator on a nitrogen cylinder.

Internally the valves are constructed from stainless steel, including the flexible bellows and the valve stem. The valve stem has a replaceable soft tip manufactured from KEL-F, a highly inert plastic, to form a reliable seal against the valve body under conditions of repeated cycling.

In all there are eleven pneumatic valves used throughout the system. Seven of these are of the normally closed type and the remaining four are normally open. Figure 3.1 shows a schematic diagram of the valve set-up for the flow system.

The carrier gas enters through either valve 1 or 2 depending on which carrier gas is desired. These valves are normally closed. After passing through the inlet valves, the gas passes into the manifold, from where the gas is distributed to the mass flow controller inlets, and to the manual valve for the window flow. The dual channel mass flow controller outlet flows are indicated by the arrows at A, B, C, and D. A and B are supplied from mass flow controller 1, and C and D from mass flow controller 2.

The flows from B and C, namely the bubbler flows pass through normally open valves 3 and 6 and into the bypass line in the "fail safe condition". Here these flows are mixed with flow A, the bypass flow, from mass flow controller 1 which keeps this line purged at all times. The combined gas flow then passes out through normally open valves 9 and 10, and out to exhaust.

Alternatively, valves 3 and 6 can be closed and the bubbler flows, B and C, are thus diverted into the bubbler lines by opening the normally closed bubbler inlet valves 4 and 7, and the normally closed bubbler outlet valves 5 and 8. The bubbler flows are then mixed with the dilution flow D before entry into the reactor. The waste products flow

out to exhaust through valve 10, a normally open valve, after passing through a particle filter to remove condensed reaction products such as cadmium, and an activated carbon filter to remove unreacted alkyls (see section 3.3.9).

Valve 11, a normally closed valve, separates the system from the evacuating system. To perfom an evacuation procedure valve 11 is opened and the exhaust valve 10 is closed. In fact these two valves have been electronically interlocked, to prevent valve 10 from being left open whilst pumping down, in order to protect the evacuating system and avoid air contamination of gas lines. Before evacuation, the bubblers must be isolated by closing pneumatic valves 4,5,7 and 8; and closing the manual bellows valves on the bubblers.

3.3.3 Manifold

The manifold is essentially a gas reservoir which feeds the mass flow controllers. It acts as a distribution point to the various flow controlling devices and enables gas pressure equalisation at the inlets to the mass flow controllers.

The manifold consists of a 1" diameter stainless steel tube of 10" length. Each end has been blanked off by welding a machined cap to it. A series of holes, two for the inlet gases and five for the feeds to the flow devices, were drilled, after which Swagelock weld fittings were attached. There are two gas input lines as it was proposed to use either a helium or a nitrogen carrier gas.

3.3.4 Flow controllers

Five separate flows of gases require to be controlled. These are the dilution flow, the bubbler flows, the bypass flow and the window flow. All these flows with the exception of the window were controlled by electronic mass flow controllers. The window flow was controlled by a manual needle valve as it was not crucial to control this flow as accurately as the others.

Two mass flow controllers are employed. Each is a Precision Flow Devices Inc. PFD 112 dual channel controller. Three of the total of four channels have a range of up to 200 sccm. These are the lines for the reactants and the bypass. The dilution flow line has a maximum range of 3 slm.

The mass flow controllers have an integral valve on each channel which is able to servo thus enabling the flow rate to be controlled. The input signal to the servo valve

is provided by the error signal from the mass flow controller sensor, which operates on the thermal transfer principle.

The sensor consists of a thin walled tube onto which are wound two resistance sensing coils, which can give a measure of temperature, and also a heating coil. As the gas stream passes through the sensor tube, the gas is warmed by the heating coil, and the temperature difference between the two resistance coils is measured as a voltage. This voltage difference is directly related to the thermal properties of the gas and the mass flow rate, according to the equation :-

$$V_{diff} = K C_p v$$

where V_{diff} is the differential voltage, K is the instrument constant, C_p is the specific heat capacity of the gas and v is the flow rate.

The differential voltage, V_{diff}, is processed electronically and then compared with the program voltage as set by the operator. The difference between the two is used to position the servo valve precisely thus achieving the desired flow rate.

The window flow was monitored using a flow tube. A Brooks Instruments 1355 Sho-Rate 150 purgemeter, with a maximum flow range of up to 6 litres/min nitrogen is fitted to the system. The flow tube is a tapered glass tube with a stainless steel ball as the float indicator.

A Nupro manual bellows valve is used to control the flow through the flow tube, and is connected prior to the inlet to the tube. The tube must be mounted vertically for correct operation and has been mounted together with the manual valve onto a metal plate which is attached to the framework of the system.

3.3.5 Bubbler

The reactant, in liquid form, is contained in a stainless steel bubbler arrangement which is supplied complete with manual valves on the inlet and outlet arms. Figure 3.2 shows a schematic diagram of the bubbler cross-section. The inlet arm extends to the diptube which reaches the bottom of the bubbler container. This is to ensure maximum saturation of the incoming carrier gas with the reactant contained in the bubbler. The internal walls and the diptube are coated with ptfe to prevent contamination of the reactants from the stainless steel container.

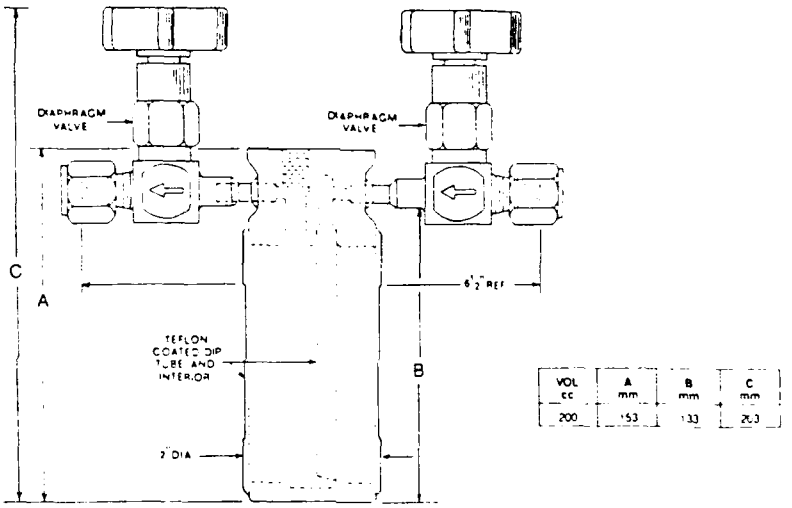

FIG. 3.2. DIMETHYL CADMIUM BUBBLER (AFTER REF. (86)).

Assuming low flow rates through the bubbler and a long bubble path through the liquid reactant, i.e. relatively large "bubble" residence times in the reactant fluid, we can assume complete saturation of the incoming carrier gas with the reactant. If the reactant saturated vapour pressure is p atmospheres, then for each 1cc of carrier gas at 1 atm. entering the bubbler (1+p) cc will emerge at the same pressure. Each 1 cc of this emerging gas will thus contain p/(1+p) cc of the reactant vapour. Hence the partial pressure of the vapour in this stream is p/(1+p) atmospheres. This is the maximum partial pressure obtainable at any given temperature. Due to the strong temperature dependence of the metalorganics, increased partial pressures of the reactants can be obtained by heating the bubbler; the saturated vapour pressure follows the Arrhenius relation, log p = A-B/T, where A and B are constants and T the temperature. Saturated vapour pressures for dimethylcadmium over the temperature range 0 to 45°C are plotted in figure 3.3.

A reduction in partial pressures of the reactants in the reactor can be achieved using the dilution flow, which can be mixed with the flow emerging from the bubbler prior to its entry into the reactor.

If the rate of the emerging flow from the bubbler is x cc/min, and the rate of the dilution flow it is mixed with is y cc/min, then the final reactant partial pressure is xp/[(x+y)(1+p)] atmospheres. Hence accurate control of the concentrations of the reactants into the reactor is possible.

3.3.6 Reactor

The reactor is the vessel in which the reactions and subsequent depositions occur. The design criteria for the reactor are that it should be capable of withstanding high temperatures, it should be transparent to the ultraviolet radiation in the frequency range of interest, 200-300nm, and should be capable of providing a reasonably laminar flow of reactant species over the substrates.

A relatively simple design was decided upon due to considerations of economy and ease of replacement and modification at a later stage. Figure 3.4 shows the reactor.The reactor consists of a vitreosil silica quartz open furnace tube of 50mm outside diameter with a 2.5mm wall thickness. This is transparent to ultraviolet radiation of wavelengths between 200 nm and 400 nm as shown in the transmission curve of figure 3.5.

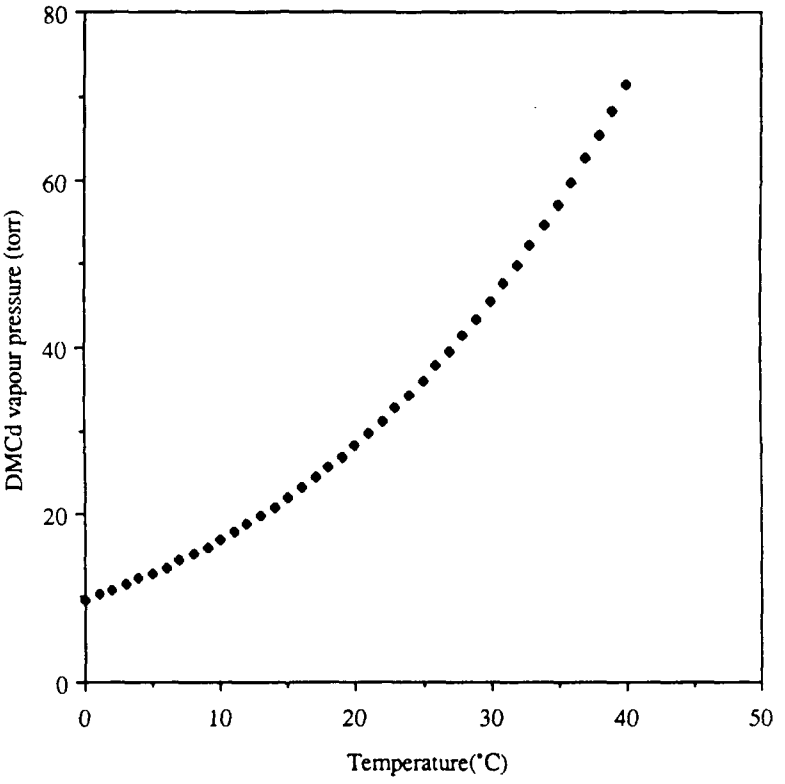

FIG. 3.3. VARIATION OF DIMETHYLCADMIUM SATURATED VAPOUR PRESSURE AS A FUNCTION OF TEMPERATURE.

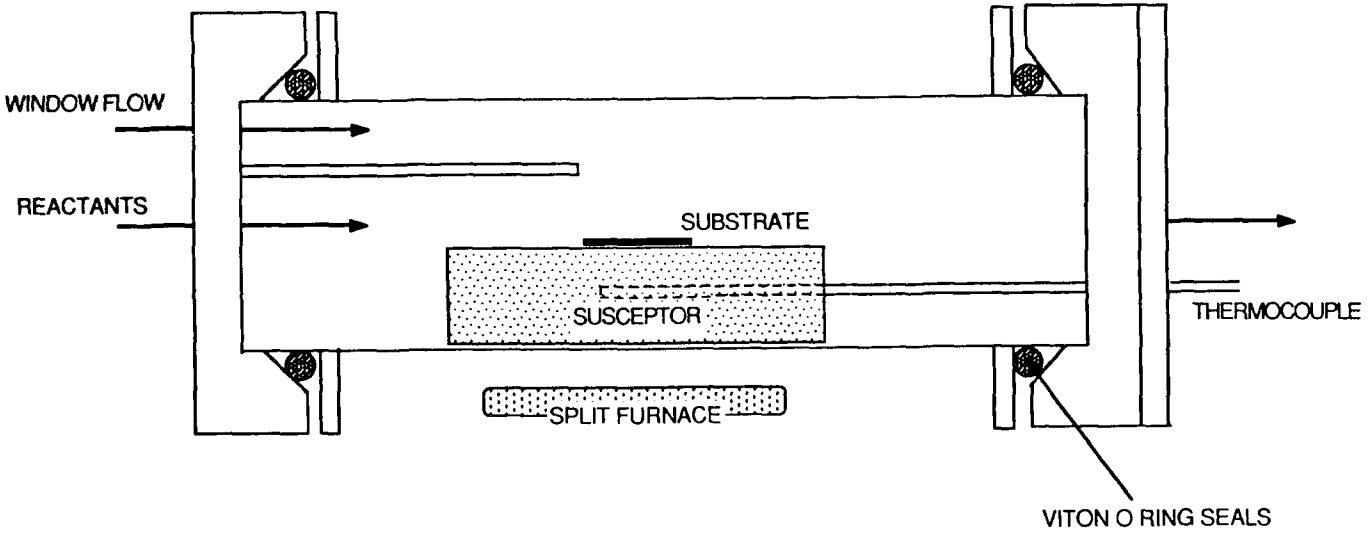

FIG. 3.4. REACTOR DESIGN.

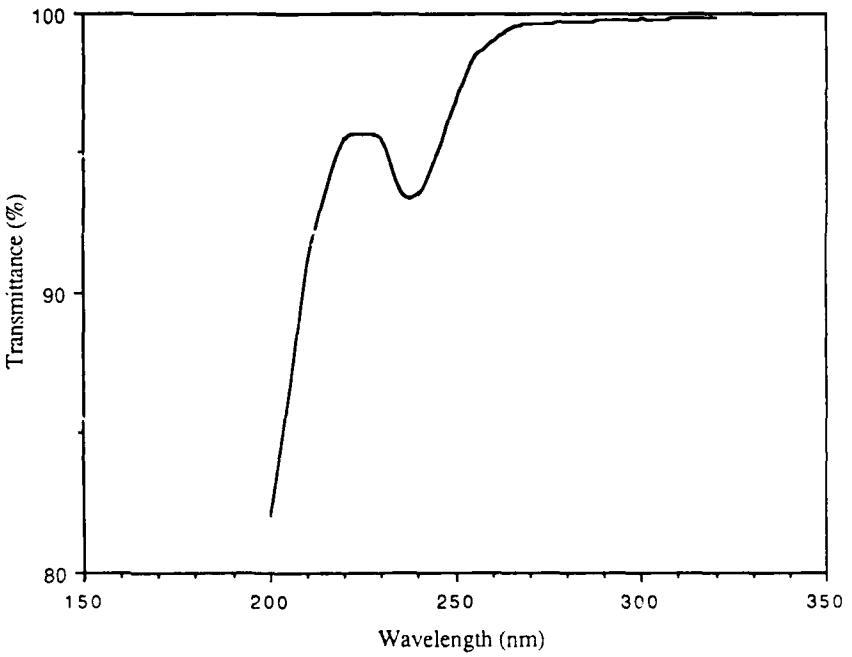

FIG. 3.5. UV TRANSMITTANCE CURVE FOR VITREOSIL WITH A 2.5mm PATH LENGTH[87].

The reactor is attached to the rest of the system by specially machined stainless steel inlet and outlet end ports. These ports are sealed to the reactor tube using "O" ring seals. The "O" ring seals are of Viton rubber which is more chemically resistant than normal neoprene type.

The inlet port has two gas input lines. These are the mixed gas flow line and the window flow line. These are introduced above and below the flow separator plate respectively. This flow separator plate is welded onto the inlet port to prevent any mixing of the gases entering the reactor from the two gas input lines and extends four inches into the reactor tube. The window flow is introduced over the top of the reactor tube in order to keep the top section of the tube clear of any deposits which are likely to form and which would otherwise cause attenuation of the incident ultraviolet radiation passing through the top of the reactor.

Below the reactant flow inlet, a stainless steel sheathed chromel-alumel thermocouple enters the reactor through a bored 1/8" diameter Swagelock connector and is inserted into the graphite substrate holder. to measure the substrate temperature.

The outlet port of the reactor has a flat end cap which can be unbolted from the body of the port to allow access into the reactor tube for insertion and removal of the substrate samples. The gas flow out of the reactor is via a Swagelock weld connection at the side of the output port body.

3.3.7 Susceptor

The susceptor is essentially a thermal mass which provides mechanical support for the substrates. As the susceptor must be capable of the transfer of heat energy to the substrate, it must have a high thermal conductivity, and be able to withstand high temperatures. Also the susceptor material should be inert.

The susceptor was machined from a block of high density graphite, and shaped to fit into the reactor tube. A 1/8" hole was drilled into the susceptor, into which the thermocouple extending from the reactor input port fits.

The substrates are normally placed close to the leading edge of the susceptor, and the susceptor edge is placed at the end of the flow separator plate. This minimises any turbulence effects and composition changes over the substrates caused by mixing between the reactant and window flows.

The distance between the susceptor and window flow is crucial, as this determines the attenuation of the ultraviolet radiation and hence the amount of radiation reaching the substrates.

3.3.8 Substrate heater

The sample substrates can be heated to temperatures of ~600 °C, using an electrical resistance split furnace. This is essentially a ceramic unit with a 350 watt coil wound internally. As the furnace is split and has a semi-circular cross section it fits below the susceptor, external to the reactor tube. The furnace is mounted on a heat resistant plate, and when in position below the susceptor provides uniform heating to the susceptor without obscuring the top illuminating ultraviolet radiation.

A second, similar furnace is available, and is used in conjunction with the susceptor heating furnace to bake out the reactor. These furnaces are controlled from the central electronics console via a Eurotherm 810 microprocessor based temperature controller.

3.3.9 Filters

A stainless steel mesh large area particle filter is placed immediately after the reactor. Its purpose is to prevent dust from being swept downstream into the exhaust system. Such particulates could damage the valve seats on the pneumatic valves thus preventing them from sealing. The filter consists of a Balston SMC-100-12 reusable stainless steel mesh filter cartridge and it has a 3 micron size filtration rating. The cartridge is cylindrical in shape with a length of 64 mm and a diameter of 38 mm.

An housing has been constructed for the filter cartridge out of stainless steel. The incoming unfiltered gases enter via a stainless steel Swagelock weld connector which directs the flow into the internal part of the cartridge. The filtered gases then flow out via the exit Swagelock. Flat Viton seals at either edge of the cartridge ensure all incoming gas is filtered. A stainless steel end plate has been machined to enclose the cartridge within the housing. This seals onto the housing by means of an "O" ring. The end plate is secured onto the housing by using bolts, which may be rei ved for easy removal of the cartridge for cleaning purposes.

A large area carbon filter supplied by Emcel is fitted to the exhaust line to prevent any toxic gases being exhausted into the fume cupboard. The carbon is in granular form for maximum absorption properties and is supplied in an integral housing. with 1/4" input and output tubing and is thus simply swaged into the exit of the exhaust

line. The unit is fully disposable and has a limited lifetime dependent upon its usage.

3.3.10 Exhaust valve

A non-return exhaust valve is fitted at the very end of the exhaust line after the carbon filter unit. This is a one way relief valve whose function is to prevent back flow of air into the system, when an evacuation procedure has been performed, but to permit flow of gas throughout the system out to atmosphere if necessary.

The valve consists of a poppet which resists the incoming flow through a spring pressing against one end of the valve body. The spring tension is such that it will crack at a preset pressure of 1/3 psi, i.e. when a pressure differential of this value appears between the valve inlet and outlet, gas will be able to flow out of the system. A soft "O" ring on the poppet performs the sealing against the main body of the valve when flows along the opposite direction are present.

The materials used in the valve construction are 316 and 306 stainless steel for the valve body and the cracking spring respectively and Viton for the "O" ring seal.

3.3.11 Solenoid valves

The pneumatically operated valves are switched via a bank of minaturised solenoid valves. These solenoid valves, when actuated, direct the gas pressure into the selected pneumatic valve through plastic tubing. Thus, there is a separate solenoid valve corresponding to each pneumatic valve.

The array of seven solenoid valves is mounted onto a sub-base assembly to which the gas pressure is applied. The gas is also discharged through this assembly when any of the valves is deactivated.

The solenoids operate on application of a d.c voltage of 24 volts which is provided by the central electronic console. All switching and monitoring for these valves is performed on the console. Solenoid valves were chosen for their compactness, low electrical power consumption and their durability and long life at high cycling rates. The valves chosen were the Microsol Pilot valves. These valves consist of a solenoid and a rigidly fastened body. The solenoid includes a coil and its magnetic circuit which is encapsulated wihin synthetic material. There is a magnetic core which acts as a plunger and locates into the valve body via a return spring when the solenoid valve is de-energised. When energised the plunger is drawn by the solenoid admitting air into the

outlet line and hence to the pneumatic valves.

3.3.12 Molecular sieve

A molecular sieve is used as the drying agent for the carrier gases and is contained within a drying tower.

The molecular sieve used is Fisons 4A grade "Davison" type. This is in the form of crystalline sodium alumina silicates, of 4 Ångstrom pore size, and is particularly suited for absorbing water and other polar molecules. Carbon dioxide and oxygen are also absorbed by the 4A grade sieve.

The drying column is constructed from a brass tube of length 3/4 m and a diameter of 4cm. The longest practical length possible was used to provide the gas flow with the maximum path length through the drying agent for maximum drying efficiency. End caps with a fine mesh to prevent the molecular sieve from being blown into the system were soldered onto the brass tube. The end caps have copper tubing inserted and sealed into them to provide the inlet and outlet flows to and from the sieve.

Periodically the molecular sieve is re-activated to drive off the adsorbed molecules. This is performed by means of a heating tape wound onto the full length of the drying tower with a thermocouple/temperature controller monitoring the sieve temperature. There is a valve connected to the evacuating system, which when open allows the sieve to be pumped whilst it is being baked out.

The carrier gases supplied to the drying tower are either white spot nitrogen or high purity helium. These are contained in standard gas cylinders with pressure regulators distributing the gas directly into the molecular sieve. The outlet from the tower is connected to the MOCVD inlet valves

3.4 Pumping system

The pumping system consists of a diffusion pump and rotary pump arrangement which is capable of evacuating the entire flow system to a base pressure of less than 10^{-6} torr. An efficient pumping system is of the utmost importance as the quality of the depositions is heavily influenced by the level of contamination present within the system. Thus prior to any experimental work the complete system is evacuated thoroughly after which an inert gas is introduced without the system being subjected to the surrounding atmosphere. A secondary function of the pumping system is to enable leak detection of the entire system, the better the vacuum obtainable the better the leak detection limit.

An Edwards direct drive, dual stage rotary pump was chosen as the backing for the diffusion pump for reasons of reliability and of achieving fast pumpdown speeds. The diffusion pump is an Edwards $1^1/2$ inch with an integral baffle valve. The pumping system was deliberately kept as close as possible to the reactor to ensure that any pressure differential effects were minimal. This was expected to be a problem due to the long and complex flow paths in the MOCVD system, and also because of the narrow bore tubing utilised throughout the system.

The vacuum is measured in two stages, from atmosphere down to $\sim 10^{-2}$ using a Pirani gauge, which is located at the rotary pump, and from 10^{-2} torr to $\sim 10^{-7}$ torr using a Penning located at a diffusion pump port. Ideally the vacuum sensing should be performed at the reactor but this is impractical becase of the corrosive environment within the reactor and also from a construction point of view.

3.5.1 Electronic control console

All procedures required to operate the MOCVD system are performed remotely outside the fume cupboard at the central electronics control console.

The front panel of the control box has a schematic flow diagram of the MOCVD system similar to the diagram of figure 3.1 etched on it. Each pneumatic valve is represented by a light emitting diode which indicates the current status of the valve, and hence the consequent flow direction through the MOCVD system. The desired valve position can be selected at the control panel.

The control box houses the power supplies for this mimic display and also for the operation of the pneumatic valves. Mounted on the control panel adjacent to the valve status indicators are the pneumatic valve selector switches.

Also constructed within this box are the power supplies and monitoring equipment for the mass flow controllers, the split furnace heating unit and the panel mounted susceptor temperature controller. A digital temperature indicator, monitoring the bubbler temperature, is also powered from this control box.

A block diagram of the power supply circuitry and of the ancillary circuitry is shown in figure 3.6. Mains power supply of 240 volts a.c, 50 Hz, is converted to a d.c voltage of 24v at point 2, by a network consisting of a toroidal step down transformer, feeding a Wheatstone bridge circuit and a dual capacitor circuit. Thus at point 2 voltages of +24v and -24v are available. From here four voltage regulator networks are fed to obtain regulated voltages of values +15v, +7.5v, +5v and -15v d.c. The regulators are integrated circuits which with their ancillary circuitry provide the constant output voltages required regardless of any small fluctuations at the regulator inputs. A positive voltage is applied to the 7815, 78HG and the T03 regulators, whilst the negative ouput potential from the capacitors is applied to the 7915 regulator. The former three regulators provide the outputs of +15v, +7.5v and +5v respectively whist the latter gives -15v.

3.5.2 Mass flow controller circuitry

The +15v, -15v and the 7.5v regulated supplies are fed directly to the mass flow controllers. The +15v and -15v are also fed into the valve override system. Here the selection of the negative or positive value of the voltage causes the mass flow controller valves either to open fully or to close bubble tight. With a floating voltage the mass flow controller performs in its normal feedback controlled mode. Selection of the override system is achieved through four three way switches with each switch

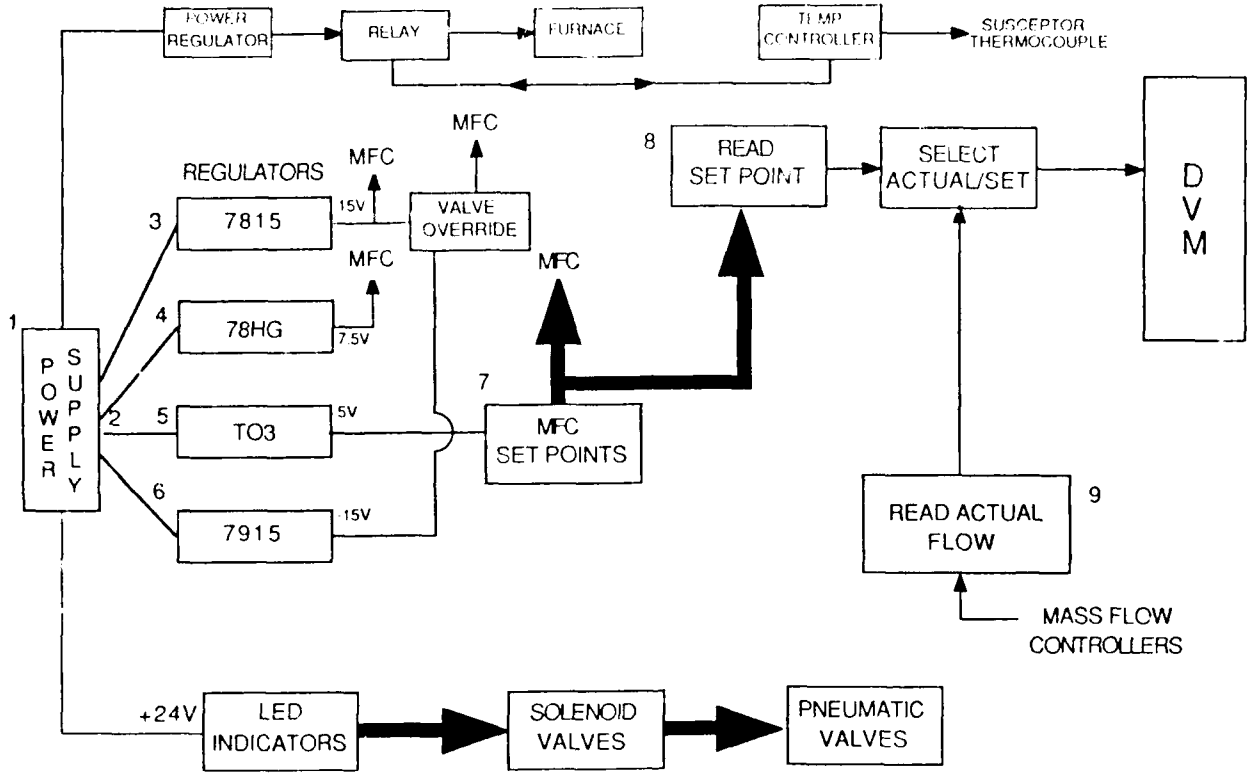

FIG. 3.6 BLOCK DIAGRAM OF MOCVD POWER SUPPLY CIRCUITRY.

controlling one channel of the mass flow controller independently.

The +5v supply from regulator T03 is fed into the mass flow controller set point system as signified by block 7. This is simply a variable resistor network which outputs the required value of voltage selected for each channel of the mass flow controllers. The voltage selection is achieved from multi turn dialing knobs, which record the position of the potentiometers. Each mass flow controller channel is controlled separately by its own dial/potentiometer combination. The set voltage output from unit 7 is then applied to the mass flow controller feedback control circuitry and also to unit 8, where a 4 way rotary switch selects a particular channel. The set value of the selected mass flow controller channel can then be displayed on the digital voltage meter by selecting the read set point mode at unit 9 which is a 4 pole two way switch. Alternatively the volt meter will indicate the actual flows through the mass flow controller channels with the display switch at its second position of read set point. The signal of the actual flow is output from the mass flow controllers and the particular channel to be monitored can be selected using a 4 way rotary selector switch at unit 9 similarly to the read point selection procedure.

3.5.3 Digital temperature monitor

A second tapping is taken off the 78HG 7.5v regulator, and this is required to power the digital temperature indicator. This indicator senses the temperature of the reactant bubbler with a chromel-alumel thermocouple.

3.5.4 PID Temperature controller

The temperature controller for the split furnace is also powered from the mains input as is the furnace power regulator. This is a solid state phase controlled regulator with an external potentiometer to control the input power to the split furnace. There is a solid state relay between the regulator and the furnace which is switched by the three term temperature controller. The relay is protected from electrical spiking by a capacitive filter.

The temperature controller can be programmed to suit the desired function and is connected to the temperature sensing chromel-alumel thermocouple using temperature compensating cable. The controller gives a direct readout of the susceptor temperature and also whether it is swiching the relay on a heating or cooling cycle.

A +24v tapping is taken directly off the power supply capacitor. This is fed to the 4 pole double throw swiches on the front fascia panel. The switches if selected distribute the voltage to the solenoid valves and consequently operate the pneumatic

valves. The valve status light emitting diodes are also powered from the 4-pole switches, and indicate by turning green or red depending on the pneumatic valve position. The

indication corresponds to the switch position which biases the light emitting diode circuit either positively or negatively.

3.6 Ultraviolet lamp

The ultraviolet lamp is a 1 kW mercury/xenon high pressure arc lamp. The lamp has two closely spaced electrodes between which an arc is struck. These electrodes are surrounded by a mercury/xenon vapour mixture at high pressures (under operating conditions) contained within a quartz envelope. An arc between the two electrodes is set up by applying a high voltage to ionise the gas and create a conduction path through it. The resulting output spectrum consists of a series of pressure broadened mercury lines in the ultraviolet and visible from 240 -700nm, followed by a continuum in the infrared to 2500nm. The mercury lines can be seen in the spectrum of figure 3.7.

The lamp is mounted in a universal lamp housing. This has a 3" f/0.7 UV grade fused silica lens which is able to focus the beam as desired. A spherical reflector in the housing receives the radiation from the rear of the lamp and this increases the output power by thirty percent.

The radiation exits the lens housing as a horizontal beam and therefore to achieve the vertical illumination necessary for the reactor design a polished aluminium reflector is needed to divert the beam onto the substrate. Mounted in the side of the housing is a fan which provides forced air cooling for the lamp.

The lamp power supply outputs a high start up voltage to the lamp, and then maintains the established arc at a reduced voltage. A safety interlock cuts off the power supply to the lamp if the fume cupboard sash is opened.

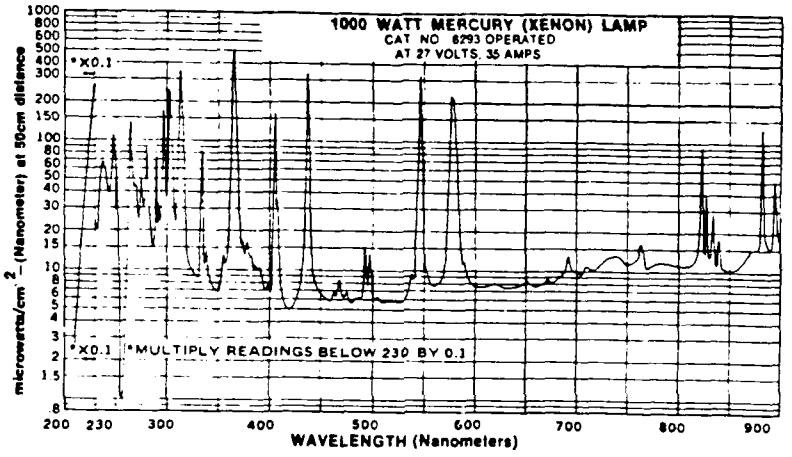

FIG. 3.7. SPECTRUM FOR 1 kW Hg-Xe ARC LAMP (AFTER REF (88)).

3.7 R.S.R.E Equipment

Under the CASE award scheme, a great deal of the experimental work was performed at R.S.R.E (Malvern). The major differences between the system utilised at R.S.R.E and the system constructed at Birmingham will now be briefly described.

The R.S.R.E system although similar has a somewhat higher specification. Compound growth of II-VI materials is possible due to the inclusion of diethyltelluride and dimethylmercury bubblers in addition to the dimethylcadmium bubbler. Also the reactor has been designed to accept elemental mercury, which may be used as an alternative to the dimethylmercury bubbler.

The additional choice of a hydrogen carrier is available. This is purified by diffusing through a palladium/silver alloy membrane system. High purity helium is also available.

A Beckman hygrometer is fitted to the inlet flow line, to monitor the moisture level of the incoming helium downstream of the molecular sieve. This is able to measure the moisture content to a level of 1 ppm.

The susceptor heating is performed by an infra red lamp mounted within an elliptical reflector, which provides for more rapid heating than is achieved with the split furnace arrangement used on the Birmingham system.

A Dataquad mass spectrometer analyser head is mounted on the vacuum system. This is extremely useful for detecting molecular species produced in the growth system, e.g. for detecting photo-fragments produced by the ultraviolet. It also serves as an aid for leak detection.

This facility can be used in conjunction with the liquid nitrogen cold trap in the pumping line prior to the pumps, which normally serves as protection of the pumping system against residual alkyls. Different species entrapped in the cold trap can be analysed by the mass spectrometer as they evaporate in accordance to their vapour pressures as the cold trap warms to room temperature. A cold trap is also present on the diffusion pump to reduce contamination by preventing oils from the pump diffusing back into the MOCVD system.

A closed circuit televison camera constantly monitors the substrate during a growth run and provides a constant visual check during growth. This is particularly

useful when the ultraviolet lamp is in operation.

A Druck pressure monitor gives an indication of the pressure within the system. This is observed when the carrier gas is input to the system after evacuation to enable the exhaust valve to be opened without risk of the system being exposed to air.

The ultraviolet lamp is an Illumination Industries 3kw, water cooled mercury lamp. This lamp is focussed, using an elliptical reflector, to a ~1cm strip on to the substrate. Alternatively it may be used in its defocussed mode where a reduction of intensity by a factor of ninety at the substrate is obtained. The lamp spectrum is shown in figure 3.8.

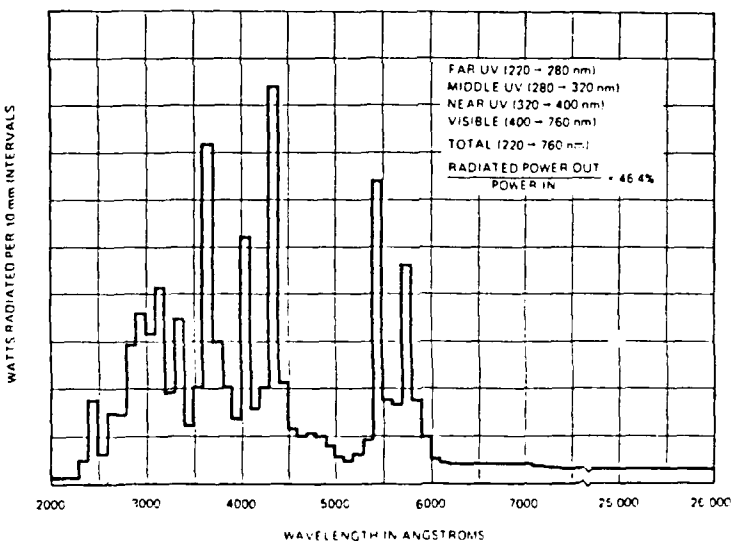

FIG. 3.8. SPECTRUM FOR 3kW Hg ARC LAMP (AFTER REF (89)).

Chapter 4: Experimental

4.1.1 Substrate material

The GaAs substrates were all of (100) orientation, cut 2° off towards (110), and supplied by Mining and Chemical Products with one face polished. These were either Cr doped semi-insulating (batch XK 5962) or Si doped (XK 5441). The CdTe substrates were of similar orientation and supplied by Cominco. Si substrates were also (100) orientation and supplied by Wacker Chemitronic GmbH. Sapphire substrates were basal plane (0001) and obtained from PBK Micron.

4.1.2 Substrate preparation

GaAs substrates were prepared by degreasing and etching a cleaved piece typically of 1cm x 1.5cm size. This was degreased in trichloroethane for 1 minute in an ultrasonic bath after which it was transferred into fresh trichloroethane heated to 100°C for 15 minutes. The substrate was then removed and nitrogen blow dried prior to etching in a 5:1:1 H_2SO_4:H_2O:H_2O_2 solution for 20 minutes. After etching the substrate was rinsed in distilled water and given a final cascade rinse with deionised water for 2 hours. Once this rinsing was complete the substrate was rinsed in warm propanol for 5 minutes followed by immersion into fresh propanol for storage until transfer into the growth reactor was possible.

The CdTe substrates preparation was similar with the etching stage replaced by pad polishing using 2% bromine/methanol solution.

The GaAs substrate preparation for the deposition of cadmium at Birmingham was as above although the final cascade rinse in deionised water was replaced by three separate 15 minute rinses due to the limited supply of deionised water.

The sapphire substrates were thoroughly degreased in trichloroethane for 5 minutes in an ultrasonic bath followed by warm propanol for 15 minutes.

The Si substrates were etched for 10 minutes in a buffered HF solution (NH_3F:40%HF, 4:1) for oxide removal and then rinsed in deionised water.

4.1.3 TEM specimen preparation

Cross-sectional TEM specimens were prepared in the following manner. For layers on GaAs, Si and CdTe substrates two pieces approximately 5mm x 10mm were

cleaved and glued, layer surfaces together, using epoxy adhesive. Silicon support blocks were also glued to either side to provide mechanical support during the grinding stages. The specimen was then clamped and allowed to set for more than 12hours. It was then sliced using using a diamond impregnated circular saw to give slices of ~1mm thickness. These were then ground mechanically either on a cast iron plate or using a VCR Dimpler until a thickness of ~50μm was reached. These slices were then polished on both sides using 6μm and 1μm diamond paste. Discs of 2.8mm diameter were cut out from the polished slices using an ultrasonic drill after which brass support rings of 70μm thickness, 2.8 OD and 2.3 mm ID were glued on to provide additional strength.

Sapphire specimens were prepared as above although the initial cleavage step was replaced by cutting using a diamond saw; silicon support blocks were not required.

Final ion beam thinning to thin the specimens to electron transparency was carried out using Ion Tech ion beam thinners fitted with B11 ion beam guns. These guns were suitably modified for the reactive ion beam milling.

For CdTe layers, reactive iodine etching was employed using plasma currents of 10μA at 5keV with an incident angle of 12°. For the cadmium deposits, argon milling was used at 0.15mA, 5keV, and an incident angle of 14°.The latter ion beam thinner was equipped with a liquid nitrogen cooled stage.

Planar TEM specimens were prepared by ultrasonically cutting 2.8mm discs from the substrate and then jet polishing from the reverse of the layer side until perforation of these occurred. A 2% bromine/ethanediol mixture was used for the GaAs and a 8:1:1 HF:HNO_3:H_2O solution for the Si substrates.

4.2.1 Secondary ion mass spectrometry (SIMS)

SIMS profiles were determined using a Cameca IMS-3f secondary ion mass spectrometer with a 1μA oxygen primary beam with a 250μm raster. Depth profiles for gallium were obtained by recording counts for ^{69}Ga ions. Profiles were also obtained for selected impurities. Profiling the specimens was only undertaken up to the interface to prevent contamination of the sample chamber with gallium. This equipment is at RSRE.

4.2.2 Scanning electron microscopy (SEM)

Scanning electron microscopy was carried out in a Cambridge S250 operating at 20kV or on a Philips 500 operating at 25kV at RSRE. This was used principally to view the surface morphology of the grown deposits and to determine layer thicknesses by viewing cleaved edges. A Philips 500 SEM and an ISI 100A were also used at Birmingham.

4.2.3 X-ray diffraction

A Philips single crystal X-ray diffractometer operating at 35kV, 20mA with nickel filtered Cu Kα radiation was used to determine the crystallinity of the CdTe layers.

4.2.4 Transmission electron microscopy (TEM)

Prepared TEM foils were viewed in a JEOL 4000FX TEM operating at 400kV, a Phillips EM 400T at 100kV or a Phillips EM 300 at 100kV. The high resolution microscopy was carried out on a JEOL 4000EX TEM at RSRE.

Chapter 5: Cadmium telluride depositions; results and discussion

Twenty growth runs were performed and layers were chosen for characterisation by x-ray diffraction, transmission electron microscopy (TEM), scanning electron microscopy (SEM) and secondary ion mass spectroscopy (SIMS). Growths were performed over a range of temperatures from 230°C to 350°C using both UV and thermal dissociation to deposit onto gallium arsenide and cadmium telluride substrates. The UV radiation was incident on the substrate in either the focussed or defocussed mode. Table 5.1 lists the flow conditions, the reactant partial pressures, the growth temperature, the substrate and the dissociation method utilised for each deposition along with the growth rates obtained.

5.1 Heterodeposition onto Gallium Arsenide substrates

CdTe Deposition was carried out onto GaAs substrates oriented (100) 2° towards (110) which were supplied by Mining and Chemical Products with one face polished.

5.1.1 UV focussed conditions

The first series of experiments was performed with the UV focussed using an elliptical reflector which focussed the beam to a 1cm strip on to the substrate. This resulted in a beam intensity of ~1Wcm^{-2} (at 254 nm) at the substrate surface.

5.1.1.1 DETe rich conditions

Run 1 was performed with DMCd and DETe input partial pressures of 0.06 and 5.1 torr respectively, and the criterion for these conditions was based upon the flow conditions used for the growth of CMT. Growth was performed at 230°C in this case and a growth rate of 1.5μm/hr obtained. Cross-sectional TEM (XTEM) shows that this layer is polycrystalline with an average grain size of ~500Å (figure 5.1). Figure 5.2 shows a diffraction pattern of the layer and shows the polycrystalline rings which have been indexed as (111), (222), (400) etc. The surface morphology of the layer as viewed in the SEM showed a poor surface with many lumps present (figure 5.3).

Further growth runs were performed with the same flow and temperature conditions with differing treatments of the substrate prior to growth.

Run	Substrate	Flows (cc/min)			Partial Pressure (torr)		Growth Temperature(°C)	Method	Growth Rate (μmhr^{-1})
		DMCd	DETe	Dilution	DMCd	DETe			
1	GaAs	3	1000	1000	0.06	5.1	230	UV focussed	1.5
2	GaAs	3	1000	1000	0.06	5.1	230	UV focussed	1.5
3	GaAs	3	1000	1000	0.05	4.6	230	UV focussed	1.5
4	GaAs	3	1000	1000	0.04	3.1	350	Thermal	0.6
5	GaAs	10	40	500	0.54	0.54	350	UV focussed	3.2
6	GaAs	10	40	500	0.46	0.45	350	Thermal	0.62
7	GaAs	10	40	500	0.54	0.54	300	UV focussed	2.2
8	GaAs	10	40	500	0.51	0.51	250	UV focussed	0.66
9	GaAs	10	40	500	0.46	0.45	300	Thermal	0.26
10	GaAs	20	47	933	0.53	0.37	300	UV focussed	0.75
11	GaAs	27	69	904	0.81	0.54	300	UV focussed	0.75
12	GaAs	27	69	904	0.81	0.54	250	UV focussed	1.1
13	GaAs	32	69	898	1.08	0.54	300	UV focussed	1.2
14	GaAs	30	62	908	1.08	0.54	250	UV focussed	0.4
15	GaAs	30	62	908	1.08	0.54	250	UV defocussed	0.15
16	GaAs	30	62	908	1.08	0.54	250	UV defocussed	0.15
17	GaAs	19	620	919	0.34	3.49	300	UV defocussed	1.1
17	CdTe	19	620	919	0.34	3.49	300	UV defocussed	1.04
18	GaAs	19	62	919	0.54	0.54	300	UV defocussed	2.3
19	GaAs	24	62	914	0.81	0.54	300	UV defocussed	0.7
19	CdTe	24	62	914	0.81	0.54	300	UV defocussed	1.38
20	GaAs	24	62	914	0.81	0.54	300	Thermal	0.135

TABLE 5.1

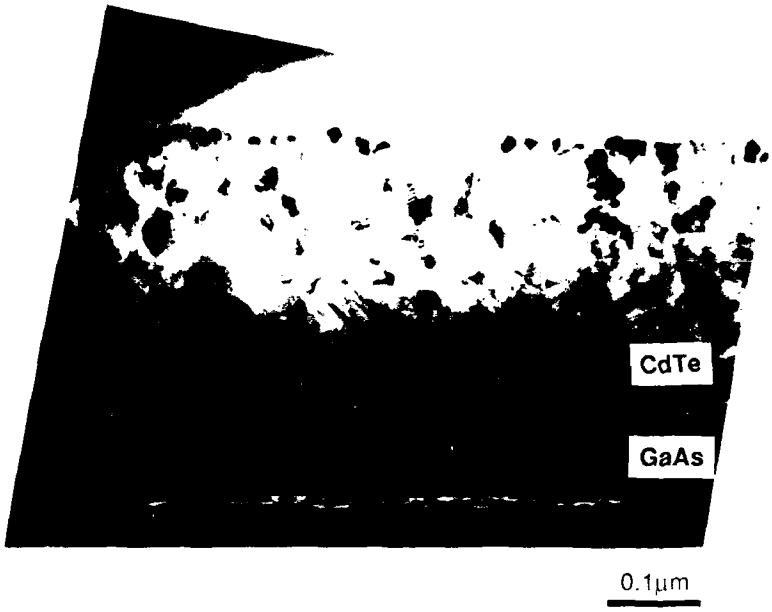

FIG. 5.1. CROSS-SECTIONAL TEM MICROGRAPH OF A CADMIUM TELLURIDE LAYER DEPOSITED ON A GALLIUM ARSENIDE SUBSTRATE AT 230°C WITH DETe RICH CONDITIONS AND FOCUSSED UV.

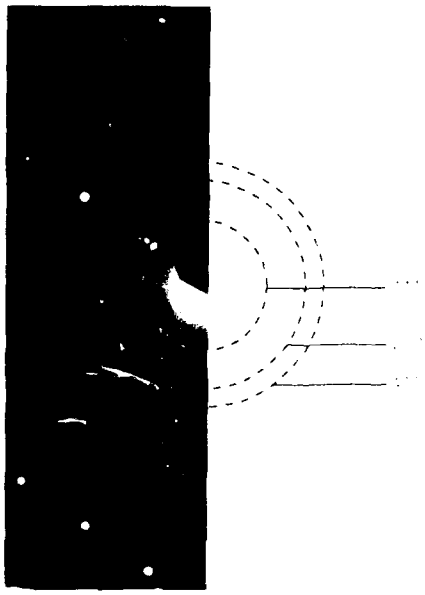

FIG 5.2. DIFFRACTION PATTERN OF A CADMIUM TELLURIDE LAYER DEPOSITED ON A GALLIUM ARSENIDE SUBSTRATE AT 230°C WITH DETe RICH CONDITIONS.

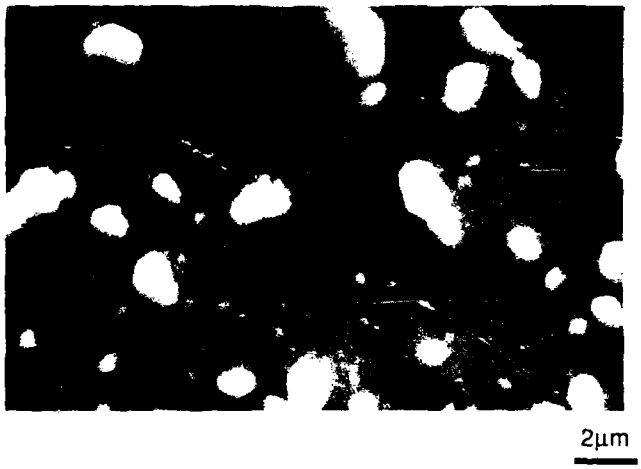

FIG 5.3. SURFACE MORPHOLOGY OF A CADMIUM TELLURIDE LAYER DEPOSITED ON A GALLIUM ARSENIDE SUBSTRATE AT 230°C WITH DETe RICH CONDITIONS AND FOCUSSED UV.

Photodissociation of dimethylmercury, with an expected production of highly reactive methyl radicals, which were expected to have a cleaning effect on the substrate, was carried out. No change in the crystalline structure of the layer (Run 2) was obtained with again polycrystallinity resulting; however it is not certain that this treatment would have affected the substrate.

Heat cleaning the substrate at a temperature of 480°C in a stream of hydrogen for a period of 10 minutes in an attempt to desorb the surface oxide results in a change of microstructure. Although this heat cleaning temperature is below the typical desorption temperature of ~580°C it can still be expected to cause partial oxide desorption and/or surface reconstruction. Figure 5.4 shows the substrate surface and the crystallographic nature of the layer (Run 3) is evident with the faceted polycrystallites clearly visible. The TEM diffraction pattern as shown in figure 5.5 shows that the preferred orientation of the layer is (111) with no (400) contribution and this orientation is confirmed by the hexagonal growth features. Growth rates were the same in all cases and neglecting any growth rate dependence on orientation this would be expected as similar process conditions were used throughout.

5.1.1.2 DMCd:DETe=1

The next step was to investigate the effect of increasing the DMCd input partial pressure. At a temperature of 350°C and flow conditions giving rise to a DMCd:DETe ratio of unity a growth run with focussed UV illumination conditions was carried out (Run 5). This resulted in growth of an epitaxial layer with the same orientation as the GaAs substrate, namely (100) on (100). The defect structure of this layer shows a heavily dislocated region at the interface and twinning at 54.74° to the interface, beginning on the substrate surface corresponding to two different (111) slip planes (figure 5.6). A decrease in the dislocation density on nearing the layer surface is observed and is a direct consequence of the layer thickness. The diffraction pattern, shown in figure 5.7, has been taken with the SAD aperture over both the substrate and the layer and shows the similar orientation of the two. The different spacing of the two sets of spots is due to the difference in lattice parameter of the CdTe and the GaAs with the spots with the greater separation corresponding to the smaller lattice parameter of the GaAs.

The success in obtaining an epitaxial layer with unity alkyl flow conditions led us to attempt to deposit at reduced temperatures with similar flow conditions. Thus a similar flow was carried out at 300°C (Run 7). The change in the crystallinity of this layer

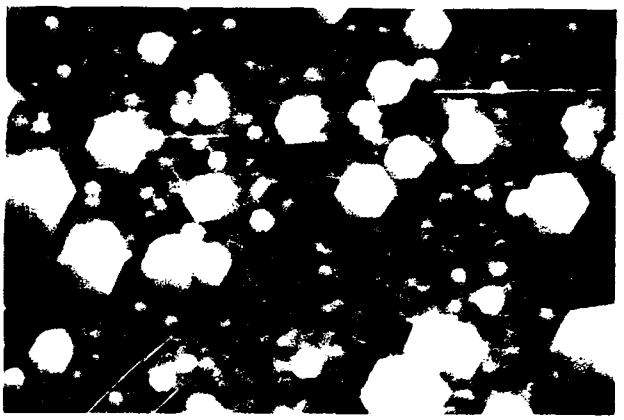

FIG 5.4. SURFACE MORPHOLOGY OF A CADMIUM TELLURIDE LAYER DEPOSITED ON A HYDROGEN CLEANED GALLIUM ARSENIDE SUBSTRATE AT 230°C WITH DETe RICH CONDITIONS AND FOCUSSED UV.

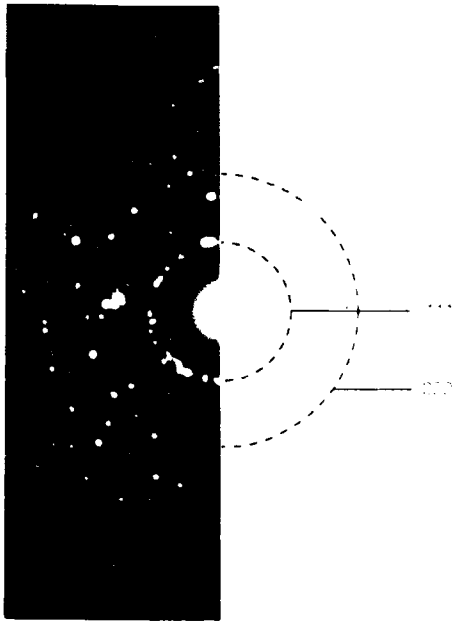

FIG 5.5. DIFFRACTION PATTERN OF A CADMIUM TELLURIDE LAYER DEPOSITED ON A HYDROGEN CLEANED GALLIUM ARSENIDE SUBSTRATE AT 230°C WITH DETe RICH CONDITIONS AND FOCUSSED UV

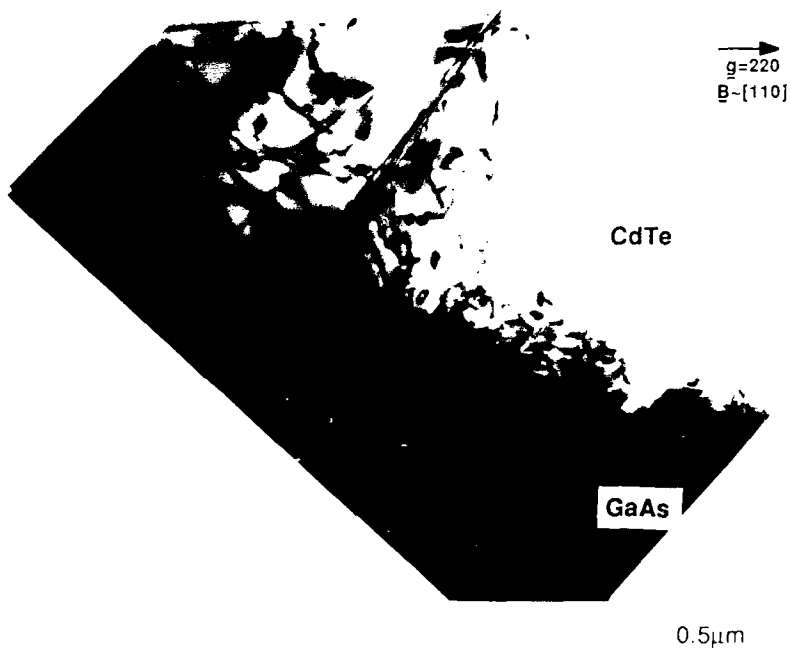

FIG. 5.6 CROSS-SECTIONAL TEM MICROGRAPH OF A CADMIUM TELLURIDE LAYER DEPOSITED ON A GALLIUM ARSENIDE SUBSTRATE AT 350°C WITH UNITY ALKYL RATIO AND FOCUSSED UV

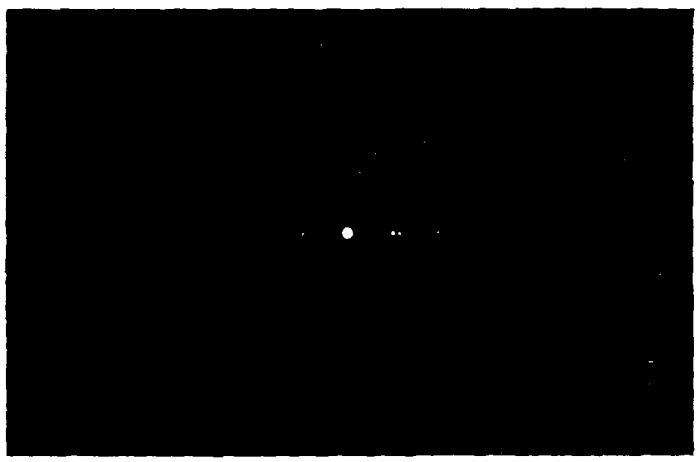

FIG. 5.7. DIFFRACTION PATTERN OF A CADMIUM TELLURIDE LAYER DEPOSITED ON A GALLIUM ARSENIDE SUBSTRATE AT 350°C WITH UNITY ALKYL RATIO AND FOCUSSED UV. THE SELECTED AREA APERTURE HAS BEEN PLACED OVER THE LAYER AND THE SUBSTRATE

is quite dramatic with a strongly polycrystalline deposit obtained, as evidenced from SEM (figure 5.8). This shows that randomnly oriented crystallites of varying size between 0.5μm and 5μm are growing in a columnar manner. This is in stark contrast to the polycrystalline layers deposited with DETe rich conditions, which although polycrystalline show no type of columnar structure to them, have a smoother morphology and are less porous. The diffraction pattern for this layer is similar to that of Run 3, (figure 5.3) and shows a preferential (111) growth direction.

At a further reduced temperature of 250°C this columnar type of growth is obtained (Run 8) although to a somewhat lesser degree due to the reduced growth rate at this lower temperature (figure 5.9).

5.1.1.3 DMCd:DETe=1.5

Further increase of the DMCd partial pressure was carried out to improve low temperature crystallinity. Growth was carried out at a ratio of 1.5 and at a temperature of 300°C and the surface morphology improved from the strong columnar polycrystalline morphology to a specular but nevertheless rough surface (figure 5.10). Observation by XTEM reveals that this layer (Run 11) is also columnar polycrystalline although more densely packed than the layer obtained with unity alkyl ratios. The layer is heavily faulted and microtwinning within the individual grains is evident as can be seen from figure 5.11. The diffraction pattern for this layer is similar to that of figure 5.5 showing no evidence of (400) type reflections.

Decreasing the temperature to 250°C for Run 12 resulted in the increased faceting of these features as seen from the SEM micrograph in figure 5.12. A XTEM micrograph (figure 5.13) shows this structure to be columnar polycrystalline but with a far higher degree of point nucleation at the substrate, and is indicative of reduced surface diffusion of atomic species at the growth interface or an increase in the density of nucleation.

5.1.1.4 DMCd:DETe=2

Further increase of the DMCd to obtain a reactant input ratio of 2 at 300°C (Run 13) results in a further improvement in the morphology and single crystal growth is achieved. The dislocation network associated with the lattice mismatch as seen for Run 5 is not observed in this case. However TEM (figure 5.14) indicates that a layer of polycrystallinity exists at the interface and extends some 0.1-0.2μm into the CdTe after which single crystal CdTe has grown with the same orientation as the substrate.

FIG. 5.8. SURFACE MORPHOLOGY OF A CADMIUM TELLURIDE LAYER DEPOSITED ON A GALLIUM ARSENIDE SUBSTRATE AT 300°C WITH UNITY ALKYL RATIO AND FOCUSSED UV.

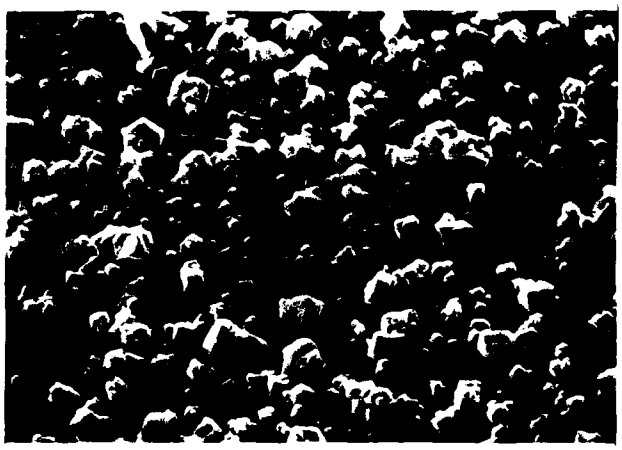

FIG. 5.9. SURFACE MORPHOLOGY OF A CADMIUM TELLURIDE LAYER DEPOSITED ON A GALLIUM ARSENIDE SUBSTRATE AT 250°C WITH UNITY ALKYL RATIO AND FOCUSSED UV.

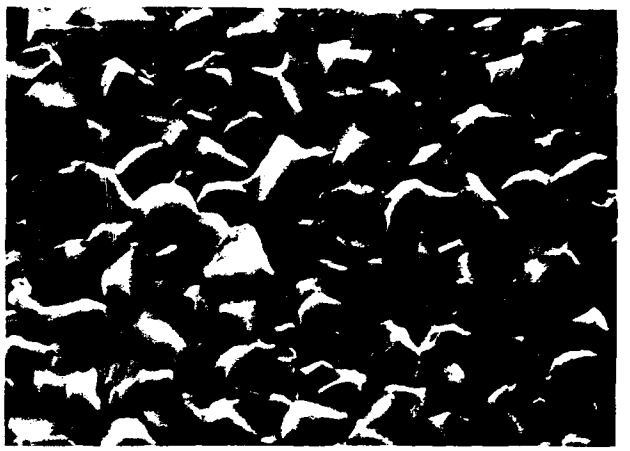

FIG. 5.10. SURFACE MORPHOLOGY OF A CADMIUM TELLURIDE LAYER DEPOSITED ON A GALLIUM ARSENIDE SUBSTRATE AT 300°C WITH DMCd:DETe=1.5 AND FOCUSSED UV.

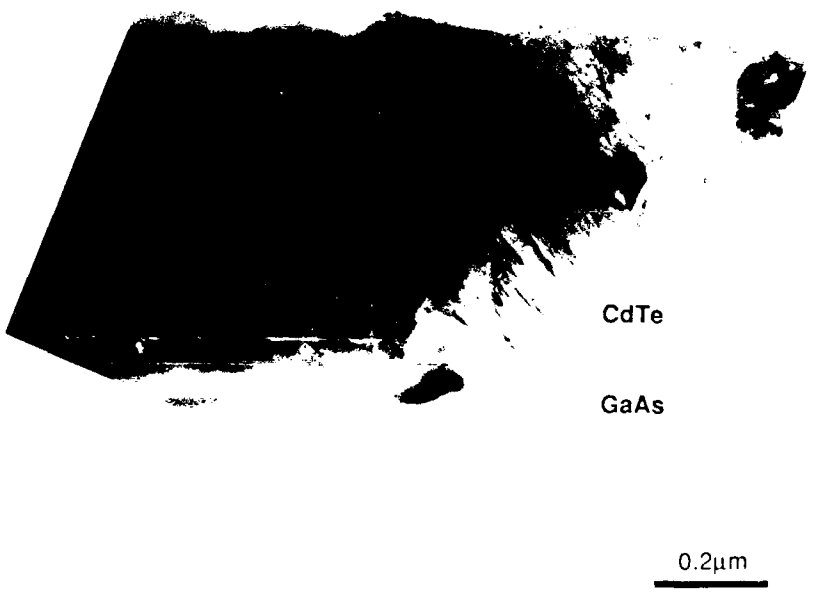

FIG. 5.11. CROSS-SECTIONAL TEM MICROGRAPH OF A CADMIUM TELLURIDE LAYER DEPOSITED ON A GALLIUM ARSENIDE SUBSTRATE AT 300°C WITH DMCd:DETe=1.5 AND FOCUSSED UV.

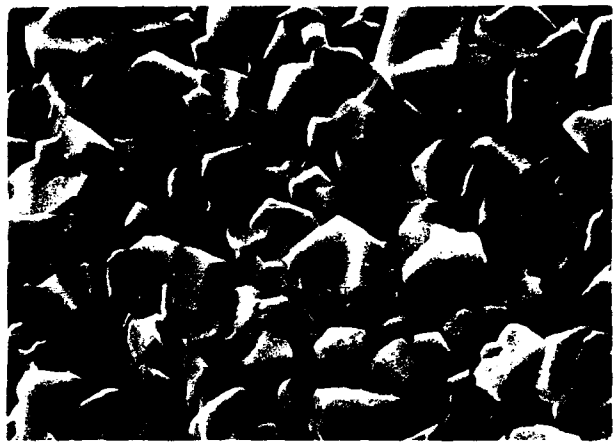

FIG. 5.12. SURFACE MORPHOLOGY OF A CADMIUM TELLURIDE LAYER DEPOSITED ON A GALLIUM ARSENIDE SUBSTRATE AT 250°C WITH DMCd:DETe=1.5 AND FOCUSSED UV.

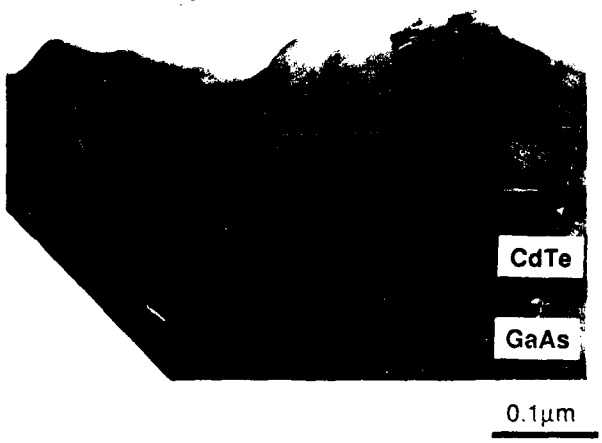

FIG. 5.13. CROSS-SECTIONAL TEM MICROGRAPH OF A CADMIUM TELLURIDE LAYER DEPOSITED ON A GALLIUM ARSENIDE SUBSTRATE AT 250°C WITH DMCd:DETe=1.5 AND FOCUSSED UV.

FIG. 5.14. CROSS-SECTIONAL TEM MICROGRAPH OF A CADMIUM TELLURIDE LAYER DEPOSITED ON A GALLIUM ARSENIDE SUBSTRATE AT 300 °C WITH DMCd:DETe=2 AND FOCUSSED UV. THE SPECIMEN HAS BEEN TILTED TO SHOW THE BEND CONTOURS OF THE SINGLE CRYSTAL REGION.

Decreasing the temperature to 250°C once again leads to a breakdown of epitaxial growth and results in the poor random columnar type of growth achieved earlier.

5.1.2 UV defocussed conditions

The UV lamp was defocussed to investigate the effect of reduced UV intensity on the deposition of CdTe. When used in the defocussed mode a beam intensity of 12mwcm^{-2} was obtained at the substrate surface.

5.1.2.1 DMCd:DETe=1

With the defocussed lamp and a unity input ratio (Run 18) and at a temperature of 300°C the CdTe exhibits a matt, satin like surface. SEM (figure 5.15) reveals the surface to be rough with sharp and spurious peaking.

Nevertheless, despite the poor surface morphology cross-sectional TEM (figure 5.16) shows the layer to be epitaxial with a heavily dislocated interface region. However there is little penetration of the dislocation structure into the layer beyond this densely dislocated region of ~0.2μm, although occasional microtwins do protrude into the layer further than this distance. The orientation relationship is again of the (100) CdTe||(100) GaAs type.

5.1.2.2 DMCd:DETe=1.5

With increase of the DMCd:DETe to 1.5 (Run 19) a large improvement in crystallinity and surface morphology was obtained. The surface is highly specular and smooth with only occasional dimpled features on the surface (figure 5.17). As with the layer deposited at a unity input ratio this layer is epitaxial although with a much reduced dislocation density. This can be seen in the XTEM micrograph of figure 5.18 and is confined to less than 250Å of the interface.

5.1.2.3 DMCd:DETe=2

With the UV defocussed, an input ratio of 2 (Run 16) and a reduced temperature of 250°C a highly specular layer surface resulted. A reduction of the growth rate was obtained. XTEM (figure 5.19) shows that this layer is also polycrystalline with a strong columnar structure, although the grain sizes are of a larger average size. Many of these grains still exhibit a great deal of microtwinning.

FIG. 5.15. SURFACE MORPHOLOGY OF A CADMIUM TELLURIDE LAYER DEPOSITED ON A GALLIUM ARSENIDE SUBSTRATE AT 300 C WITH UNITY ALKYL RATIO AND DEFOCUSSED UV.

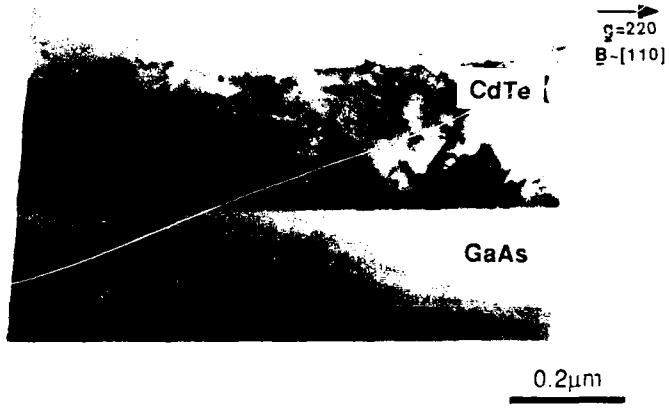

FIG. 5.16. CROSS-SECTIONAL TEM MICROGRAPH OF A CADMIUM TELLURIDE LAYER DEPOSITED ON A GALLIUM ARSENIDE SUBSTRATE AT 300°C WITH UNITY AKYL RATIO AND DEFOCUSSED UV.

FIG. 5.17 SURFACE MORPHOLOGY OF A CADMIUM TELLURIDE LAYER DEPOSITED ON A GALLIUM ARSENIDE SUBSTRATE AT [illegible] DMCd DETe=1.5 AND DEFOCUSED UV

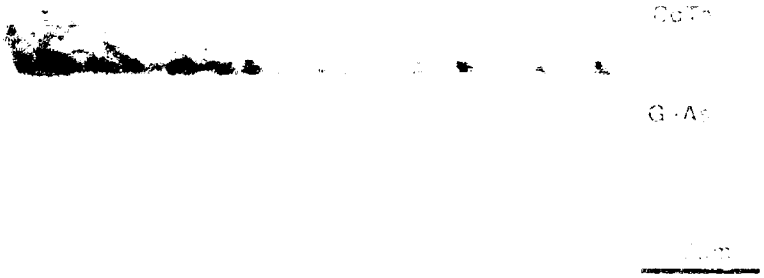

FIG. 5.18 CROSS-SECTIONAL TEM [illegible] LAYER DEPOSITED ON A GALLIUM ARSENIDE [illegible] DMCd DETe=1.5 AND DEFOCUSED UV

FIGURE 19. CROSS-SECTIONAL TEM MICROGRAPH OF A CADMIUM TELLURIDE LAYER DEPOSITED ON A GALLIUM ARSENIDE SUBSTRATE AT 250°C WITH [illegible]

5.2 Homoepitaxial growth

Deposition was carried out onto CdTe substrates oriented (100) 2° towards (110) which were supplied by Cominco with one face polished.

5.2.1 DMCd:DETe=1.5

Growth onto CdTe substrates was undertaken at the optimum growth conditions achieved for the growth onto GaAs, i.e. an alkyl ratio of 1.5, defocussed UV lamp conditions and a temperature of 300°C. The surface morphology is extremely good with a featureless and specular surface (figure 5.20). Although cross-sectional SEM failed to distinguish the layer from the substrate, XTEM shows a high quality layer with few defects visible; some dislocations below the substrate surface are replicated in the layer (figure 5.21). There is a complete absence of the misfit dislocation network seen at the interface of the CdTe-GaAs system. A growth rate of 1.38μm/hr was obtained and was a factor of two higher than for the deposition onto GaAs. This may be related to nucleation difficulties on the latter substrates or to changes in surface reconstruction at the interface. This latter would then influence the diffusion of atomic species at the growth interface and is consistent with a surface kinetic process. This is also supported by the slightly inferior surface morphology of the layer deposited on the GaAs substrate (Run 19) under similar conditions.

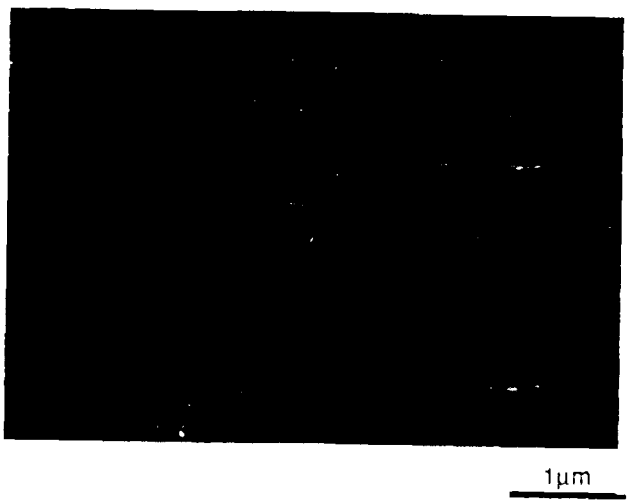

FIG. 5.20. SURFACE MORPHOLOGY OF A CADMIUM TELLURIDE LAYER DEPOSITED ON A CADMIUM TELLURIDE SUBSTRATE AT 300°C WITH DMCd:DETe=1.5 AND DEFOCUSSED UV.

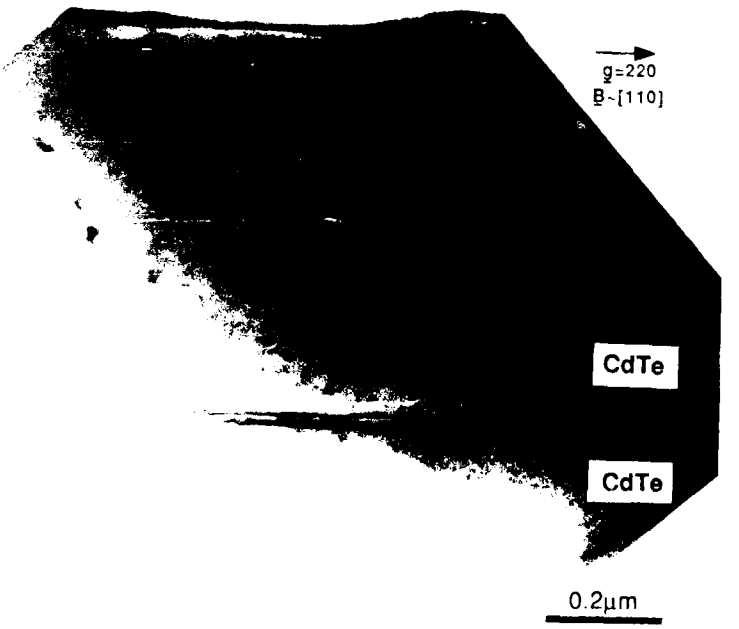

FIG. 5.21. CROSS-SECTIONAL TEM MICROGRAPH OF A CADMIUM TELLURIDE LAYER DEPOSITED ON A CADMIUM TELLURIDE SUBSTRATE AT 300°C WITH DMCd:DETe=1.5 AND DEFOCUSSED UV.

5.3 Thermal depositions

The following experiments were carried out using purely thermal means, i.e. without the assistance of the UV radiation.

5.3.1.1 DETe rich conditions

A thermal growth (Run 4) was carried out at a temperature of 380 C with similar DMCd and DETe concentrations to Runs 1-3 namely DETe rich conditions. Although the temperature was increased a growth rate reduction from 1.5 to 0.6 microns per hour was observed due to the dissociation of the metal organics occurring only pyrolytically. The surface of the layer does not exhibit the lumps seen on the layer deposited photolytically using otherwise similar growth conditions. The surface of the layer is highly specular but the layer is once again polycrystalline (not epitaxial).

Figure 5.22 shows a XTEM micrograph of a thermally grown layer at a relatively low thermal growth temperature of 410 C showing the dislocation structure at the interface. This specimen was grown by GEC (Hirst Laboratories) and forwarded for XTEM examination. The substrate was given a prebake at 580 C for approximately 10 minutes prior to growth and the layer, in contrast to the previously grown epitaxial layers, has a (111) orientation on the (100) GaAs substrate and an azimuthal orientation as indicated by $<110>_{CdTe} \| <110>_{GaAs}$ and $<112>_{CdTe} \| <110>_{GaAs}$.

The flow conditions were such that growth was carried out under Te rich conditions (DMCd:DETe = 0.81) at a tellurium partial pressure of 0.81 torr. Visible on the sample are stacking faults (figure 5.23) and dipoles (figure 5.24) and these may be indicative of the higher growth temperature utilised and the consequent greater stresses in the layer.

A Burgers vector analysis was performed for the dislocations extending from the interface into the CdTe layer using the g.b=0 invisibility criterion. Figure 5.25 shows a schematic Kikuchi map centred on [101] for the zinc blende structure. The arrows indicate the operating diffracting vectors used for the Burgers vector determination and the corresponding two beam images are shown in figure 5.26 as indicated alongside. All micrographs have been taken with the deviation parameter, s set positive of Bragg.

The micrograph of figure 5.26(a) has been obtained with a beam direction, B close to [2$\bar{1}$1] and a diffracting vector g=022. The dislocations, marked as A, are clearly visible under these tilt conditions. However with B=[11$\bar{2}$], g=2$\bar{2}$0 and B=[10$\bar{1}$], g=1$\bar{1}$1

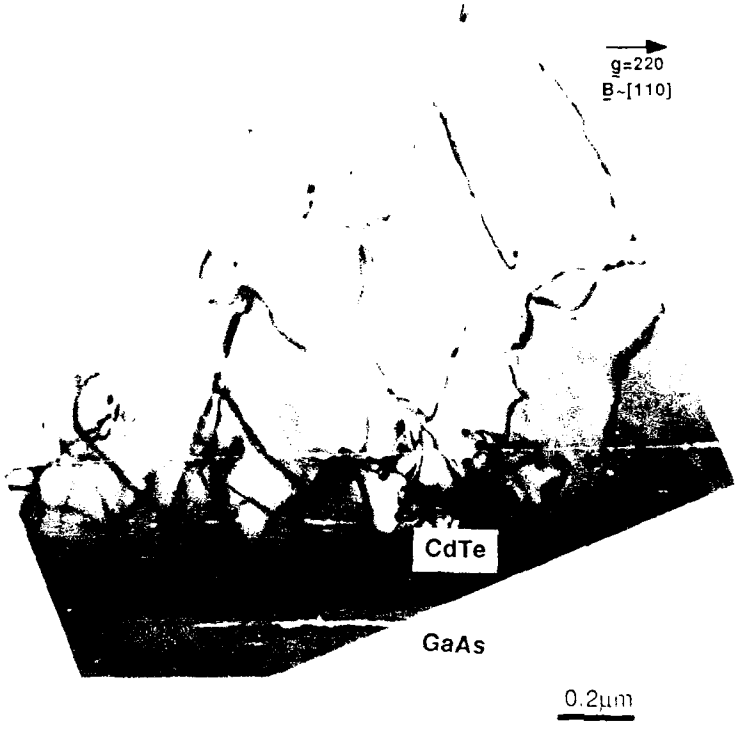

FIG. 5.22. CROSS-SECTIONAL TEM MICROGRAPH OF A CADMIUM TELLURIDE LAYER DEPOSITED THERMALLY ON A GALLIUM ARSENIDE SUBSTRATE AT 410 °C WITH DMCd DETe=0.81

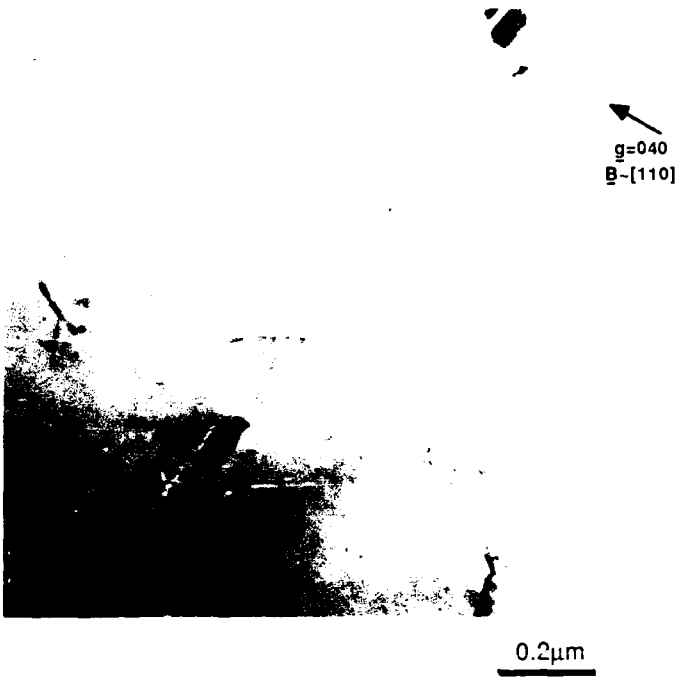

FIG. 5.23. STACKING FAULT IN A CADMIUM TELLURIDE LAYER DEPOSITED THERMALLY ON A GALLIUM ARSENIDE SUBSTRATE AT 410°C WITH DMCd:DETe=0.81.

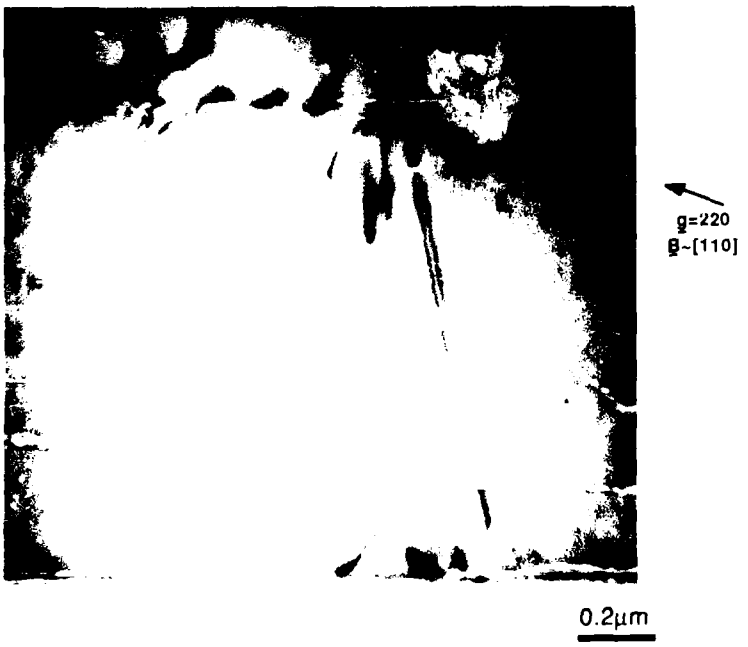

FIG. 5.24. DIPOLES IN A CADMIUM TELLURIDE LAYER DEPOSITED THERMALLY ON A GALLIUM ARSENIDE SUBSTRATE AT 410°C WITH DMCd:DETe=0.81.

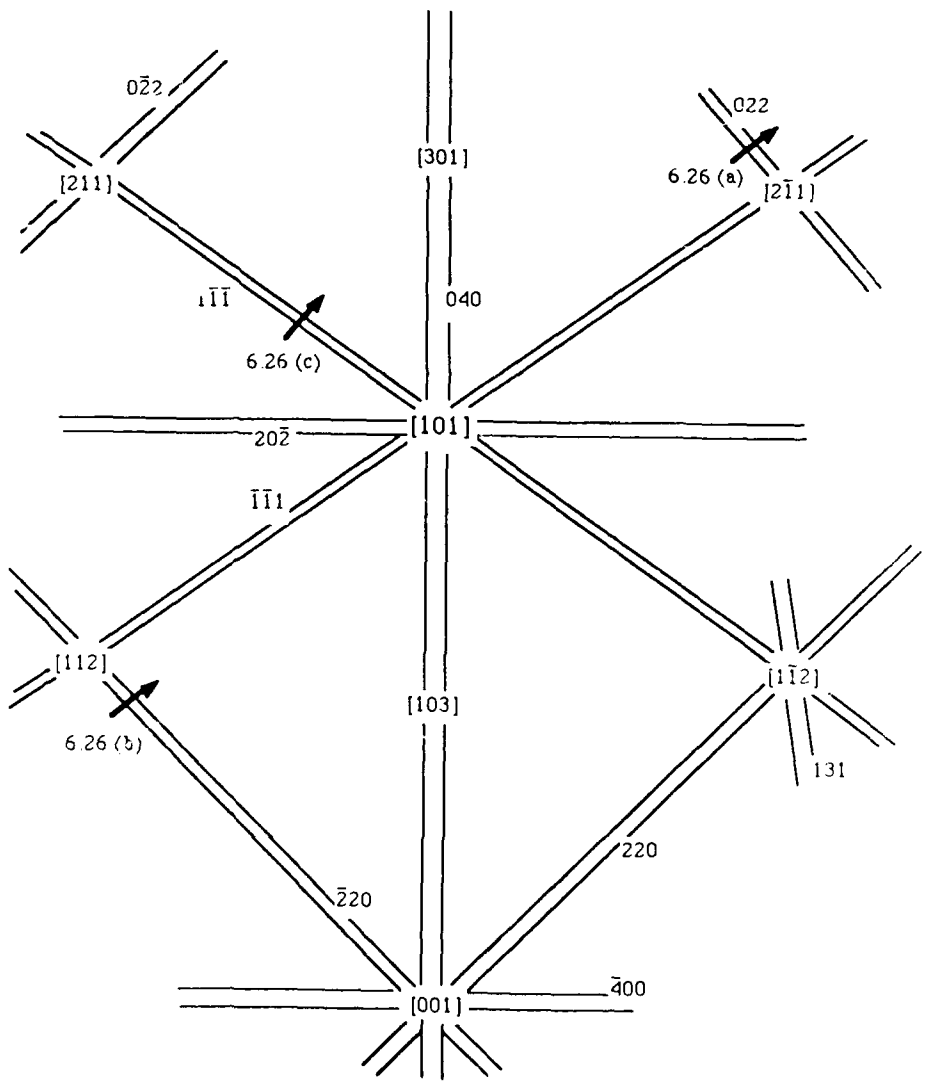

FIG. 5.25. SCHEMATIC KIKUCHI MAP FOR THE ZINC BLENDE STRUCTURE CENTRED ON [101].

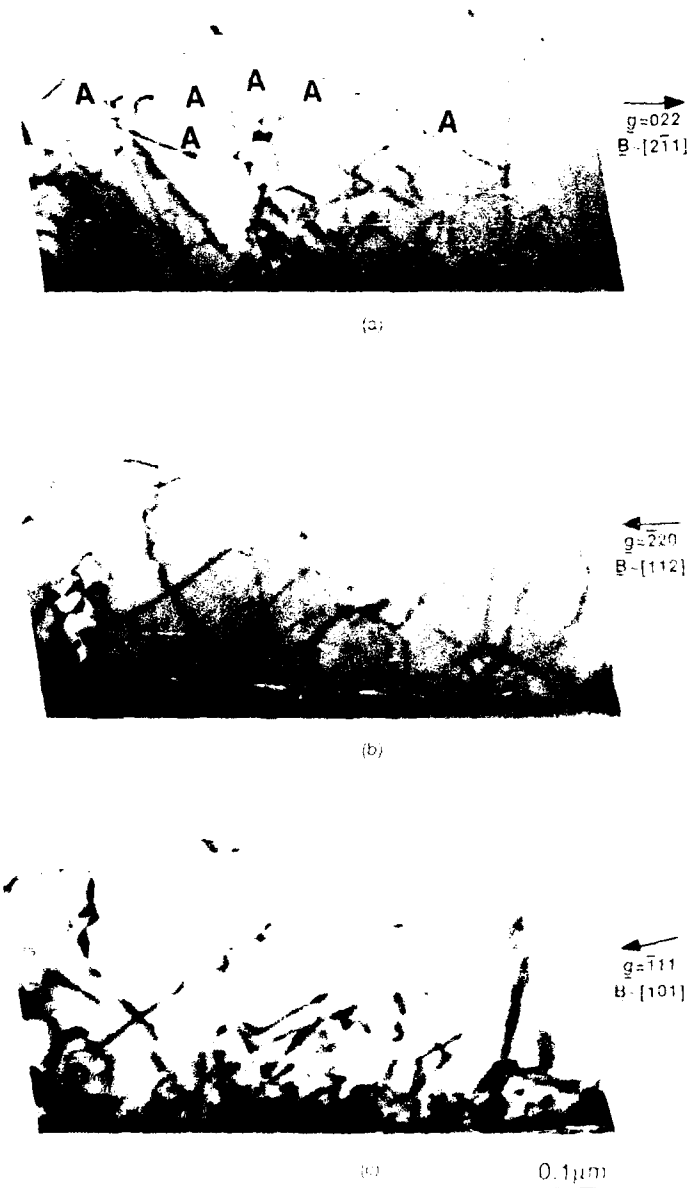

FIG 5.26 BURGERS VECTOR DETERMINATION OF DISLOCATIONS IN A CADMIUM TELLURIDE LAYER DEPOSITED ON A GALLIUM ARSENIDE SUBSTRATE

the dislocations are invisible as shown in figures 5.26(b) and 5.26(c). As these dislocations remain visible for all other diffracting conditions it may be concluded that the Burgers vectors of these particular dislocations are ±a/2[110]. Further analysis of a similar nature shows the presence of all the other five remaining types of <110> dislocation

5.3.2 DMCd:DETe=1

Increasing DMCd to the same value as the DETe, namely an input ratio of one resulted in epitaxial growth at a temperature of 350°C (Run 6). The growth on the (100) GaAs substrates is of a (100) orientation.

The dislocation structure shows the presence of a large dislocation network at the interface and a great deal of microtwinning emanating from the substrate layer interface which continues into the layer (figure 5.27). The dislocation density does not reduce away from the interface as shown earlier for Run 5. This is due to the comparative thicknesses of the two layers (1.6μm for Run 5 c.f 0.3μm for this thermally deposited layer).

Further thermal growths were carried out at 300°C with a unity input ratio, but unlike the thermally deposited layer at 350°C this layer is polycrystalline. Increase of the DMCd:DETe ratio was next performed and at a value of 1.5, an improvement in the crystallinity was observed. The microstructure was as in figure 5.18, with the dislocated region confined to <25nm of the interface.

FIG. 5.27. CROSS-SECTIONAL TEM MICROGRAPH OF A CADMIUM TELLURIDE LAYER DEPOSITED THERMALLY ON A GALLIUM ARSENIDE SUBSTRATE AT 350°C WITH UNITY ALKYL RATIO.

5.4 UHV deposited CdTe on GaAs

TEM examination of two layers of CdTe deposited by a UHV evaporation technique onto (100) GaAs substrates was undertaken. These layers were grown at RSRE by Dr DC Rodway and were provided for cross-sectional TEM.

Prior to growth the GaAs substrates were given an in-situ prebake at 610°C and growth was carried out at temperatures of 210°C and 290°C for layers DCR 9 and DCR 13 respectively.

TEM revealed that DCR 9 has grown with a (111) orientation whereas DCR 13 has a (100) orientation. Figure 5.28 shows a HRTEM micrograph of DCR 13, the (100) oriented layer in which the (111) planes have been imaged. The contrast points represent closely spaced pairs of atomic columns as it is not possible to distinguish between the individual Cd and Te atoms. The micrograph shows that the interface between the CdTe and the GaAs is free from any oxide or amorphous layer. Also along the interface, on average every seven atomic planes, an extra plane of atoms is visible. Imaging at a lower magnification (figure 5.29) over a greater area shows microtwinning in the layer beginning on the substrate surface. At a much reduced magnification using conventional diffraction contrast imaging a large dislocation network can be seen in figure 5.30, and is very similar to the dislocation structure of Runs 5,6 and 18, of the photoenhanced growths. Although this diffraction contrast image does not appear to be consistent with the high resolution image showing the regular array of misfits it must be noted that with the latter the length of interface is only ~280Å.

DCR 9 deposited at 210°C shows a markedly different dislocation structure. Figure 5.31 shows a diffraction contrast image of this sample and in common with the (100) layer a large dislocation density close to the interface can be seen. However the dislocations lie predominantly on the (111) planes parallel to the interface and continue to do so throughout the entire layer.

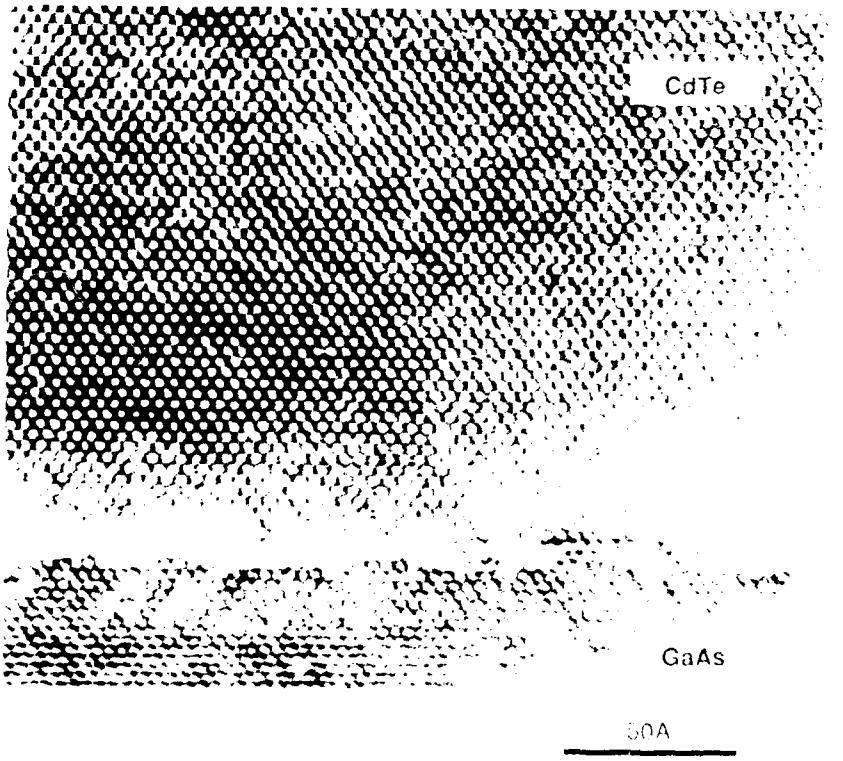

FIG. 5.28 HIGH RESOLUTION CROSS-SECTIONAL TEM MICROGRAPH OF A [illegible] CADMIUM TELLURIDE LAYER DEPOSITED ON A GALLIUM ARSENIDE SUBSTRATE AT 290°C BY A UHV EVAPORATION PROCESS.


CdTe
GaAs
100A

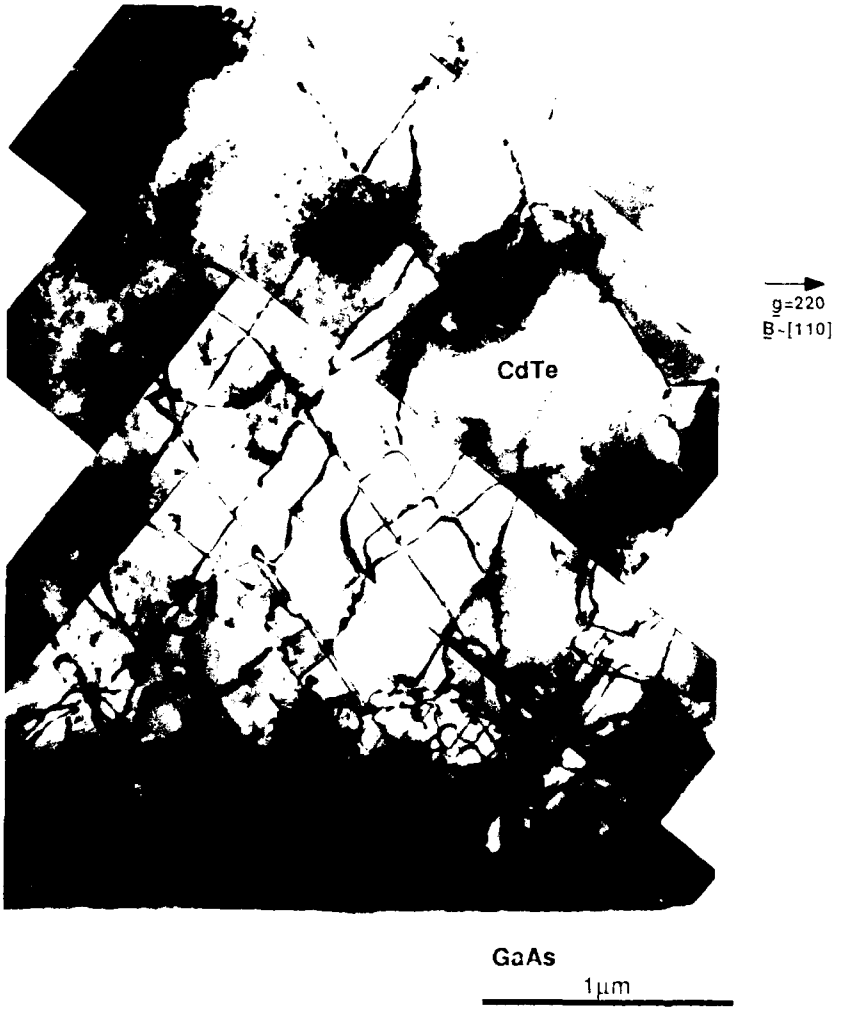

FIG 5.30. CROSS-SECTIONAL TEM MICROGRAPH OF A (100) CADMIUM TELLURIDE LAYER DEPOSITED ON A GALLIUM ARSENIDE SUBSTRATE AT 290°C BY A UHV EVAPORATION PROCESS.

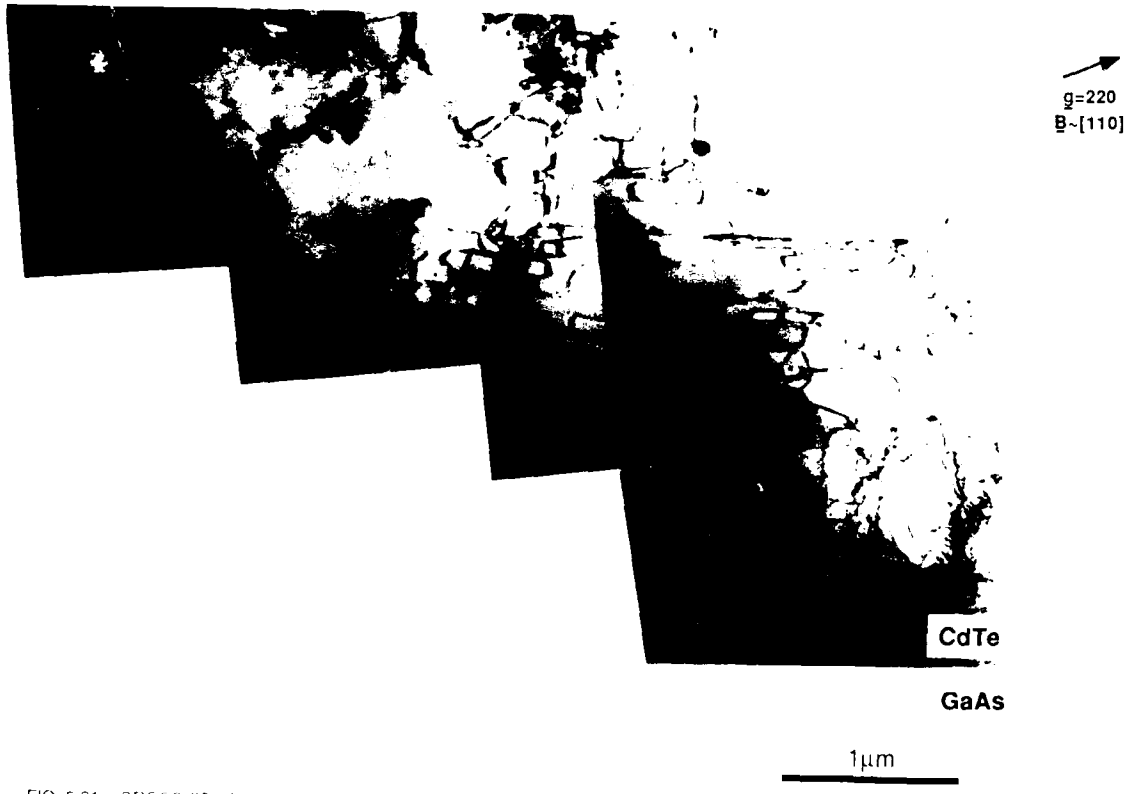

FIG. 5.31 CROSS SECTIONAL TEM MICROGRAPH OF A (111) CADMIUM TELLURIDE LAYER DEPOSITED ON A GALLIUM ARSENIDE SUBSTRATE AT 210 C BY A UHV EVAPORATION PROCESS

5.5 X-ray diffraction

5.5.1 Single crystal layers

The epitaxial layers were assessed for their crystalline quality using single crystal x-ray diffractometry. The values of the FWHM together with the growth temperatures and layer thicknesses are tabulated in table 5.2.

Figure 5.32 shows the x-ray diffraction trace of Run 6, a thermally grown layer. The FWHM of the 400 peak is ~1100arcsecs, the maximum of which occurs at a Bragg reflection angle(2θ) of 56.7°.

Similarly for Run 5, deposited photolytically at 350°C, a FWHM of 1385 arc secs was measured. However as the thicknesses of the two layers are different (0.3μm c.f. 1.5μm) a true comparison cannot be made between the quality of these two layers. However the crystallinity of the thermally grown layer is better as the lower FWHM was also the thinner layer. Run 13 shows a similar FWHM to Run 5 of ~1385 arcsecs for approximately the same layer thickness, however XTEM does show the presence of a polycrystalline region at the interface.

For Run 18 the x-ray diffraction curve (figure 5.33) shows peak splitting of the $K\alpha_1$ and of the $K\alpha_2$ wavelengths and the rocking curve has a peak width of 969 arc secs. This indicates the far higher crystalline quality of the layer compared to the earlier layers, although the layer thickness of 2.3μm is also the greatest in this case with less contribution from the interface region.

The rocking curve width for Run 19 has a FWHM of 1523 arc secs and this relatively large value is to be expected due to the layer thickness of ~0.7μm. Also noted from the rocking curve (figure 5.34) is that the peak maximum is shifted to 57.08°, a shift of 1368 arc secs from the expected (400) reflection. This may be due to uniform strain in the layer and is possibly related to the XTEM observation showing a reduction in dislocation structure which would be expected to strain relieve the layer. Using this value of twice the Bragg reflection angle for the (400) peak, the corresponding lattice parameter of the reflecting planes, i.e those parallel to the interface can be calculated to be equal to 6.4465 Å.

5.5.2 Polycrystalline layers

Run 16, the columnar polycrystalline sample deposited at 250°C with defocussed UV, shows a high degree of preferred orientation in the (100) direction with

RUN	METHOD	TEMPERATURE (°C)	THICKNESS (μm)	FWHM (arcsecs)
5	UV focussed	350°C	1.6	1385
6	Thermal	350°C	0.3	1100
13	UV focussed	300°C	1.2	1385
16	UV defocussed	250°C	0.3	1680
18	UV defocussed	300°C	2.3	969
19	UV defocussed	300°C	0.7	1523
21	Thermal	300°C	0.27	1800

TABLE 5.2

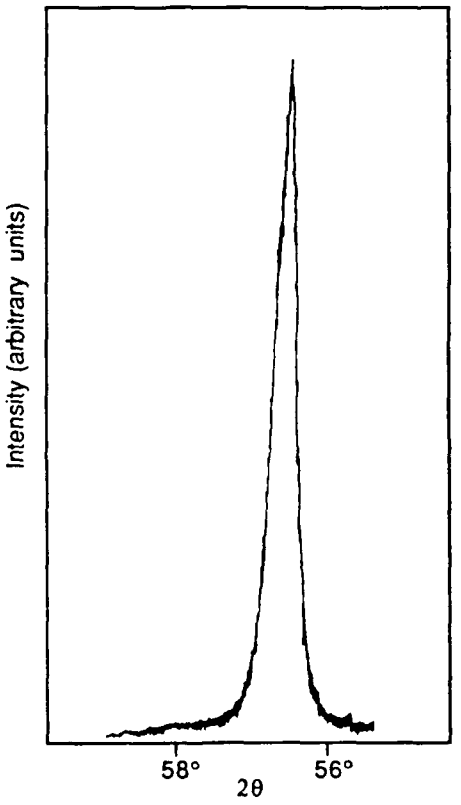

FIG. 5.32. X-RAY DIFFRACTION PEAK FOR THE (400) REFLECTION FROM A 0.3μm THICK CADMIUM TELLURIDE LAYER DEPOSITED THERMALLY ONTO A (100) GALLIUM ARSENIDE SUBSTRATE AT 350°C WITH DMCd:DETe=1.

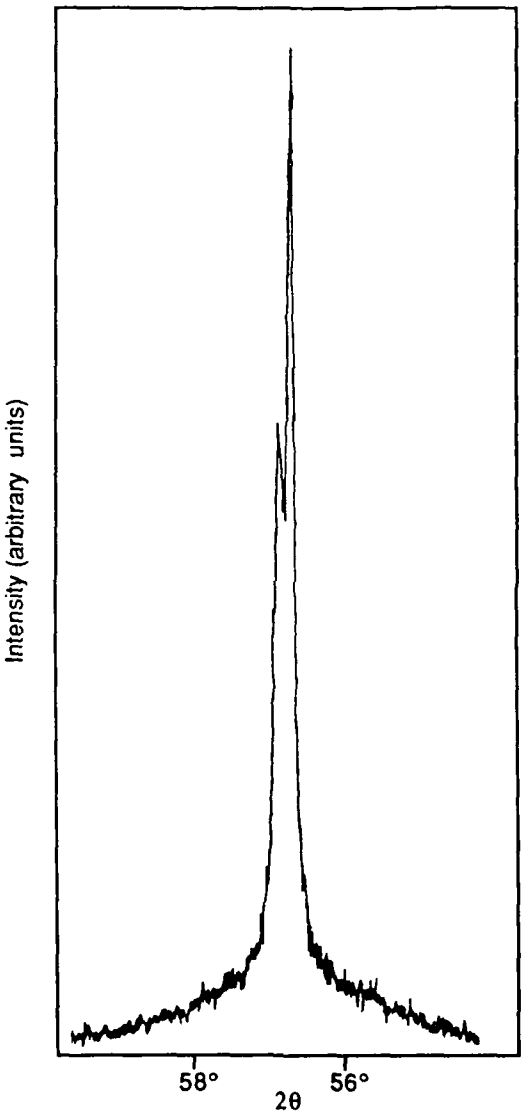

FIG. 5.33. X-RAY DIFFRACTION PEAKS FOR THE (400) REFLECTION FROM A 2.3μm THICK CADMIUM TELLURIDE LAYER PHOTO-DEPOSITED ONTO A (100) GALLIUM ARSENIDE SUBSTRATE AT 300°C WITH DMCd:DETe=1 AND DEFOCUSSED UV.

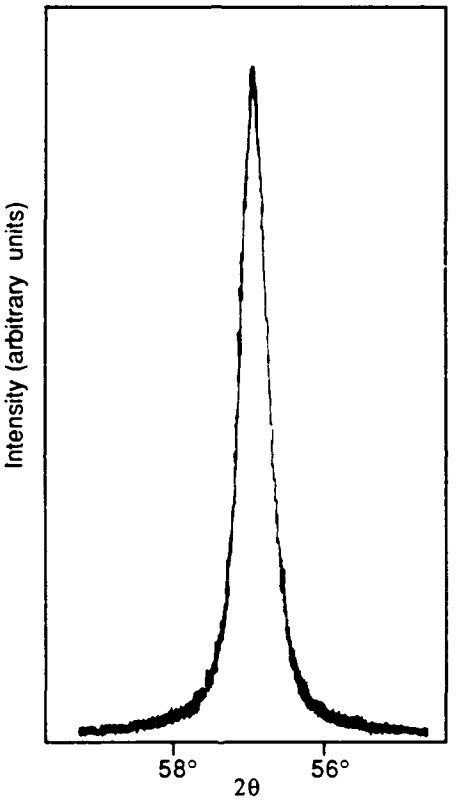

FIG. 5.34. X-RAY DIFFRACTION PEAK FOR THE (400) REFLECTION FROM A 0.7μm THICK CADMIUM TELLURIDE LAYER PHOTO-DEPOSITED ONTO A (100) GALLIUM ARSENIDE SUBSTRATE AT 300°C WITH DMCD:DETE=1.5 AND DEFOCUSSED UV.

a FWHM of 1680 arc secs. The spectrum for this layer is shown in figure 5.35 and the polycrystalline nature of the layer is apparent from the high background level detected throughout the entire scan.

X-ray diffraction on Runs 1, 2 and 3 shows a high background throughout the angular range although peaking at ~47° is superimposed onto the background signal and corresponds to a hexagonal tellurium phase of (200) orientations (figure 5.36).

This suggests that at least one factor preventing successful epitaxial growth is the excessively tellurium rich conditions utilised which then result in the simultaneous deposition of tellurium with CdTe.

In addition for Run 3 strong peaking at 23.8° due to the preferential (111) contribution (figure 5.37) is in agreement with the TEM diffraction pattern of this layer. Except for Run 16 all the other remaining polycrystalline layers, i.e. Runs 4, 7, 11, 12 and 14 similarly show a preferred orientation of (111). Comparison of the growth conditions for each of these layers indicates that this is the preferred orientation for polycrystalline growth and suggests that it is more favourable for this orientation to be achieved under high supersaturation conditions.

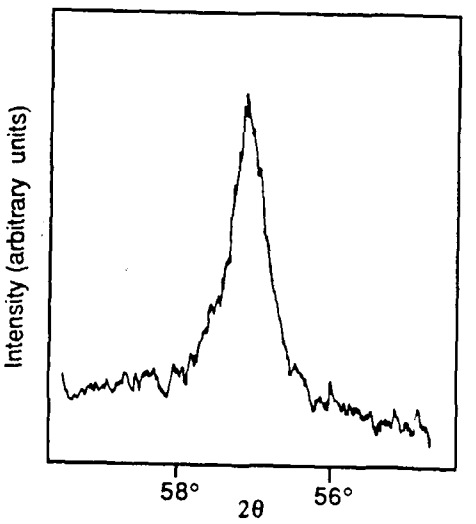

FIG. 5.35. X-RAY DIFFRACTION PEAK FOR THE (400) REFLECTION FROM A 0.3μm THICK CADMIUM TELLURIDE LAYER PHOTO-DEPOSITED ONTO A (100) GALLIUM ARSENIDE SUBSTRATE AT 250°C WITH DMCD:DETE=2 AND DEFOCUSSED UV.

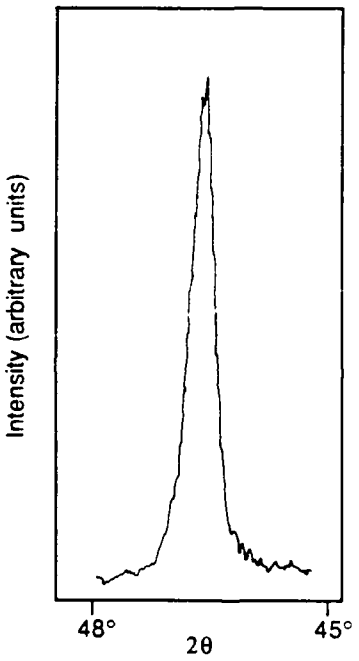

FIG. 5.36. X-RAY DIFFRACTION PEAK FOR THE TELLURIUM (200) REFLECTION FROM A POLYCRYSTALLINE CADMIUM TELLURIDE LAYER PHOTO-DEPOSITED ONTO A (100) GALLIUM ARSENIDE SUBSTRATE AT 230°C WITH DETe RICH CONDITIONS AND FOCUSSED UV.

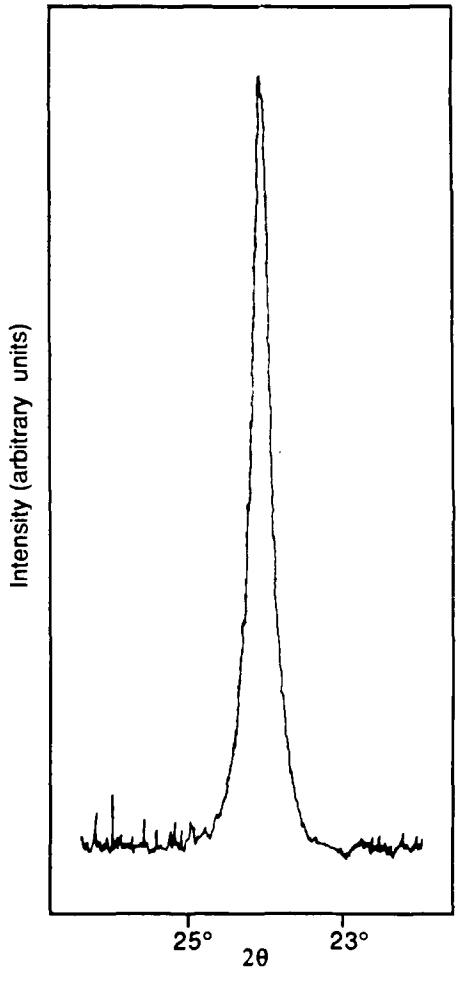

FIG. 5.37. X-RAY DIFFRACTION PEAK FOR THE (111) REFLECTION FROM A POLYCRYSTALLINE CADMIUM TELLURIDE LAYER PHOTO-DEPOSITED ONTO A HYDROGEN CLEANED (100) GALLIUM ARSENIDE SUBSTRATE AT 230°C WITH DETE RICH CONDITIONS AND FOCUSSED UV.

5.6 Secondary ion mass spectrometry (SIMS)

The SIMS depth profile for gallium through the layer of Run 5 is shown in figure 5.38. A concentration of 0.002ppma was detected throughout the layer. In comparison the layer deposited thermally at the same temperature of 350°C has a higher concentration in the layer of 7ppma (figure 5.39) and this increase is attributable to the reduced growth rate of the thermal deposition. The heavily dislocated structure which is in evidence uniformly for this layer would also contribute to this increase by providing a high mobility route for the migration of atoms by pipe diffusion. The gallium level of the photodeposited layer compares favourably with the results of Giess et al.[42] for depositions carried out at 410°C. These authors reported a concentration of ~0.1ppma in a high x CMT buffer layer at 4μm from the interface.

Run 13, deposited photolytically at a reduced temperature of 300°C has a gallium level in the layer with an average value of ~6ppma. Compared with Run 5, this layer although deposited at reduced temperature was grown for a longer duration and with reduced growth rates. Both these factors would increase the gallium diffusion into the layer. However more significantly this layer has been shown to have a polycrystalline region at the interface thus increasing the possibility of enhanced gallium diffusion along the grain boundaries, leading to an accumulation at the CdTe single crystal/polycrystalline boundary, which then subsequently diffuses into the single crystal CdTe. This is indicated by the less steep gradient (figure 5.40) through the interface.

Profiling for contamination of this layer by sodium, lithium, magnesium, iron, aluminium and silicon were also undertaken (figures 5.41(a)-(f)). Very little lithium (0.0006ppma) was detected in the layer. Sodium was detected at a level of ~0.03ppma in the layer rising to a level of 5ppma at the layer surface. Magnesium and aluminium were also found to be present at a level of less than 0.1 ppma. These levels of contamination are lower than the contamination levels quoted for the alkyls.

Aluminium and silicon show a different behaviour in that their concentrations increase towards the layer surface, immediately from the interface. The aluminium at the interface is 0.4ppma and increases to 7ppma at the layer surface whilst the silicon increases from a value of 200ppma to 3000 ppma. This behaviour is not characteristic of contamination during the growth process or diffusion from the substrate and also as the silicon contamination is well in excess of the 15ppm level in the reactant, this is more likely to be due to external contamination and is attributable to sample handling after growth or perhaps contamination in the spectrometer.

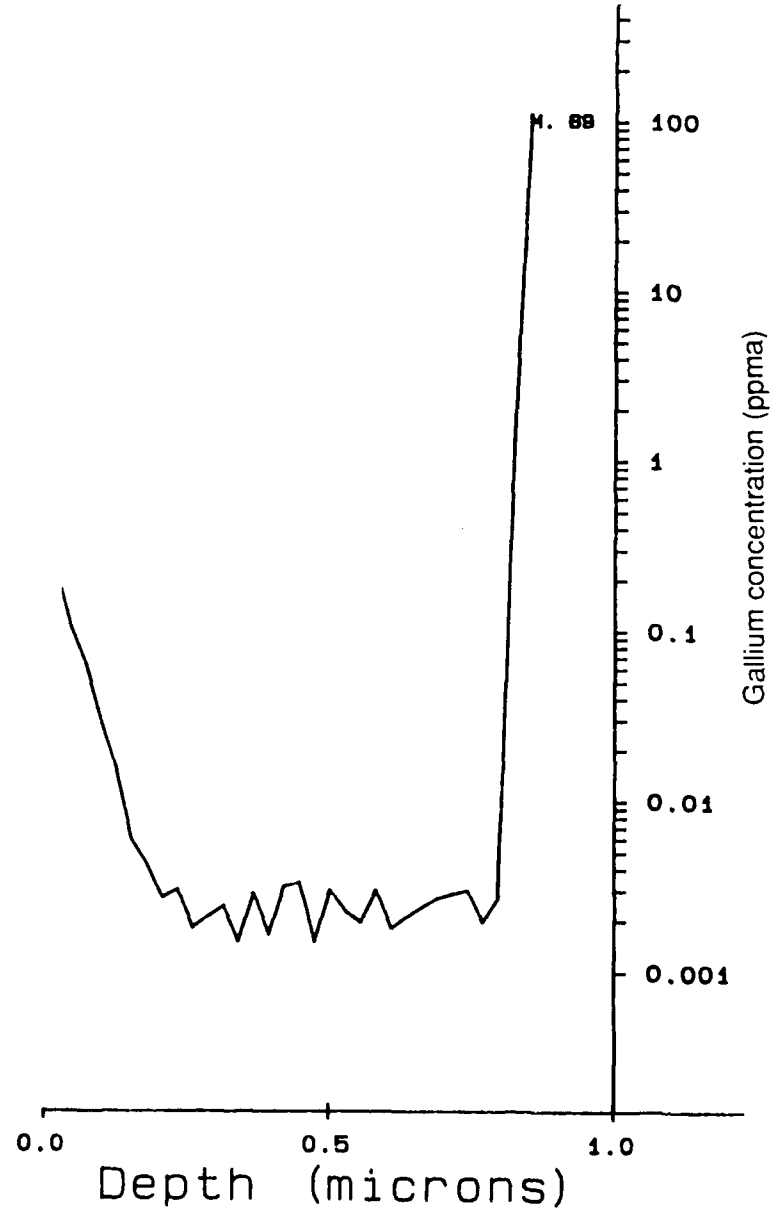

FIG. 5.38. SIMS DEPTH PROFILE FOR ^{69}Ga IN A CADMIUM TELLURIDE LAYER PHOTO-DEPOSITED ONTO A (100) GALLIUM ARSENIDE SUBSTRATE AT 350°C WITH DMCd:DETe=1 AND FOCUSSED UV.

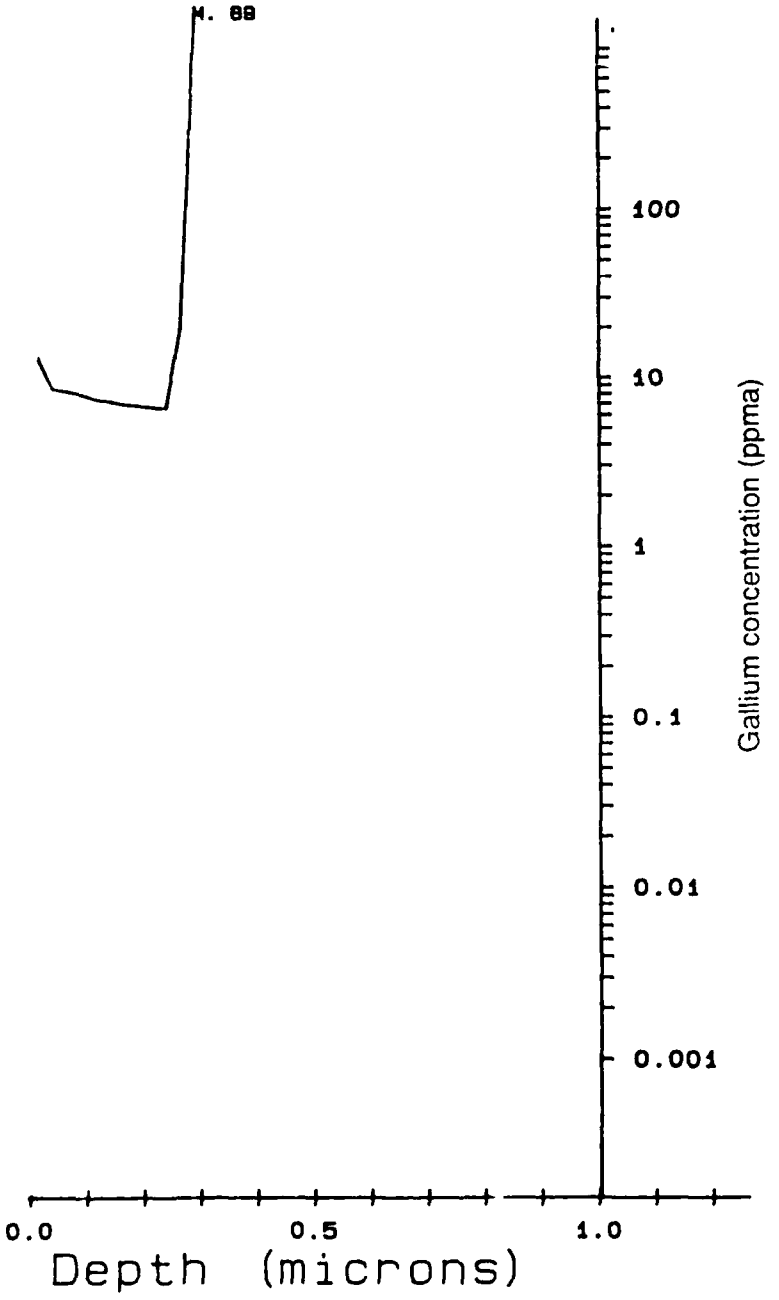

FIG. 5.39. SIMS DEPTH PROFILE FOR ^{69}Ga IN A CADMIUM TELLURIDE LAYER DEPOSITED THERMALLY ONTO A (100) GALLIUM ARSENIDE SUBSTRATE AT 350°C WITH DMCd:DETe=1.

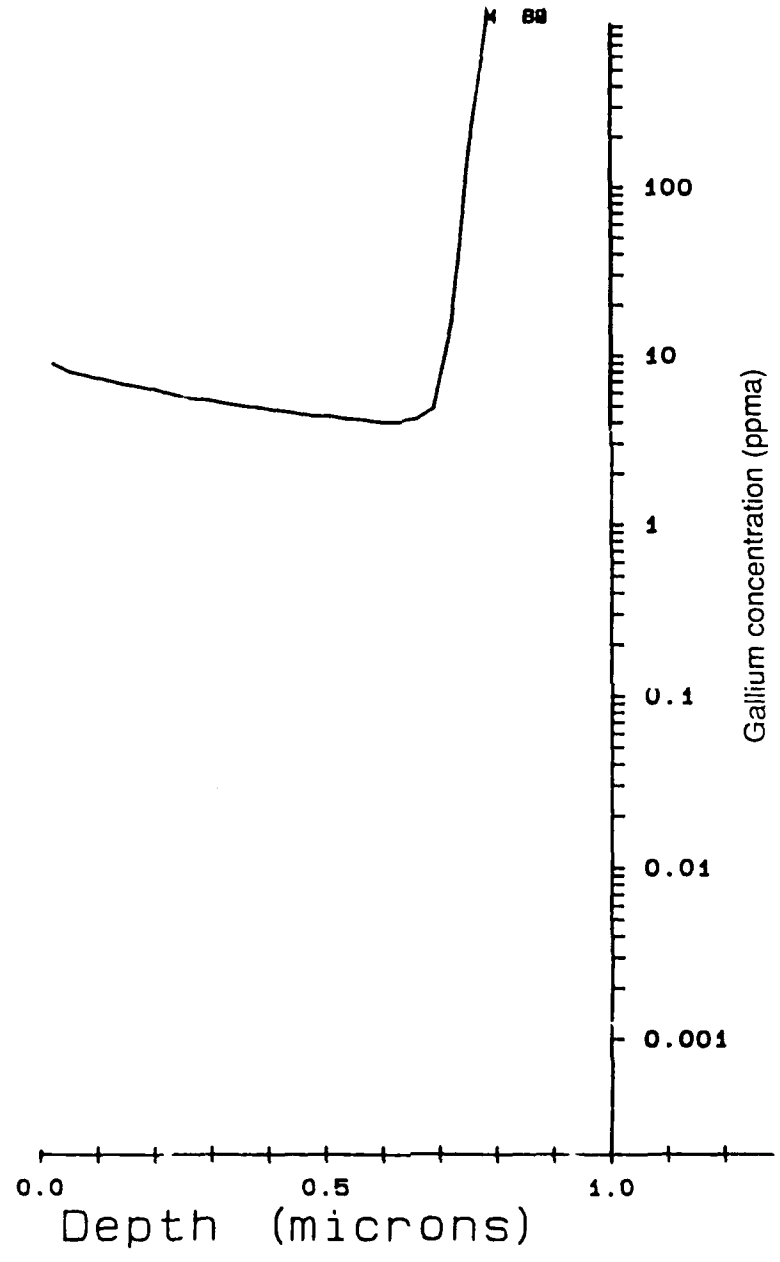

FIG. 5.40. SIMS DEPTH PROFILE FOR ^{69}Ga IN A CADMIUM TELLURIDE LAYER PHOTO-DEPOSITED ONTO A (100)GALLIUM ARSENIDE SUBSTRATE AT 300°C WITH DMCd:DETe=2 AND FOCUSSED UV.

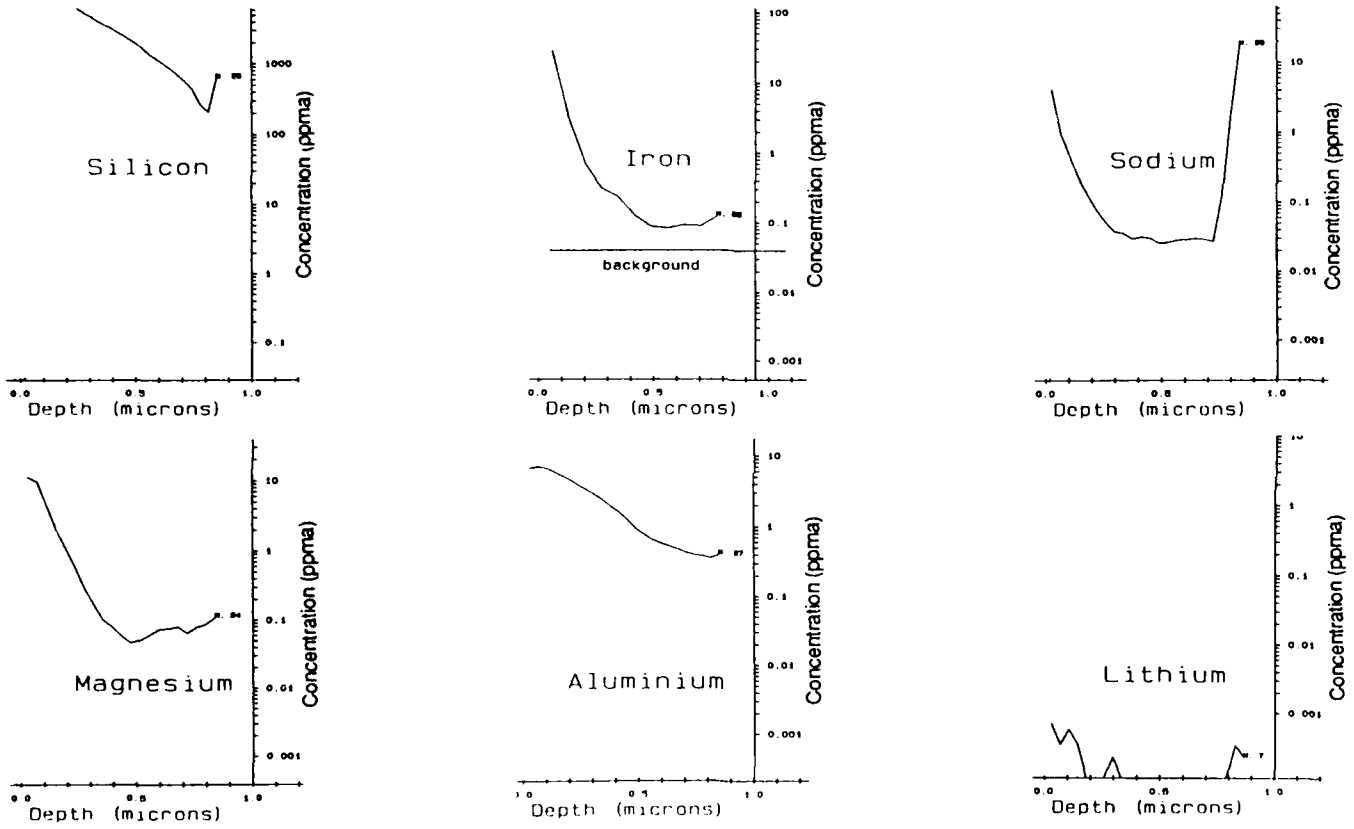

FIG. 5.41. SIMS DEPTH PROFILES FOR ^{28}Si, ^{56}Fe, ^{23}Na, ^{24}Mg, ^{27}Al AND ^{7}Li IN A CADMIUM TELLURIDE LAYER PHOTO-DEPOSITED ONTO A (100)GALLIUM ARSENIDE SUBSTRATE AT 350°C WITH DMCd:DETe=1 AND FOCUSSED UV.

5.7.1 Growth rate dependence with DMCd concentration

A curve of growth rate with variation of D.MCd partial pressure at a constant DETe partial pressure is shown in figure 5.42. The plotted points do not all correspond to the same growth temperature, e.g. the points of run 5 (350°C) and 14 (250°C) would give reduced and increased growth rates respectively if deposited at 300°C. However it is clear that the general trend is for a growth rate reduction with increasing DMCd concentration. This graph also shows that at higher DMCd partial pressures the growth rate approaches saturation at values greater than 0.8 torr. Even once the DMCd partial pressure exceeds the DETe value the growth rate continues to change when it would be expected that the DETe partial pressure would be rate controlling. This is further illustrated by the curve of the growth rate versus fractional input ratio (figure 5.43) which shows a family of curves at the temperatures of 250°C, 300°C and 350°C (projected) for both focussed and defocussed UV conditions. It is quite clear from this data that as the DMCd:DETe input ratio is increased the growth rate decreases.

5.7.2 Growth rate dependence with DETe concentration

Figure 5.44 shows a curve of the growth rate versus DETe partial pressure and the growth rate approximately follows a cube root dependence with DETe partial pressure. Increase of DETe over the DMCd concentration has little effect on the growth rate thus indicating the rate controlling species is the DMCd.

5.7.3 Site blocking

The decrease in the growth rate at increased DMCd concentrations is indicative of a site blocking mechanism whereby DMCd species adsorb onto the substrate surface and somehow prevent formation of CdTe by inhibiting adsorption or reaction with DETe molecules.

An alternative explanation of this effect may be attributable to an adduct or complex reaction mechanism where a significant increase in the concentration of any one of the alkyls would lead to the increase in the reactions occurring in the gas phase and a corresponding decrease in the surface reaction rate. However this explanation would seem to be unlikely for the following reasons:-

1. Increase of the alkyl input ratio at fixed DETe partial pressure,(i.e. greater DMCd concentrations) would be expected to lead to a greater degree of nucleation in the vapour phase and consequently a degradation of epitaxy. This does not occur and in fact results in enhanced crystallinity.

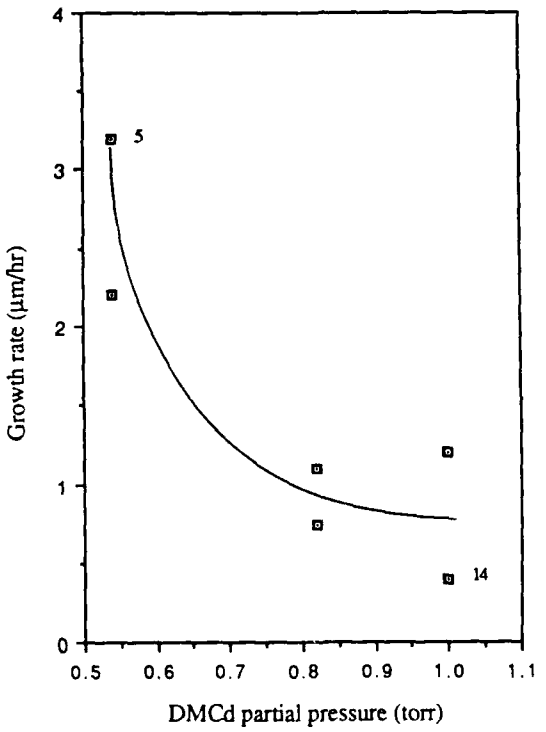

FIG. 5.42. CADMIUM TELLURIDE GROWTH RATE VARIATION AS A FUNCTION OF DMCd PARTIAL PRESSURE FOR DEPOSITIONS ONTO (100) GALLIUM ARSENIDE SUBSTRATES WITH UV ILLUMINATION.

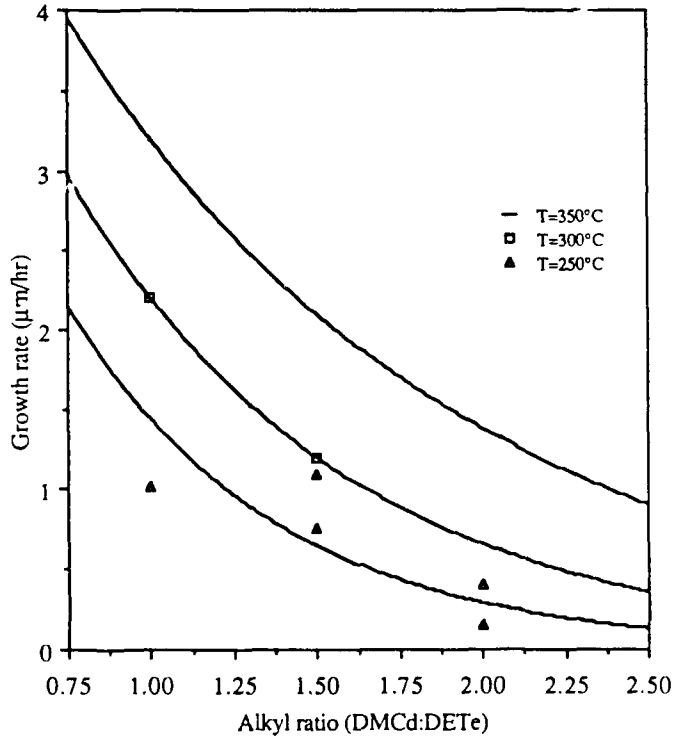

FIG. 5.43. CADMIUM TELLURIDE GROWTH RATE VARIATION AS A FUNCTION OF DMCd:DETE ALKYL RATIO FOR DEPOSITIONS ONTO (100) GALLIUM ARSENIDE SUBSTRATES WITH UV ILLUMINATION.

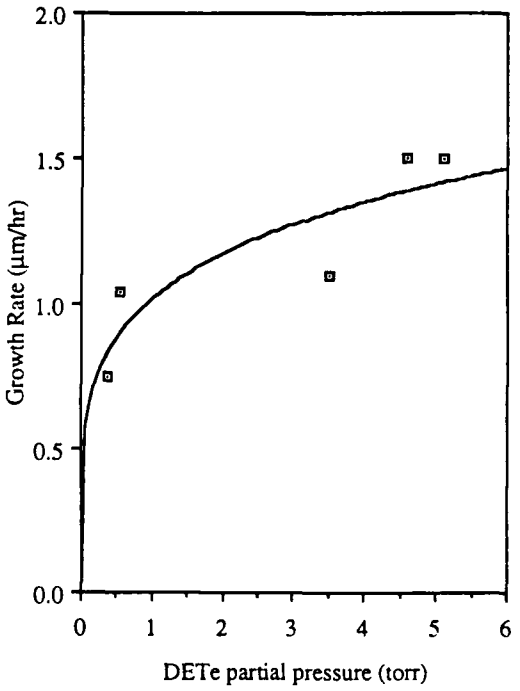

FIG. 5.44. CADMIUM TELLURIDE GROWTH RATE VARIATION AS A FUNCTION OF DETe PARTIAL PRESSURE FOR DEPOSITIONS ONTO (100) GALLIUM ARSENIDE SUBSTRATES WITH UV ILLUMINATION.

2. With defocussed UV conditions the effect is similar even though a substantial reduction of the Cd and Te supersaturations is obtained and vapour phase growth would not be as severe. This is also supported by the increase in the crystalline quality of the deposits at the lower UV intensities which indicates the reduction in probability of homogeneous vapor phase nucleation.

A plot of the logarithm of DMCd partial pressure against the logarithm of the growth rates in figure 5.45 shows a slope of negative gradient equal to 2, indicating that the growth rate is falling with a dependence on the inverse square root of DMCd partial pressure.

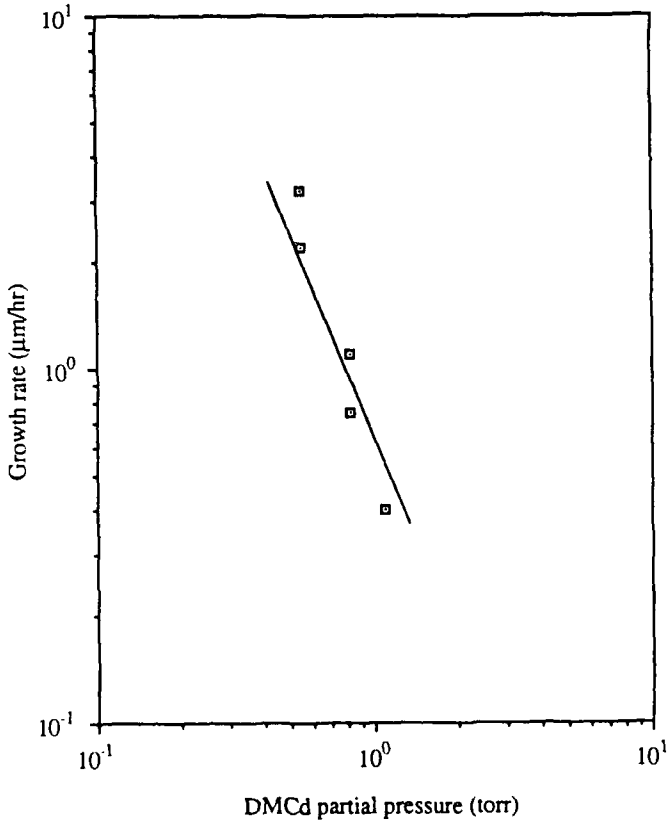

FIG. 5.45. CADMIUM TELLURIDE GROWTH RATE VARIATION AS A FUNCTION OF DMCd PARTIAL PRESSURE FOR DEPOSITIONS ONTO (100) GALLIUM ARSENIDE SUBSTRATES WITH UV ILLUMINATION.

5.8 Adsorption

In an attempt to model this decrease in the growth rate as a function of the DMCd partial pressure we may consider the adsorption of DMCd and DETe on the substrate surface.

If we assume that the DETe and the DMCd are adsorbed on x and y surface sites respectively thus:-

$$DETe(g) + xs \rightarrow DETe^{*}$$

and similarly for the DMCd,

$DMCd(g) + ys \rightarrow DMCd^{*}$, where * denotes a surface adsorbed species.

Then in the case of DETe adsorption the rate of adsorption r_1, is proportional to the partial pressure of the alkyl and the fraction of the surface which is available for adsorption, θ

$$\text{i.e.} \qquad r_1 = k_1 \theta \, p^{1/x}_{DETe} \quad \text{.....5.1}$$

and the desorption rate of the DETe from the substrate is proportional to the amount present on the surface, θ_{DETe} hence giving a desorption rate r_{-1} of

$$r_{-1} = k_{-1} \theta_{DETe} \quad \text{.....5.2}$$

Then for adsorption-desorption processes occurring under equilibrium conditions, the rate of adsorption equals the rate of desorption ($r_1 = r_{-1}$) and, also using the fact that the fraction of the surface unoccupied θ is given by $\theta = 1 - \theta_{DETe} - \theta_{DMCd}$, yields the following expressions for the adsorption isotherms for θ_{DETe} and θ_{DMCd} :-

$$\theta_{DETe} = \frac{\beta_{DETe} p^{1/x}_{DETe}}{1 + \beta_{DETe} p^{1/x}_{DETe} + \beta_{DMCd} p^{1/y}_{DMCd}} \quad \text{..... 5.3}$$

$$\theta_{DMCd} = \frac{\beta_{DMCd} p^{1/y}_{DMCd}}{1 + \beta_{DMCd} p^{1/y}_{DMCd} + \beta_{DETe} p^{1/x}_{DETe}} \quad \text{..... 5.4}$$

where β equals k_1/k_{-1} and is the ratio of adsorption to desorption rate constants.

Including the effect of inhibitors which do not take part in the actual deposition reaction but which occupy surface adsorption sites,

$$\theta_{DETe} = \frac{\beta_{DETe} p_{DETe}^{1/x}}{1+\beta_{DETe} p_{DETe}^{1/x}+\beta_{DMCd} p_{DMCd}^{1/y}+\beta_i p_i^{1/n}} \quad \text{.....5.5}$$

where p_i is the partial pressure of the inhibitor which occupies n surface sites on adsorption (per molecule). An equivalent equation may be written for the DMCd adsorption.

Alternatively if the adsorption of the DMCd and the DETe occur independently, that is to say the reactants do not occupy similar types of sites, then θ_{DETe} and θ_{DMCd} simplify to :-

$$\theta_{DETe} = \frac{\beta_{DETe} p_{DETe}^{1/x}}{1+\beta_{DETe} p_{DETe}^{1/x}} \quad \text{.....5.6}$$

and similarly for θ_{DMCd}. If the effect of inhibitors is again taken into account then the following expression is obtained for the DETe:-

$$\theta_{DETe} = \frac{\beta_{DETe} p_{DETe}^{1/x}}{1+\beta_{DETe} p_{DETe}^{1/x}+\beta_i p_i^{1/n}} \quad \text{.....} \quad 5.7$$

An equivalent expression for the DMCd adsorption may be also written.

5.8.1 Langmuir-Hinshelwood model

The Langmuir-Hinshelwood model assumes that both the DMCd and the DETe are adsorbed on the substrate surface. This may occur either competitively or independently giving a growth rate, $R = K\theta_{DETe}\theta_{DMCd}$.

Considering firstly the case of competitive adsorption without the effect of inhibitors substitution of equation 5.3 and 5.4 gives the following growth rate:-

$$R = \frac{k\beta_{DETe}\beta_{DMCd} p_{DETe}^{1/x} p_{DMCd}^{1/y}}{(1+\beta_{DETe} p_{DETe}^{1/x}+\beta_{DMCd} p_{DMCd}^{1/y})^2} \quad \text{.....} \quad 5.8$$

Secondly, for independent adsorption substituting equation 5.6 and its equivalent for DMCd coverage gives

$$R = \frac{k\beta_{DETe}\beta_{DMCd}p_{DETe}^{1/x}p_{DMCd}^{1/y}}{(1+\beta_{DETe}p_{DETe}^{1/x})(1+\beta_{DMCd}p_{DMCd}^{1/y})} \quad \ldots\ldots\ldots \quad 5.9$$

Taking $\beta_{DETe}p_{DETe}<<1$, which means that the substrate surface is not saturated by DETe (a reasonable assumption as it is known that β_{DETe} is small[10]) and also assuming strong adsorption by DMCd, i.e. $\beta_{DMCd}p_{DMCd}>>1$, then for the former case equation 5.6 simplifies to

$$R = \frac{k\beta_{DETe}p_{DETe}^{1/x}}{\beta_{DMCd}p_{DMCd}^{1/y}} \quad \ldots\ldots\ldots \quad 5.10$$

and for the case of independent adsorption using the same assumptions equation 5.7 gives:-

$$R = k\,\beta_{DETe}\,p^{1/x}_{DETe} \quad \ldots\ldots\ldots \quad 5.11$$

Thus in this latter case the growth rate is invariant with the partial pressure of the DMCd and hence is clearly not applicable. In the former case of competitive adsorption the growth rate decreases with increasing DMCd partial pressure.With a site dependence of 1, i.e. y=1, $R \alpha 1/p$ and greater y values give a reduced growth rate dependence with DMCd partial pressures.

The reaction rate may be further modified by the presence of inhibitors which occupy surface adsorption sites thus preventing adsorption of the active DMCd and DETe species. These inhibitors may be reaction products from the adsorbed DMCd or DETe, the helium carrier gas or even the DMCd or DETe reactants which though occupying surface adsorption sites do not take part in the reaction.

The inclusion of the inhibitors leads to the modification of the rate equations as follows:-

for competitive adsorption

$$R = \frac{k\beta_{DETe}\beta_{DMCd}p_{DETe}^{1/x}p_{DMCd}^{1/y}}{(1+\beta_{DETe}p_{DETe}^{1/x}+\beta_{DMCd}p_{DMCd}^{1/y}+\beta_i p_i^{1/n})^2} \quad \ldots\ldots\ldots \quad 5.12$$

and for independent adsorption

$$R = \frac{k\beta_{DETe}\beta_{DMCd}p_{DETe}^{1/x}p_{DMCd}^{1/y}}{(1+\beta_{DETe}p_{DETe}^{1/x}+\beta_i p_i^{1/n})(1+\beta_{DMCD}p_{DMCd}^{1/y}+\beta_i p_i^{1/n})} \quad \ldots\ldots\ldots \quad 5.13$$

Then again assuming $\beta_{DETe}p_{DETe}$ is small, i.e.weak adsorption of DETe and for large $\beta_i p_i$:-

$$R = \frac{k\beta_{DETe}\beta_{DMCd}p_{DETe}^{1/x}p_{DMCd}^{1/y}}{\beta_i^2 p_i^{2/n}} \quad \ldots\ldots\ldots 5.14$$

for both forms of adsorption.

If the inhibitor is a reaction product which remains adsorbed after decomposition of the DMCd then the assumption of large $\beta_i p_i$ may not be valid due to small β_i, i.e. it would be expected that the reaction products would desorb rapidly. However if the reaction proceeds by adsorption of DMCd which then decomposes to leave adsorbed cadmium on the substrate surface prior to reaction with DETe, as proposed by Ghandi and Bhat[19] for the thermal growth of CdTe, the preceding assumption may be justified. In this case then it is reasonable to assume that p_i is proportional to p_{DMCd} giving a growth rate variation as follows

$$R \propto \frac{p_{DETe}^{1/x}}{p_{DMCd}^{2/n-1/y}} \quad \ldots\ldots\ldots \quad 5.15$$

which for n=1, y=2 gives R proportional to $1/(p_{DMCd})^{3/2}$ and approaches an inverse square dependence as y becomes large with n =1.

The different values of n and y are not inconsistent with the reaction proceeding by dissociation of the adsorbed DMCd yielding Cd as in this case n (site occupancy of adsorbed Cd) would be smaller than y (occupancy of DMCd) simply from considerations of the size of the adsorbed species.

The growth rate dependence on the cube root of DETe partial pressure is given by x=3, i.e. triple site occupancy. This does appear to be at variance with Ahlgren et al.[34] who have proposed a site coverage of one DETe molecule per two sites to obtain a square root dependence of growth rate with DETe partial pressure. However the growth system these authors investigated was HgTe which involved elemental mercury which may influence site coverages.

Thermal deposition of CdTe using di-isopropyltelluride and dimethylcadmium also show a growth rate reduction with increasing Cd:Te reactant ratios from 16μm/hr to 6μm/hr with ratios from 0.36 to 2 (Irvine and Giess[90]). The dependence of this reduction is proportional to the inverse square root of DMCd and corresponds to a y value of 2 for competitive adsorption without inhibitors (equation 5.8). Although this seems to be inconsistent with the $1/p^2$ dependence obtained, differences in size of the Te source molecules between the two ... es would be expected to affect the amount of adsorption of the DMCd and hence the pressure dependence. With DIPTe the larger molecule may prevent as much adsorption of the DMCd as occurs in the case of DETe leading to a less steep growth rate reduction.

The best fitting model describing both the growth rate reduction with increase of DMCd ($\alpha 1/p^2$) and increase of growth rate with DETe partial pressure ($\alpha p^{1/3}$) is that with either competitive or independent adsorption, with the adsorbed Cd behaving as an inhibitor. Though the competitive adsorption, without considering the effect of inhibitors, also gives the cube root increase of growth rate with DETe partial pressure, the reduction with DMCd is given only by an inverse relationship. With inhibitors the experimental results are approached with n=1, x=3 and large y. If x=y=3, then reasonable agreement is obtained with the experimental observations.

5.9 Homogeneous nucleation

The poorer crystallinity obtained at reduced growth temperatures and increased UV intensities may be modelled by considering the excess chemical potential for homogeneous nucleation which is given by:-

$$\Delta\mu = RT \ln[p_v/p_e] \quad \ldots\ldots\ldots \quad 5.16$$

where R is the universal gas constant, T the temperature and p_v and p_e the reactant vapour pressure and the equilibrium vapour pressure respectively.

Thus relatively larger values of this excess chemical potential lead to an increase in the probability of homogeneous vapour phase nucleation and result in poorer crystalline quality. This is achieved at either increased reactant partial pressure (greater p_v) or at reduced temperatures (lower p_e). The supersaturation may be reduced by reducing the bubbler flow rate or by defocussing the UV. Work by Irvine et al.[91] has succeeded in identifying a region where a balance between p_v and p_e results in successful epitaxy below a certain value of excess chemical potential, the critical value for homogeneous nucleation.

An extreme example of homogeneous vapour phase nucleation can be seen in the difference in the surface morphology of Runs 1 and 4, where the dissociation was photoenhanced and purely pyrolytic respectively. The surface of Run 1 showed many non faceted particles distributed randomly on the layer which have formed in the vapour phase and have settled on the surface. In contrast the thermal deposition exhibits a complete lack of these features.

5.9.1 Growth rate dependence on UV intensity

Figure 5.46 shows a graph of the growth rate versus temperature at a constant value of DETe partial pressure (0.54 torr). The data points corresponding to different DMCd and DETe ratios are plotted for both focussed and defocussed lamp conditions. As in the graph of growth rate versus reactant input ratio (figure 5.43) it is apparent that at any one temperature increasing the DMCd:DETe results in growth rate reduction which has already been attributed to a site blocking mechanism. More significantly, paired points for focussed and defocussed conditions can be identified for each input ratio and these show that almost similar growth rates are achieved even though a x90 reduction in UV intensity is obtained in the defocussed case. Thus the extra supersaturation generated in the vapour does not result in greater incorporation of Cd and Te atoms into the growing layer over the level with defocussed conditions (i.e. the

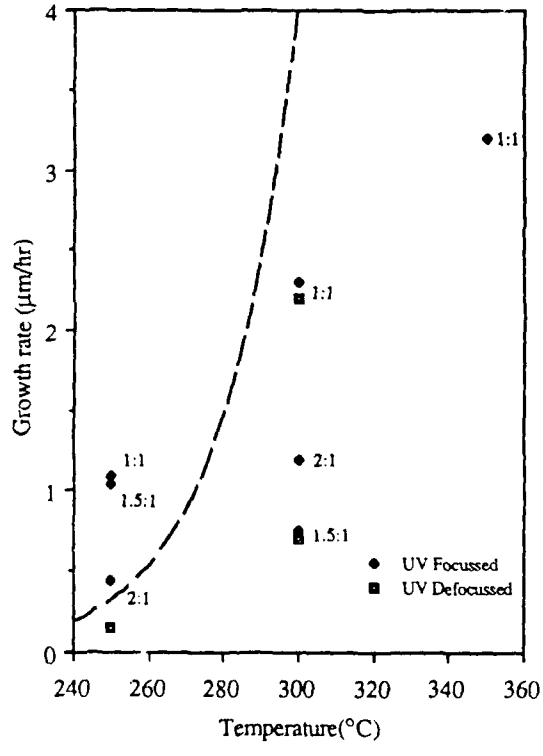

FIG. 5.46. CADMIUM TELLURIDE GROWTH RATE VARIATION AS A FUNCTION OF TEMPERATURE FOR DEPOSITIONS WITH FOCUSSED AND DEFOCUSSED UV ONTO (100) GALLIUM ARSENIDE SUBSTRATES. THE CORRESPONDING DMCd:DETe ALKYL RATIO IS MARKED. THE GRAPH ALSO SHOWS THE CRITICAL CURVE FOR HOMOGENEOUS NUCLEATION AFTER IRVINE AND MULLIN[91].

ratio of the rate of vapour phase nucleation to the rate of the surface reaction is greater with focussed UV).

Therefore with the defocussed beam conditions the maximum epitaxial growth rate has been attained and any further increase in the UV intensity although leading to a greater supersaturation does not lead to greater deposition rates but only serves to break up the epitaxial growth and thus this is also consistent with equation 5.16 and the resultant poorer crystallinity with the focussed lamp.

The effect of increased UV intensity on the excess chemical potential for nucleation in the vapour phase can be calculated by assuming that all the UV photons absorbed by the DMCd result in an equivalent number of cadmium atoms generated in the vapour phase, and with a knowledge of the absorption cross-section, the UV path length through the reaction cell, and the temperature. With a UV intensity when using a focussed beam of $1Wcm^{-2}$ there are 1.3E 22 photons $m^{-2}s^{-1}$ entering the reactor. The number of absorbed photons and hence the cadmium atom production rate I_A equals the difference between the incident uv intensity and the "outgoing" intensity,

$$\text{i.e. } I_A = I_O - I, \text{ where } I = I_o \exp[-\sigma pL/kT] \quad \ldots\ldots\ldots \quad 5.17$$

and I_O is the incident intensity, p the partial pressure of reactant, L the uv path length and σ the cross section for dissociation.

Thus for a cross-section at 254nm of 5E-18 cm^2, a path length of 1cm, a temperature of 300°C and a DMCd partial pressure of 0.54 torr the number of cadmium atoms produced in the vapour equals 5.7E 16 $cm^{-2}s^{-1}$. Which for a total flow rate of 1000sccm (or flow velocity of $4.2cms^{-1}$) gives a cadmium atom concentration of 1.36E 16 cm^{-3} which is equivalent to a Cd vapour pressure of 0.82 torr or 1.08E-3 atm. Substituting this value of p_v in equation 5.16 for the excess chemical potential for homogeneous vapour phase nucleation and assuming congruent evaporation conditions ($p_{Cd} = 1/2\ p_{Te2}$), and using a value of p_e, the equilibrium pressure of Cd over CdTe at this temperature, of $\sim 10^{-12}$ atm. gives rise to a value for $\Delta\mu$ of 35kcal/mol. Similarly in the reduced UV intensity case, with an intensity of ~12 $mwcm^{-2}$ the $\Delta\mu$ value falls to $27.8kcalmol^{-1}$ and thus gives a quantitative indication to the reduced probability of vapour phase nucleation.

5.9.2 Effect of temperature on crystallinity

The effect of the reduction of temperature (with constant flow conditions) is

illustrated by reference to the micrographs of Run 5 (figure 5.6) and Run 7 (figure 5.8) where in the former case the growth is epitaxial and is obtained at the greater temperature whereas at the lower temperature of 300°C the layer is polycrystalline. Similarly a reduction of temperature from 300°C to 250°C (at constant flow conditions) resulted in a change from a dense packed columnar polycrystalline microstructure, Run 11, to one with a greater level of point nucleation and enhanced faceting, Run 12.

This illustrates the reduced surface diffusion and mobility of the atomic species at the lower temperatures leading to a greater probability of less ordered nucleation or random site nucleation. Also as predicted by equation 5.1 the greater probability of nucleation in the vapour phase will assist in the breakdown of epitaxy and help promote random nucleation at the reduced temperatures as $\Delta\mu$ approaches $\Delta\mu_{CRIT}$.

The dashed curve transposed onto the graph of figure 5.46 represents the maximum growth rates achievable before the effect of homogeneous vapour phase nucleation results in polcrystalline growth as has been predicted by Irvine et al.[91] The obtained growth rates agree well with this fitted curve. In the majority of cases the greater the deviation below the curve the better the resulting crystallinity, and it also shows the potential for higher epitaxial growth rates at higher temperatures.

The crystallinity of the single crystal layers (obtained with varying flow conditions) similarly shows a greater degree of crystalline perfection at the higher temperatures. A graph plotting the FWHM of the (400) CdTe x-ray diffraction peak against deposition temperature is shown in figure 5.47. This graph shows the improvement in the crystalline perfection of the CdTe layers with increasing temperature.

Although this graph does indicate the general trend it must be noted that a direct comparison of the individual layers is not reliable due to the differing thicknesses of the layers. Reduced layer thicknesses will result in a broadening of the rocking curve width due to an increase in the non uniform strain in the layer. Another limitation is that the diffraction process depends upon the interaction between a large number of planes and as the layer becomes thinner the process becomes more inefficient.

It is also observed from the growth experiments that control of the DMCd:DETe input ratio is more critical at the lower temperatures, i.e. at 350°C an input ratio of one could be tolerated resulting in epitaxial growth whereas at reduced temperatures the better crystallinity occurs at larger DMCd concentrations. This indicates that at the lower temperatures large deviations from stoichiometry are less likely to be tolerated and this

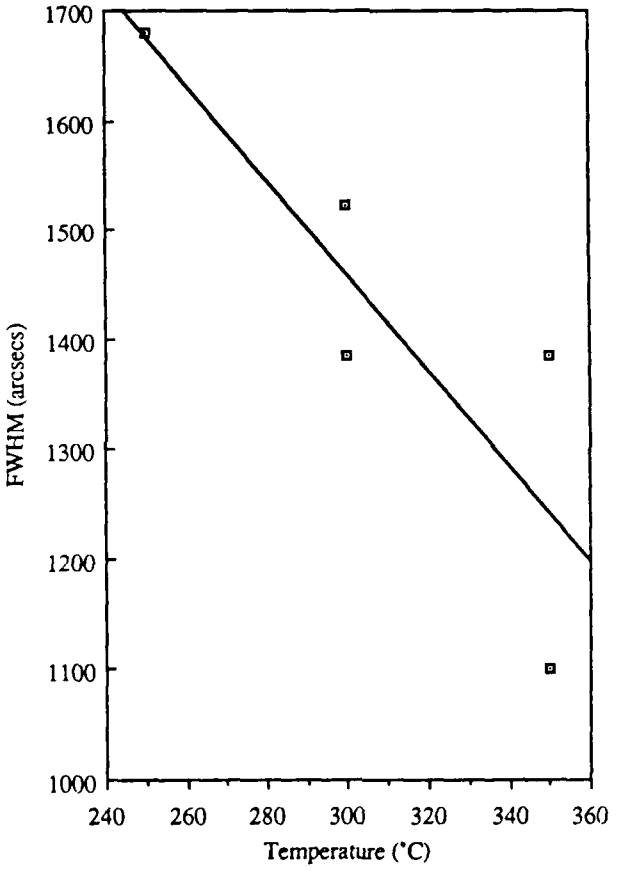

FIG. 5.47. VARIATION OF THE FWHM OF THE CADMIUM TELLURIDE (400) X-RAY DIFFRACTION PEAK AS A FUNCTION OF DEPOSITION TEMPERATURE.

may be consistent with the increased homogeneous vapour deposition at the lower temperatures and the kinetic limitations reducing lateral overgrowth on non-ideal surfaces.

5.10 Activation energy

The activation energy curve for the photodeposited layers (with focussed UV) is plotted in figure 5.48. The slope of the graph gives an activation energy of 9 kcal/mol. Also plotted on this graph are the points for the thermal deposition. Bhat et al.[10] for their thermal growths of CdTe obtained an activation energy of 22kcal/mol and this has been fitted to the thermally deposited data points. It can be seen that for the few thermal depositions undertaken the data points are in agreement with the fitted activation energy and deviate only slightly from the curve of these authors.

Although a certain amount of scatter of the data points is evident this can be attributed to the different flow conditions of the different growth runs and a variation of growth rates between epitaxial and polycrystalline deposits will also give rise to errors. For example a strong columnar structure as Run 7 will give an artificially high growth rate. The graph shows the growth rate enhancement of the photodeposited layers over the thermally deposited layers, and shows that as expected at progressively higher temperatures the thermal component becomes more important, even though considerable growth rate enhancement is evident at the higher temperature. For example at 350°C a factor of five times the thermal growth rate is obtained. Thus activation energy values for the UV enhanced process are lower compared with the activation energies of the thermally grown layers, and are indicative of a less temperature sensitive deposition process. However, some degree of temperature dependence would still be expected even in a purely photochemical process due to the temperature dependence of the absorption coefficient α, as follows in the expression for the surface reaction rate R_S,

$$R_S \alpha \exp(-\alpha L) \text{ but } \alpha \text{ is proportional to } 1/T$$

hence giving $$R_S \alpha \exp(-c/T), \text{ where c is a constant}$$

This temperature dependence is not sufficient to account for the measured value of activation energy and may be more fully explained by desorption limitations of reaction products or by nucleation difficulties at the reduced temperatures onto the GaAs substrate.

Activation energy values for CdTe photodeposited onto GaAs by Ahlgren et al.[34] gave a value of ~14kcal/mol. Although this is considerably higher than that obtained in the present work these authors did express some doubt regarding their results due to adverse UV attenuation. Nevertheless this value is considerably less than

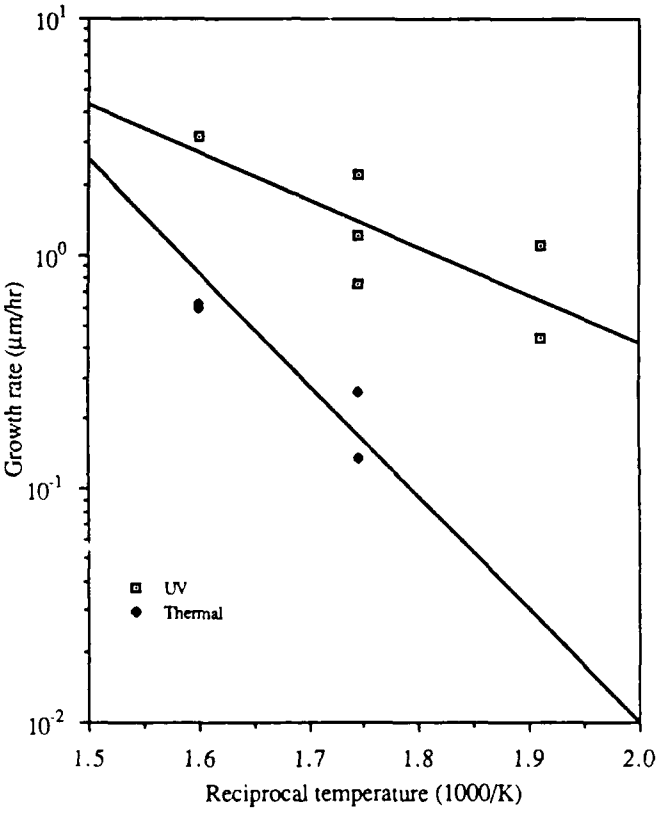

FIG. 5.48. ACTIVATION ENERGY CURVES FOR THERMALLY AND PHOTODEPOSITED CADMIUM TELLURIDE ONTO (100) GALLIUM ARSENIDE SUBSTRATES. THE CURVE FIT FOR THE THERMAL DEPOSITIONS IS AFTER BHAT ET AL.[10]

that of thermal depositions (Bhat et al.[10]) and is an indication that an important thermal step in the film growth is occurring photolytically.

Using the same argument as the vapour transport model of section 5.9.1, where the generated supersaturations for the focussed and defocussed UV were calculated to be 0.82 torr and 0.009 torr, it is possible to obtain an estimate of the upper limit of the growth rates by considering the flux of atoms diffusing through the boundary layer above the substrate. Then assuming a 1cm boundary layer and a diffusion coefficient of $1cm^2s^{-1}$ leads to growth rates of $0.4\mu m\ hr^{-1}$ for the defocussed lamp and $33\mu m\ hr^{-1}$ when the lamp is focussed. This then gives apparent efficiencies for the deposition process of ~175% and 7% respectively though this would be expected to be further reduced in practice due to free radical reactions.

The assumptions used in these calculations are that all the UV enters the reactor, i.e. no reflections occur and that as the deposition progresses no attenuation of the radiation occurs due to a build up of unwanted deposits on the reactor window. We have also assumed that all the liberated atoms form part of the layer, whereas in reality deposition onto the reactor walls, gas entrance effects, unreacted products etc. would reduce the growth rates. Also the assumption that a quantum efficiency of one, i.e. that each absorbed photon releases an atom, may not be operative and any reduction of the quantum yield will also result in lower supersaturations and hence lower growth rates. However, an increase would be obtained if the full range of the lamp spectrum were to be considered over the complete wavelength spectrum of the absorption curve.

5.11.1 Effect of alkyl ratio on crystallinity

At any fixed temperature an increase of the DMCd:DETe input ratio leads to an improvement in the crystallinity. At a temperature of 300°C a progression from the growth of randomly oriented crystallites to a more densely columnar structure through to an eventual single crystal deposit has been achieved with increase of the DMCd:DETe ratio from 1 through to 2.

An alkyl ratio of unity at this temperature gives rise to a loose microstructure of randomly oriented crystallites. At an increase to a 1.5 DMCd:DETe ratio this behaviour is somewhat suppressed leading to a more dense columnar type of layer. Further increase to a 2:1 ratio under equivalent conditions results in single crystal growth albeit with a polycrystalline interfacial region.

In figure 5.49 the FWHM of both the photodeposited and the thermally grown layers are plotted. As has already been pointed out comparison becomes difficult due to change in several key parameters, namely temperature and layer thickness. Taking this into consideration a curve for the photodeposited layers is plotted and gives an apparent decrease in FWHM (i.e. improved crystallinity) with increase of alkyl ratio.

In contrast however it would seem that the crystallinity of the thermal depositions degrades with increase of the DMCd:DETe ratio though this appears to be in agreement with the photoluminescence measurements of Ghandi et al.[23] who detected a slight deterioration of crystallinity with alkyl ratios greater than one. Although the data points in figure 5.49 show a dramatic decrease in crystallinity in going from an alkyl ratio of 1 to 1.5 this is exaggerated due to the higher growth temperature of Run 6 and therefore these points are not inconsistent with the results of Ghandi et al.

Comparison between the photodeposited and thermal layers show that at least for alkyl ratios greater than unity better crystallinity is obtained in the former case. This observation is supported by the preliminary photoluminescence data of Kisker and Feldman[40] which indicates better crystallinity for photodeposited CdTe on GaAs compared with thermal growths carried out at an alkyl ratio of 1.5

The effect on the crystallinity of UV, alkyl ratio and temperature are illustrated schematically in figure 5.50. Steps 1 and 3 are consistent with a decrease in the excess chemical nucleation potential in that p_e and p_v are increasing and decreasing respectively. Step 2 is a deviation from DMCd:DETe stoichiometry and steps 4 and 5 kinetic effects relating to increased and decreased surface diffusion respectively.

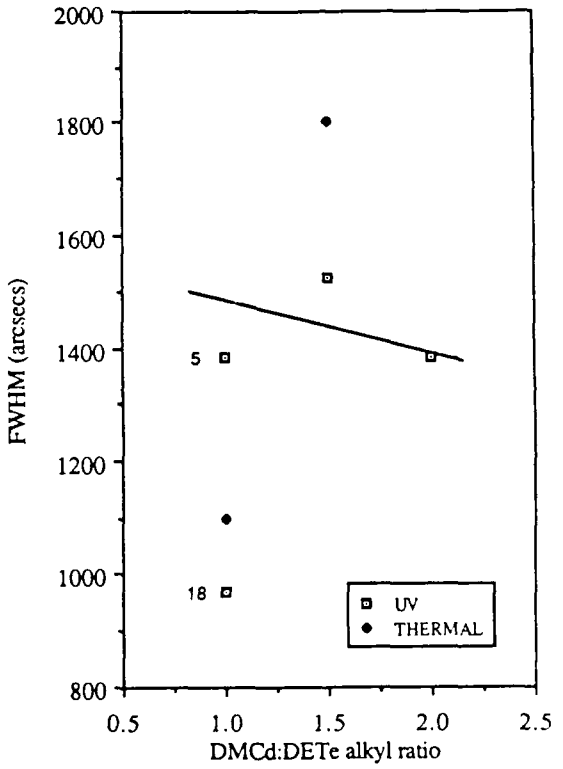

FIG. 5.49. VARIATION OF THE FWHM OF THE CADMIUM TELLURIDE (400) X-RAY DIFFRACTION PEAK AS A FUNCTION OF DMCd:DETe ALKYL RATIO.

NOTE. THE STRAIGHT LINE SHOWS THE GENERAL TREND FOR THE DEPOSITIONS UNDERTAKEN WITH UV ILLUMINATION. POINT 5 IS UNDERESTIMATED DUE TO THE HIGHER GROWTH TEMPERATURE IN THIS CASE. SIMILARLY POINT 18 IS VASTLY UNDERESTIMATED DUE TO THE GREATER COMPARATIVE THICKNESS OF THIS LAYER. TABLE 5.2 LISTS THE FWHM ALONG WITH THE GROWTH TEMPERATURE AND THE LAYER THICKNESS FOR ALL POINTS.

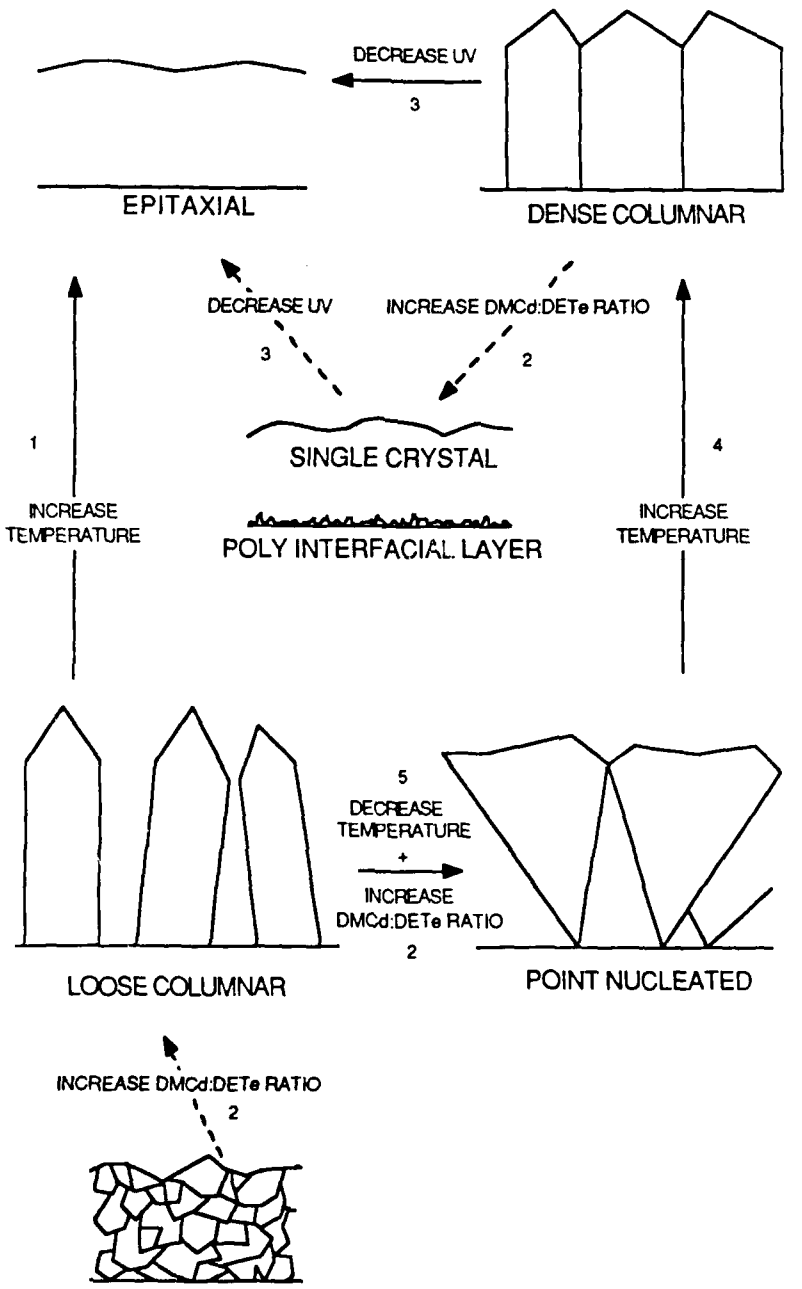

FIG. 5.50. SCHEMATIC DIAGRAM SHOWING THE EFFECT OF ALKYL RATIO, UV INTENSITY AND TEMPERATURE ON THE CRYSTALLINITY OF CADMIUM TELLURIDE LAYERS PHOTODEPOSITED ONTO GALLIUM ARSENIDE SUBSTRATES.

5.11.2 Effect of alkyl ratio on dislocation structure

The dislocation structure of the epilayers improves with increasing alkyl ratio. With defocussed lamp conditions at 300°C, increasing the input alkyl ratio from 1 to 1.5 resulted in a much improved defect structure although both of the layers were epitaxial. With the unity input ratio the defect structure extends to ~0.1μm into the layer and this dislocation network is of a sufficiently high density that the individual dislocations cannot be resolved. However at the increased input ratio almost no extended dislocations are visible although a slight disturbance is seen close to the interface.

These improvements in crystallinity and dislocation structure at increased alkyl ratios are a result of the different yields of cadmium and tellurium. The ratios of the reactants in the vapour would not be expected to be the same as the cadmium and the tellurium concentrations at the growth interface due to the different absorbance of the alkyls over the full spectral range of illumination and also due to the inevitable difference in the quantum efficiency through this range. Also the growth mechanism may not be directly proportional to the amount of cadmium and tellurium atoms in the gas phase if the mechanism involves adsorption of any or either of the reactants.

5.12 Temperature dependence of the dislocation structure

At the higher deposition temperature of 410°C there is evidence of defects in the near surface regions of the layer. The presence of dipoles and dislocation loops is indicative that a climb process may be operative. The presence of stacking faults is known to be related to a high point defect level and these may be due to high concentrations of gallium in the layer. This may be enhanced by the prebake this layer was given or possibly by poor substrate preparation. Bicknell et al.[79] also obtained stacking faults in their MBE grown layers and attributed these to contamination of the substrate.

For the photodeposited material at 350°C the dislocation network is dense throughout the layer, but from the depositions at 300°C the dislocation network is generally limited to <0.1μm from the interface. It is apparent that at increased alkyl ratios the dislocation structure is suppressed. Thus the dislocation morphology seems to be more sensitive to stoichiometry variations than to temperature.

In comparison at further reduced temperatures, i.e. those used for the UHV depositions the crystallinity again deteriorates with heavy dislocation evident throughout the layer. The limitation in this case may be kinetic with the depositing species having much reduced surface mobility.

5.13 Heterogeneous nucleation on GaAs

The growth of the single crystal layer, Run 13, illustrates that the conditions used, namely DMCd:DETe equal to 2:1, are close to those required for layer stoichiometry even though the region at the interface is bounded by a polycrystalline region. This does however give an indication of the difficulty in nucleation onto the GaAs substrate, since this result would suggest that although conditions for single crystal growth have been utilised it is not the only criterion to be satisfied, and that ordered nucleation onto the GaAs substrate surface is a separate issue which has to be considered. This difficulty in the nucleation is also consistent with the relatively high value of activation energy measured for the photochemical process and also with the greater growth rates obtained on CdTe substrates using otherwise similar process conditions.

The preferred orientation for the polycrystalline deposits has been shown to be (111). Although under low supersaturation conditions (100) growth is predominant, at high supersaturations and reduced temperatures the preference is to grow as (111). The removal of the oxide enhances the (111) growth due to a change in the substrate surface structure. Giess et al.[78] have also shown that this is the preferred orientation for growths carried out under Te rich conditions.

This preferential (111) growth is also obtained in the case of the epitaxial UHV deposited layer at reduced temperatures. This would then seem to suggest that reduced temperatures and high supersaturations, i.e. conditions which promote reduced mobility and rapid arrival of atomic species then result in insufficient time for optimum lattice site incorporation. Although there are many reports of depositing both (100) and (111) CdTe by MBE techniques these all attribute the differing orientations to differences in substrate treatment prior to growth, the presence of interfacial layers etc. but not to differences in the growth temperature.

5.14 Critical misfit dislocation free layer thickness

It is seen that in the case of layer 19 little or no extended dislocation structure is visible using diffraction contrast TEM. However it should be noted that dislocations are only introduced into a layer of a heteroepitaxial system when the layer exceeds a certain critical thickness. Layers of thickness less than this find it more energetically favourable to accommodate the mismatch strain by distortion of the lattice in an attempt to take up the same lattice parameter as the substrate (at least for the first few monolayers).

5.14.1 Tetragonal distortion

Assuming the distortion is tetragonal it is possible to calculate the change in the lattice parameter parallel to the interface on the assumption that the lattice spacing of the CdTe contracts to take up the parameter of the GaAs.

At 300K the lattice parameter of GaAs, a_{GaAs} equals 5.65Å and Poisson's ratio for CdTe, υ= 0.512. Using these values a contraction of the CdTe normal to the interface in order for the CdTe to take up the same lattice parameter as the GaAs will result in a corresponding increase of lattice parameter parallel to the interface in proportion to Poisson's ratio thus:-

$$\Delta a_{\perp}/\Delta a_{\parallel} = \upsilon \quad \ldots\ldots\ldots \quad 5.18$$

where $\Delta a_{\parallel}$ is the change in lattice parameter of the CdTe from its cubic value to that of GaAs, i.e $\Delta a_{\parallel} = a_{CdTe}-a_{GaAs}$=0.83Å. Hence from equation 5.18, $\Delta a_{\perp}$ =0.425Å giving a lattice parameter $a_{\perp\, CdTe}$ of 6.905Å.

Adopting this value of $a_{\perp CdTe}$ as the new lattice parameter the shift in the position of the (400) x-ray diffraction peak can be calculated and gives a 2θ equal to 52.98°. The measured value of the peak position for Run 19 equaled 57.08° which is equivalent to a lattice parameter, $a_{\perp CdTe}$, of 6.45Å. This peak position corresponds to a shift in the opposite direction to that predicted from assuming elastic strain producing tetragonal distortion. Although partial distortion, i.e. distortion of only some of the lattice, would result in less strain being evident giving rise to an effective lattice parameter $a_{\perp}$ less than the 6.905 Å predicted, it would not be expected that a lattice parameter less than the cubic value of 6.48Å would be obtained.

The thickness of the layer, h_c, at which the misfit strain has to be relieved by the introduction of misfit dislocations is dependent on the degree of mismatch, and is given by the following expression[92] :-

$$h_c = \frac{b(1-\upsilon\cos^2\beta)}{8\pi f(1+\upsilon)\sin\beta\cos\zeta} \ln\left(\frac{\alpha h_c}{b}\right) \quad \ldots\ldots\ldots \quad 5.19$$

where b is the magnitude of the Burgers vector, υ the Poisson's ratio of the layer, β the angle between the Burgers vector of the dislocation and the dislocation line, ζ the angle

between the interfacial plane and the slip plane of the dislocation and f the degree of mismatch as defined by $f=mod2(a_O-a)/(a_O+a)$.

For CdTe the slip system is {111},<110> hence giving a $\zeta=54.74°$ for a (100) growth orientation. The predominant dislocation in CdTe is the 60° type <101> i.e has $\beta=60°$ and $b=a/\sqrt{2}$.

Thus equation 5.19 reduces to :-

$$h_c = 1.5375 \ln\left(\frac{h_c}{1.1455}\right) \quad \ldots\ldots\ldots \quad 5.20$$

which upon solving for the smallest error value by numerical substitution for h_c gives a critical thickness of ~1.54Å.

This then suggests that for the CdTe-GaAs system misfit dislocations would occur in layers of thickness greater than a few monolayers. Of course the fact that no extended dislocations are seen in the layer of Run 19 does not preclude the possibility of a regular array of misfit dislocations at the interface as has been observed by lattice imaging using high resolution TEM of thermally grown layers by Cullis et al[80].

5.14.2 Lattice parameter variation with temperature

The change in lattice parameter as a function of temperature can be an important consideration in the effect of strain in lattice mismatched systems. Differences between the thermal expansion coefficients of layer and substrate could lead to a change in strain as the sample cools from the growth temperature to room temperature and could consequently be a possible generation mechanism for the dislocation network.

The lattice parameters of CdTe and GaAs as a function of temperature have been calculated between 200°C and 800°C using published data[93] for thermal coefficients of linear expansion between this temperature range and are plotted in figure 5.51. The change in the misfit of the CdTe-GaAs system for this temperature range is then plotted in figure 5.52, where the misfit has been defined as $(a_{CdTe}-a_{GaAs})/a_{GaAs}$ and has been expressed as a percentage. This curve shows that the misfit increases from 14.655% at a growth temperature of 300°C to 14.68% at close to room temperature.

It is unlikely that a change in the lattice mismatch of 0.17% would be responsible for the interfacial dislocation network or in fact greatly influence the

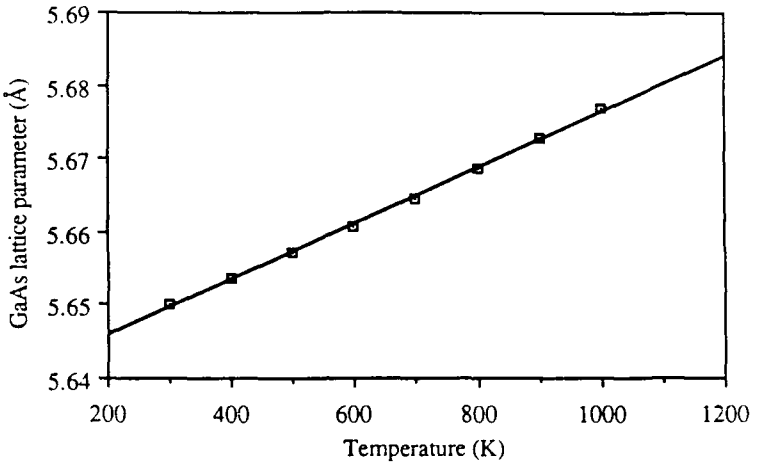

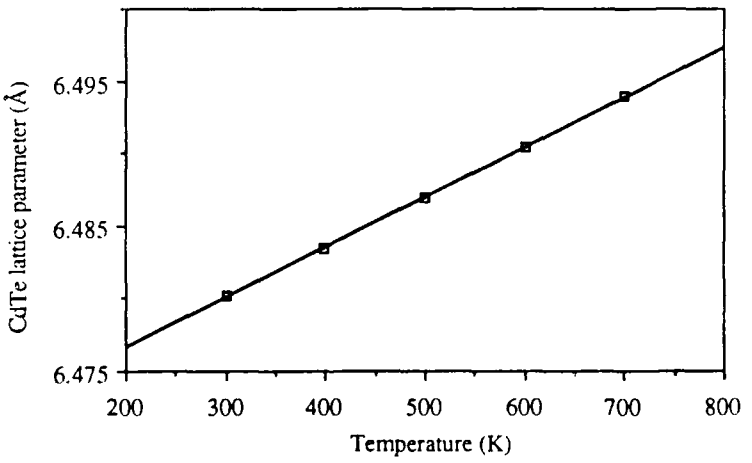

FIG. 5.51. VARIATION OF THE LATTICE PARAMETERS OF GALLIUM ARSENIDE AND CADMIUM TELLURIDE WITH TEMPERATURE.

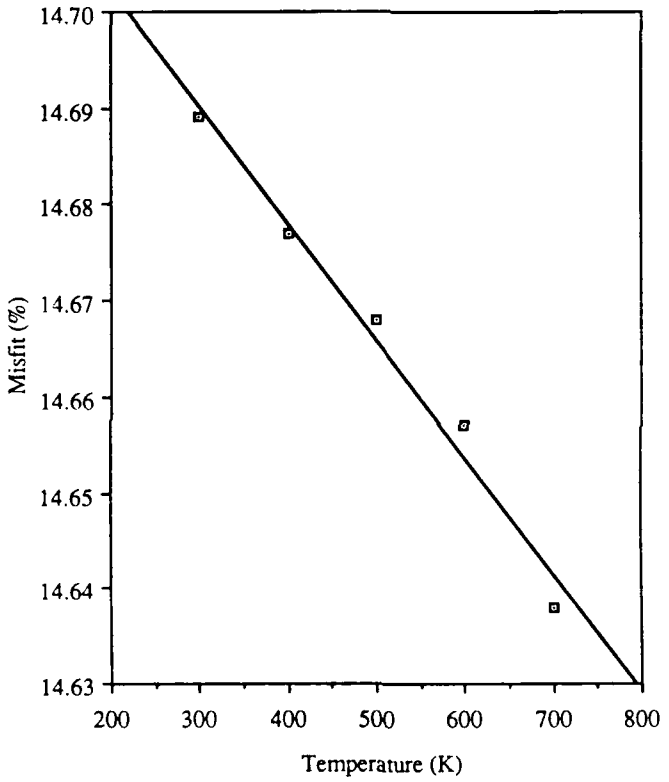

FIG. 5.52. PERCENTAGE MISFIT OF CdTe-GaAs SYSTEM AS A FUNCTION OF TEMPERATURE.

dislocation structure although it has been reported by Oe et al.[94] that a lattice mismatch of ±0.05% is enough to induce misfit dislocations in double heterostructure III-V quaternary layers.

5.15 UHV deposited CdTe on GaAs

The dislocation structure of the UHV deposited layer with (111) orientation (figure 5.31) appears to contrast with that obtained for the CVD layer deposited thermally at 410°C (figure 5.22) which also has a (111) orientation. However the projected direction, i.e. the beam direction B in the microscope or the direction perpendicular to the plane of the micrograph, was found to be different in both cases. In the case of DCR 9 the beam direction was <112> whereas in the case of the CVD deposition B=<110>. The substrate will cleave along the most densely packed planes, i.e. along the {110} in the GaAs. With reference to figure 5.53, this means that for a (111) orientation of CdTe the cleavage direction is along the <110> or the <112> direction i.e. perpendicular to each other. Hence the direction one views the cross-sectional TEM specimen is to a degree random and is dependent on which face of the as glued cross-section specimen is polished during preparation.

Therefore the dislocation structure of the micrographs may not be inconsistent with each other as effectively only the direction one views is different in each sample. The dislocation structure as drawn in three dimensions is shown in figure 5.53, and is consistent with both the <110> and the <112> beam directions.

The degree of relaxation of the lattice mismatch strain relieved by the misfit dislocation is given by $\delta = b_{eff}/d$, where d is the distance between the dislocations and b_{eff} the value of the Burgers vector projected onto the (100) plane.

Depending on whether the dislocation is a 60° type or an edge or screw type the value of $b_{eff} = |b|/2 = 2.29$Å or $|b| = 4.58$Å. From figure 5.28 the spacing between the misfit dislocations can be measured to be 31Å. Constructing a Burgers vector circuit around the dislocations shows that the Burgers vector lies parallel to the interface and the dislocations are of the pure edge type with a line direction, l=(110). Hence $\delta = 14.8\%$ and thus the presence of these misfit dislocations would relieve the mismatch strain completely. As the Burgers vector of these dislocations lies in the plane of the interface it is not possible for these dislocations to glide away from the interface. However the 60° type dislocation would be able to glide away from the interface along the (111) planes although the amount of strain relief (for the same separation distance d) would be half of the mismatch strain. Although no 60° type dislocations were detected at the interface their presence is highly probable and have in fact been detected by Cullis et al.[80,84].

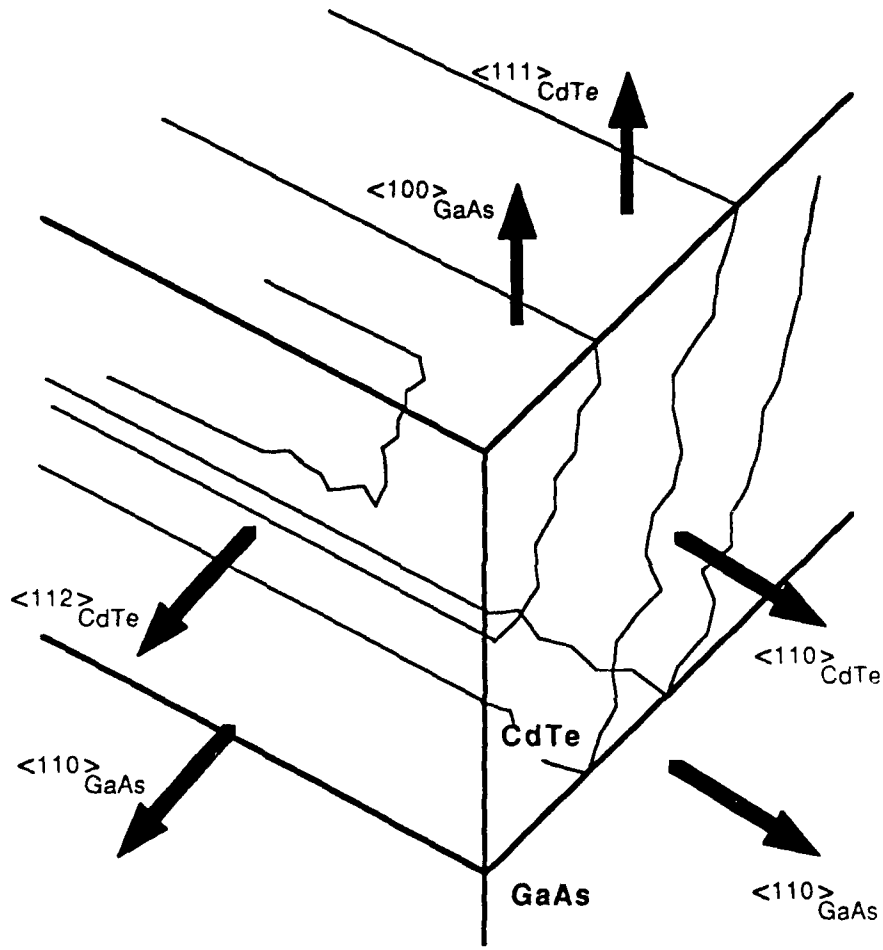

FIG. 5.53. THREE DIMENSIONAL VIEW OF THE DISLOCATION STRUCTURE OF A (111) CADMIUM TELLURIDE LAYER DEPOSITED ONTO A (100) GALLIUM ARSENIDE SUBSTRATE.

Chapter 6: Cadmium deposition; results and discussion

Deposition of cadmium was carried out by photodissociating DMCd using a 1kW Hg/Xe arc lamp over a range of flow and temperature conditions to investigate the nucleation behaviour onto sapphire, silicon and gallium arsenide substrates and to promote low temperature crystallinity. The UV was focussed over an area of $3cm^{-2}$ resulting in a UV beam intensity at the substrate of $1mWcm^{-2}$.

6.1 Sapphire substrates

The sapphire substrates were of (0001) orientation and were supplied by PBK Micron with both sides polished.

6.1.1 T=80°C

Figure 6.1 shows an SEM micrograph of a growth run carried out with a dimethylcadmium partial pressure of 3 torr at a substrate temperature of 80°C for a one hour period. This low magnification micrograph shows a high density of particles distributed randomly on the substrate surface. These features are typical of three dimensionally nucleated particles which have formed in the vapour phase as can be seen from the higher magnification micrograph of figure 6.2. These 3-D homogeneously nucleated particles have settled on the substrate after forming in the vapour phase.

Decreasing the DMCd partial pressure to 1.3 torr resulted in a lower density of the vapour phase nucleated particles. This is shown in figure 6.3 for a deposition carried out for a one hour period. In addition to these particles many smaller features of ~0.1μm size are also visible. These particles or nuclei exhibit no faceting and are domed or hemispherical in shape. These nuclei are also distributed somewhat randomly on the substrate although it is clear that at various positions some clustering of the nuclei is in evidence. This is especially true at or close to defects or scratches on the substrate surface.

Reduction of the DMCd partial pressure to 0.6 torr resulted in little deposition of any kind whatsoever using the temperature and growth duration as above. Increasing the growth time does however result in a small increase in the homogeneous vapour phase nucleated particles although there is no evidence of any heterogeneous nucleation as seen in figure 6.3 for the sample deposited at 1.3 torr.

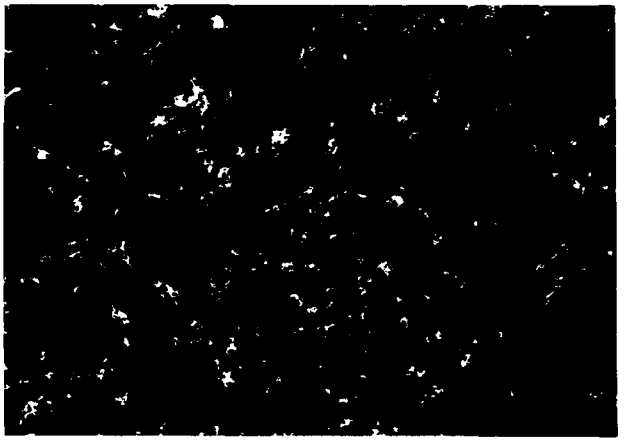

FIG 6.1. RANDOM DISTRIBUTION OF HOMOGENEOUS VAPOUR PHASE NUCLEATED CADMIUM PARTICLES ON A SAPPHIRE SUBSTRATE.

FIG. 6.2. HOMOGENEOUS VAPOUR PHASE NUCLEATED CADMIUM PARTICLE ON A SAPPHIRE SUBSTRATE.

FIG. 6.3. HETEROGENEOUS NUCLEATION IN ADDITION TO HOMOGENEOUS VAPOUR PHASE NUCLEATED CADMIUM PARTICLES ON A SAPPHIRE SUBSTRATE (80°C, 1.3 TORR PARTIAL PRESSURE, 1 HOUR).

6.1.2 T=50°C

Reducing the growth temperature to 50°C (partial pressure 1.3 torr) results in a growth morphology as shown in figures 6.4. It can be seen that, for the maximum feasible growth time of 1hour at this reduced temperature, a dense coverage of the cadmium deposit was achieved on the sapphire substrate. Also it is evident that many of the individual nuclei have developed into larger crystallites of size approaching 200nm. Faceting of the crystallites is also becoming evident at this stage and can be seen clearly from the low and high magnification SEM micrographs of figures 6.4(a) and 6.4(b).

6.1.3 T=30°C

A reduction of temperature to 30°C (at a DMCd partial pressure of 1.3 torr) led to the deposition being of a much more dense nature as can be seen from the micrograph of figure 6.5. From this figure it can be seen that the nuclei have completely covered the substrate leaving none of the sapphire surface visible and as the micrograph shows each nucleus is of an average size of ~0.05-0.07μm, similar to the earlier depositions but markedly different from the deposition at 50°C. This particular growth run was carried out for a one hour period.

Growth carried out using the same partial pressure conditions for a reduced duration of only five minutes, shows that an extremely thin layer is present on the substrate surface with as yet little or no appearance of the hemispherically shaped nuclei. This sample is shown in figure 6.6 and it can be seen that the layer is relatively uniform though slightly rippled at places. Small fissures or cracks can be seen in this layer and may be boundaries between growth islands. The small layer thickness is evident from the fact that the surface scratches on the substrate are still visible and also from the fact that viewing the sample edge on by SEM and cross-sectional TEM failed to differentiate the layer from the sapphire substrate. The latter is not unexpected due to foil bending effects obscuring information very close to the interface. This thin layer has also been obtained in the deposition at the higher temperatures as can be seen in the background of figures 6.2 and 6.3.

Similar depositions of growth times between these two extremes, namely for twenty, thirty and forty minutes respectively result in an increase in the density of the dome shaped nuclei on the uniform thin layer as was obtained in the five minute growth run. Also from the transition from obtaining a deposit consisting of isolated nuclei to the formation of a uniform coating of these nuclei it was noted that although a change in density of nuclei clearly occurred there was little change in their size between the different growth times performed.

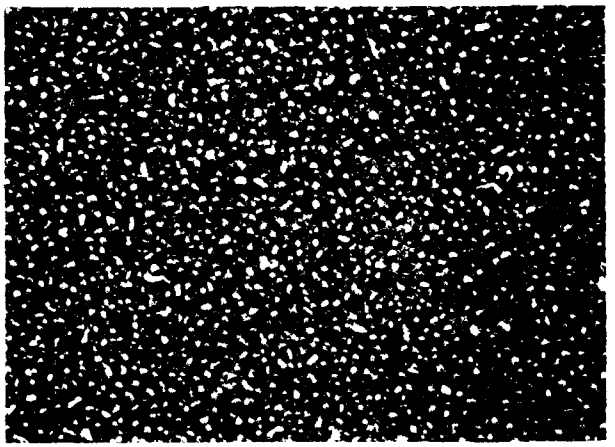

(a)

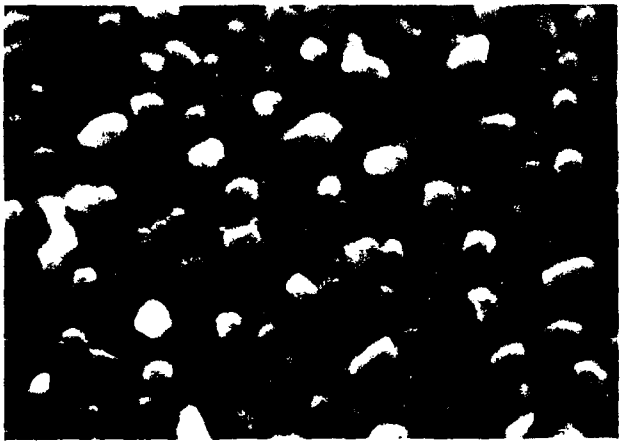

(b)

FIG. 6.4 SURFACE MORPHOLOGY OF CADMIUM DEPOSITED ON A SAPPHIRE SUBSTRATE (50°C, 1.3 TORR PARTIAL PRESSURE, 1 HOUR)

FIG. 6.5. SURFACE MORPHOLOGY OF CADMIUM DEPOSITED ON A SAPPHIRE SUBSTRATE (30°C, 1.3 TORR PARTIAL PRESSURE, 1 HOUR)

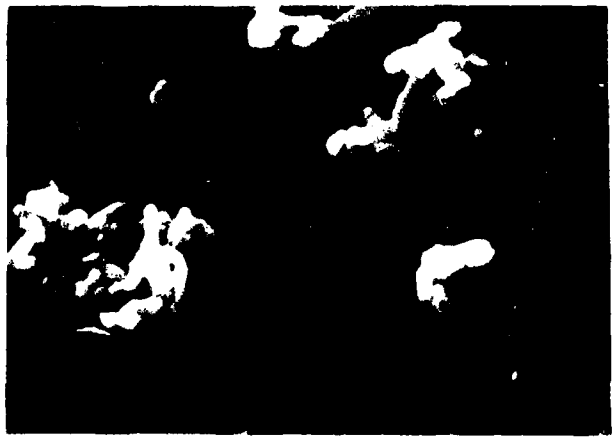

FIG. 6.6. SHORT TIME DEPOSITION SHOWING UNIFORM BACKGROUND LAYER ON A SAPPHIRE SUBSTRATE (30°C, 1.3 TORR PARTIAL PRESSURE, 5 MINS)

Although further growth runs of greater durations were carried out the deposits did not appear to be any different in surface morphology as viewed by SEM from the one hour growth run deposition of figure 6.5, i.e a high density of nuclei completely covered the substrate. The cross-sectional TEM micrograph for this layer shows in figure 6.7 that the layer has increased in thickness with successive additions of the previously observed nuclei. The size of these is again similar being circa 0.05μm resulting in a layer thickness of ~0.1μm although this was found to vary greatly over the substrate to less than ~0.05μm at some points.

Growth runs for greater lengths of time were not practicable as deposition on the reactor tube caused severe attenuation after growth runs of ~1hour.

FIG 6.7. CROSS-SECTIONAL TEM MICROGRAPH OF CADMIUM DEPOSITED ON A SAPPHIRE SUBSTRATE (30°C, 1.3 TORR PARTIAL PRESSURE, 1 HOUR).

6.2 Silicon substrates

Silicon substrates were of (100) orientation and were supplied by Wacker Chemitronic GmbH with one face polished.

6.2.1 T=40°C

Figure 6.8 shows a cross-sectional TEM micrograph of a layer deposited on a silicon substrate. This micrograph shows that the layer has a thickness of 30nm. However although the layer is extremely thin it is highly uniform. The diffraction pattern for this layer is shown in figure 6.9 and shows that the layer is amorphous. This specimen was deposited at 40°C using a partial pressure of 1.3 torr for a growth time of sixty minutes. SEM observation shows a completely featureless layer surface.

Deposition performed for short time intervals, namely 5,10 and 15 minutes, shows in figures 6.10(a)-(c), the growth and coalescence of cadmium islands on the silicon substrates.

Figure 6.10(a), a deposition for only five minutes shows very small nuclei of approximately 10nm average diameter on the substrate. The lack of contrast is due to the extreme thinness of the nuclei, and also to their amorphous nature which is evident from the lack of change in contrast with specimen tilt in the TEM. Although an accurate determination of the thickness was not possible, by comparison with amorphous carbon evaporated TEM specimens, by taking into account the difference in atomic weights of the two materials, and also due to the minimal effect of these features on the diffraction information, this may be estimated to be less than 100Å.

Figure 6.10(b) shows a micrograph of a deposition carried out for 10 minutes. It can be seen that the size of the nuclei has increased laterally to ~100nm. However there has been no substantial increase in the" thickness" of the nuclei as is apparent from the bend contours of the crystalline substrate still being visible through the nuclei and appearing as a dark band in the micrograph.

Figure 6.10(c) where the growth time has been increased to 15 minutes shows some of the cadmium islands coalescing and forming larger islands and moving towards the formation of a continuous layer.

6.2.2 T=80 C

Depositing at the slightly elevated temperature of 80 C resulted in a change in the morphology of the deposit. Flow conditions as in the low temperature growth were

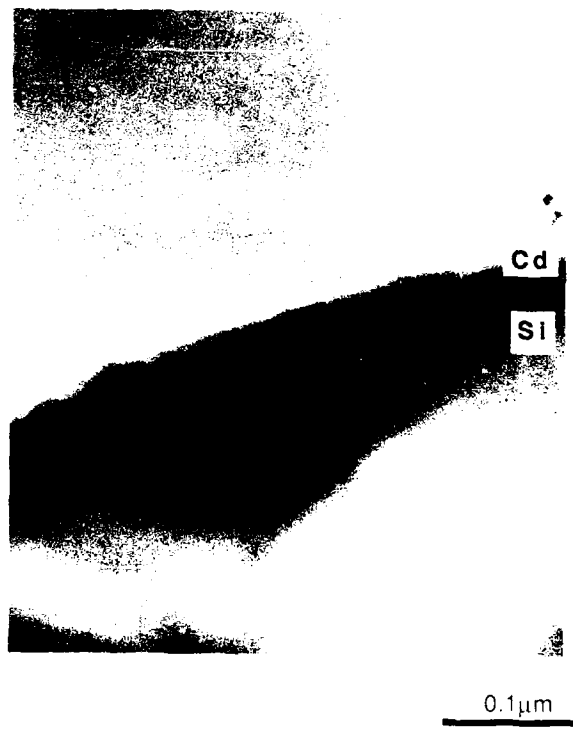

FIG 6.8. CROSS-SECTIONAL TEM MICROGRAPH OF CADMIUM DEPOSITED ON A SILICON SUBSTRATE (40°C,1.3 TORR PARTIAL PRESSURE 1 HOUR)

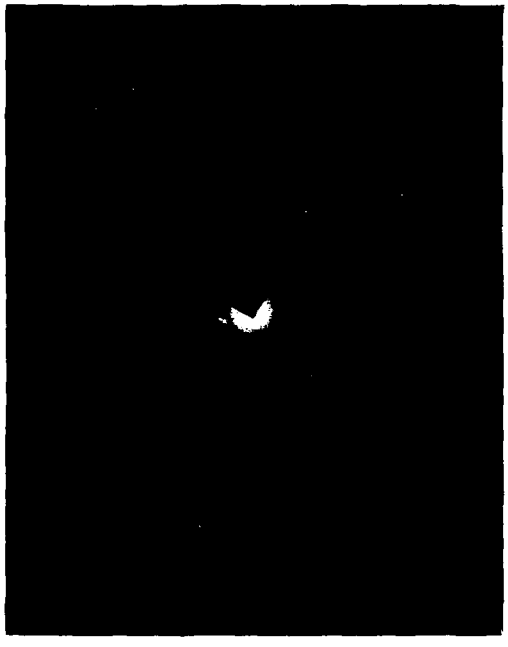

FIG. 6.9. DIFFRACTION PATTERN OF AMORPHOUS CADMIUM DEPOSITED ON A SILICON SUBSTRATE(40°C,1.3 TORR PARTIAL PRESSURE, 1 HOUR).

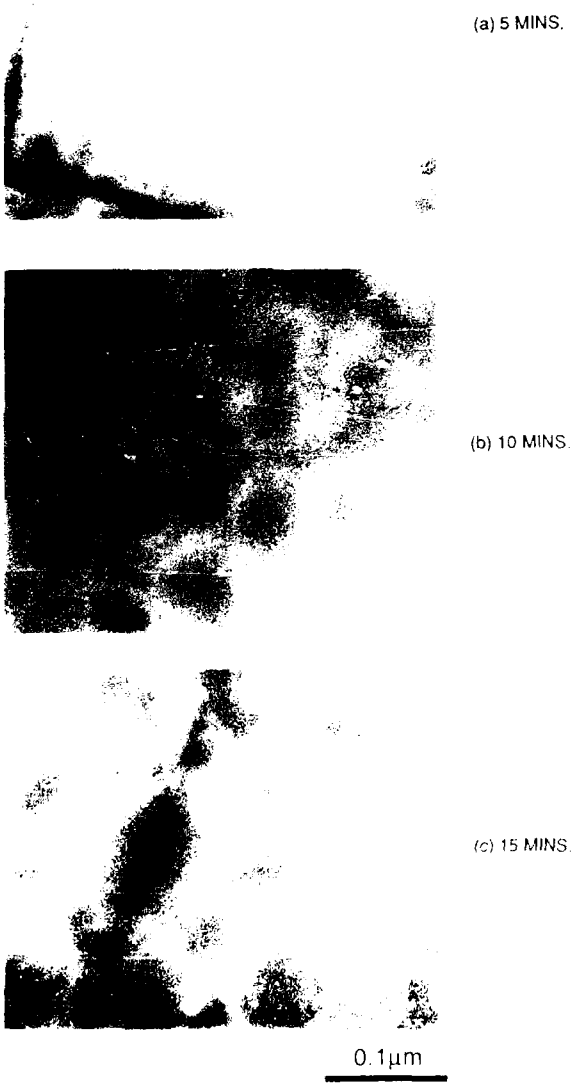

FIG. 6.10 PLANAR TEM MICROGRAPHS OF CADMIUM DEPOSITED ON SILICON SUBSTRATES FOR DIFFERENT DURATIONS (40°C, 1.3 TORR PARTIAL PRESSURE)

again utilised. A greater delay in nucleation compared with the low temperature depositions was obtained using these conditions; after 20 minutes some deposit was detectable and this is shown in the micrograph of figure 6.11(a). At successively greater growth durations of 30, 40 and 60 minutes further planar TEM specimens were prepared. The micrographs for these growth runs are shown in figures 6.11(a)-(d) and somewhat similarly to the lower temperature deposition illustrate the growth and coalescence of the nuclei into a continuous thin film. The islands of cadmium however an be seen to consist of very fine polycrystalline grains and this is in evidence from a very early growth stage.

Figure 6.11(a) shows few nuclei present on the substrate and these are generally isolated from each other. In figure 6.11(b) these individual islands can be seen to have grown in size and are in places beginning to coalesce with other neighbouring islands. Figure 6.11(c) shows many of the islands have now linked to each other and have now covered the majority of the substrate and figure 6.11(d) shows the final polycrystalline
film. This shows a micrograph of the final continuous film obtained after growing for 60 minutes and it can be seen that this has a grain size of ~50nm.

Higher temperatures failed to produce any deposition other than the homogeneous vapour phase nucleated particles, similar to that obtained in the case of the sapphire substrates, resulting in a powder like non adherent deposit.

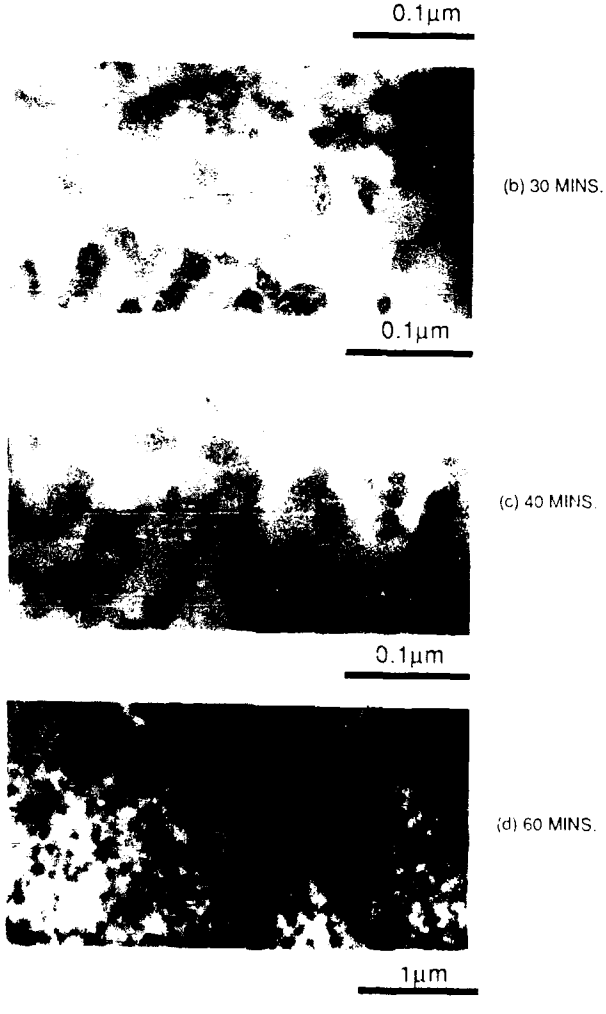

FIG. 6.11 PLANAR TEM MICROGRAPHS OF CADMIUM DEPOSITED ON SILICON SUBSTRATES FOR DIFFERENT DURATIONS (80°C,1.3 TORR PARTIAL PRESSURE).

6.3 GaAs substrates

The GaAs substrates were oriented (100) 2° towards (110) and were supplied by Mining and Chemical Products with one face polished.

6.3.1 Partial pressure >1.3 torr

Deposition onto GaAs substrates also shows the characteristic homogeneous vapour phase nucleation at high dimethylcadmium partial pressures, i.e. for partial pressures greater than ~1.3 torr. These homogeneously nucleated particles, being independent of the substrate material, have a similar morphology in all cases, unlike the heterogeneous growth whose morphology differs markedly with change of substrate material.

6.3.2 Partial pressure=1.3 Torr

6.3.2.1 Temperature=30°C

At a temperature of 30°C for a deposition period of thirty minutes some nucleation was detectable by TEM. Figure 6.12(a) shows the nucleation behaviour at an early stage where a low density of irregularly shaped islands are present on the substrate surface. Figure 6.12(b) shows a micrograph of a similarly grown deposit although the growth duration was increased to 40 minutes. It can be seen that there is a much greater surface coverage in this case and the individual islands have started to link or coalesce by the characteristic necks between the islands resulting in the formation of a network of islands into an almost continuous deposit. Also evident in this micrograph is the emergence of small, dark contrast features, which are thicker fine polycrystalline grains of ~5nm size and have formed by coalescence of the thinner islands. This is further illustrated by a growth run of longer time (figure 6.12(c)) and shows that the growth of the small crystallites has progressed. At this stage they have increased in size to 25nm and are taking up a more faceted appearance. However the growth of these crystallites has resulted in a considerable reduction of the thinner islands of cadmium and consequently leaves much of the substrate bare.

Further growth runs were carried out at successive time intervals and these show a rapid development of the faceted cadmium crystallites and a concomitant reduction or elimination in the snake-like features, suggesting that diffusion of these island features to the faceted sites is responsible for the growth of the latter. This is shown in figure 6.12(d) for a growth run carried out for 60 minutes where the crystallites have now developed to a larger size and have a more crystalline nature to them showing clear faceting. Examination between the crystallites resulted in little detection of the island features previously observed at the earlier growth stages

FIG. 6.12 PLANAR TEM MICROGRAPHS OF CADMIUM DEPOSITED ON GALLIUM ARSENIDE SUBSTRATES FOR DIFFERENT DURATIONS (30 C, 1.3 TORR PARTIAL PRESSURE)

indicating that the three dimensional growth is progressing by the sacrifice of the two dimensional nuclei.

6.3.2.2 Temperature=15°C

A reduction of the temperature to below room temperature to 15°C was then carried out and this resulted in an increase in the surface coverage by the nuclei. This deposition was carried out for a time period of 30 mins and the surface density of the cadmium is greater compared with the higher temperature depositions as is shown in figure 6.13. This figure shows some isolated crystallites of cadmium of around 200nm in size with smaller non faceted growth islands in intermediate stages of coalescence surrounding the larger crystallites. Also evident from the micrograph are the denuded regions surrounding each of the crystallites, thus suggesting the growth of the larger crystallites has occured by mass transport from the smaller islands surrounding the crystallites, causing a depletion of cadmium around the larger faceted crystallites.

6.3.2.3 Temperature=0°C

Reducing the growth temperature further shows an even greater surface coverage of the substrate as shown in figure 6.14. This shows a TEM micrograph of a deposition performed at 0°C using the same flow conditions as earlier and a deposition time of 30 mins. It can be seen that this is very similar to the depositions at the higher temperature with 200nm sized crystallites of cadmium surrounded by much smaller rounded island features. However in comparison to the higher temperature deposits the density of these islands is much greater. Similarly to the earlier deposits there also exists a small area around each crystallite which is devoid of any of the island features, although these denuded regions are narrower which is consistent with the reduced surface diffusion distances at this lower temperature.

It can also be seen on the higher magnification micrograph of figure 6.15 that many of the small individual islands exhibit black-white contrast within the island. This is direct evidence of the coalescence of two islands of different orientations. The boundary within the island is known as a double position boundary (DP) and is a special form of twinning.

Deposition with similar process conditions for increased deposition time, namely to sixty minutes resulted in a layer approximately 50nm thick as shown in the cross-sectional TEM micrograph of figure 6.16. The layer surface is shown in figure 6.17 and it can be seen that the density of the deposit is very high. There is the similar type of faceted crystallites of similar size (~200nm) distributed on the substrate as seen

FIG 6.13. PLANAR TEM MICROGRAPH OF CADMIUM DEPOSITED ON A GALLIUM ARSENIDE SUBSTRATE (15°C,1.3 TORR PARTIAL PRESSURE, 30 MINS).

FIG 6.14. PLANAR TEM MICROGRAPH OF CADMIUM DEPOSITED ON A GALLIUM ARSENIDE SUBSTRATE (0°C, 1.3 TORR PARTIAL PRESSURE, 30 MINS)

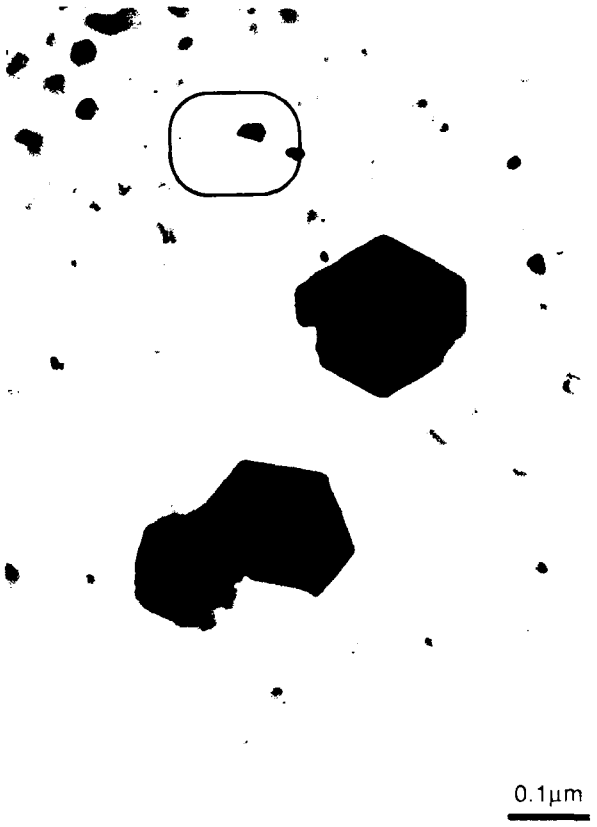

FIG 6.15. BLACK-WHITE CONTRAST OF CADMIUM ISLANDS EXHIBITING DOUBLE POSITION BOUNDARIES DEPOSITED ON A GALLIUM ARSENIDE SUBSTRATE.

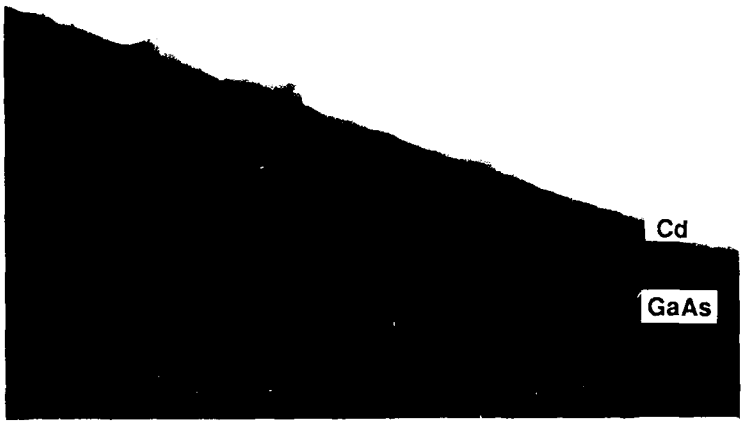

FIG 6.16. CROSS-SECTIONAL TEM MICROGRAPH OF CADMIUM DEPOSITED ON A GALLIUM ARSENIDE SUBSTRATE (0°C, 1.3 TORR PARTIAL PRESSURE, 60 MINS)

(a)

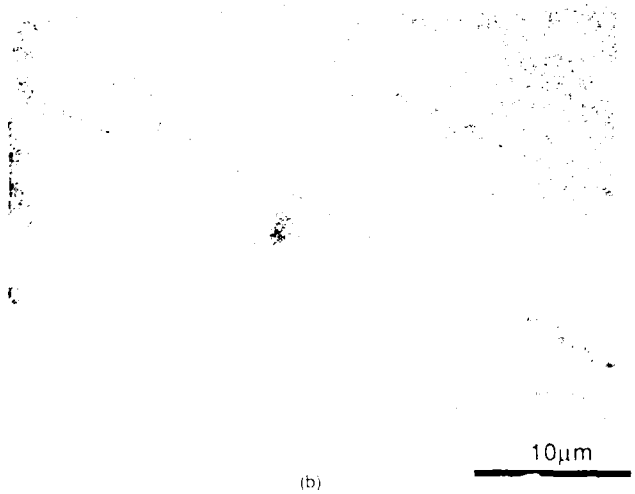

(b)

FIG. 6.17 SURFACE MORPHOLOGY OF CADMIUM DEPOSITED ON A GALLIUM ARSENIDE SUBSTRATE (0 °C, 1.3 TORR PARTIAL PRESSURE 1 HOUR)

in the earlier growth stages. However between these crystallites a dense deposit has formed although with a much finer grain size. Figure 6.17(b) shows a lower magnification SEM micrograph of the surface and a great deal of "whisker-like" growth predominantly parallel to the substrate can be seen.

6.3.3 Reduced UV intensity

T=0°C

A qualitative reduction in the UV intensity was performed to investigate the effect of reduced UV intensity on the depositions carried out at 0°C. This was undertaken by using the reactor flow separator plate to mask the UV beam over part of the substrate.

This resulted in an apparent reduction in nucleation density of the crystallites compared with the high intensity region. There existed no evidence of the densely packed structure of fine polycrystallites, as observed in the high intensity regions, surrounding the larger cadmium crystallites. It is apparent that the size of these crystallites is greater in the low intensity region, being ~250nm compared with ~180nm in the high intensity region as can be seen in figure 6.18. Also, the whisker growth is not seen in this case.

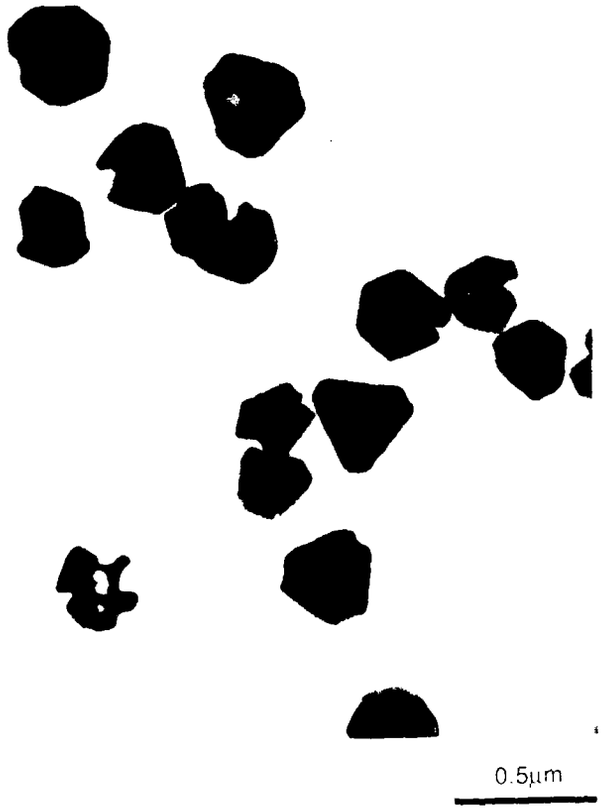

FIG 6.18 PLANAR TEM MICROGRAPH OF CADMIUM DEPOSITED ON A GALLIUM ARSENIDE SUBSTRATE IN REDUCED UV INTENSITY REGION

6.4 Prenucleation

Prenucleation types of growth run were carried out whereby depositions were performed by using the ultra-violet radiation to nucleate onto the substrate and then subsequently causing thermal decomposition of the alkyls by heating the substrate. All depositions using this method were carried out with a non contact mask placed in the beam path to prevent illumination of part of the substrate with the UV during the first step of photolytic nucleation. This type of deposition is analogous to the aluminium depositions by Tsao and Ehrlich[67] and Flicstein[95]. Although these authors employed laser illumination for the second stage of their process this latter stage was also a thermal process.

6.4.1 Silicon substrates

Two temperatures were employed for deposition onto the silicon substrates during the photolytic nucleation stage. The first deposition run was carried out at a temperature of 40°C for 30 minutes during the UV illuminated period after which the UV was switched off and the substrate temperature raised to 100°C for sixty minutes. The partial pressure was kept constant at 1.3 torr for both growth stages. Similarly this procedure was repeated with the UV illuminating nucleation step carried out at 80°C.

6.4.1.1 Temperature=40°C;100°C

In the former case it was found that in the high intensity region a uniform thin layer of 200nm thick was obtained as is shown in figure 6.19, which shows an SEM micrograph of a cleaved edge. In the low intensity region a thickness of <30nm was obtained. Cross sectional TEM showed this film to have an amorphous microstructure. A purely thermal deposition was carried out at the growth temperature of 100°C for the same period and showed that little deposition had occurred.

6.4.1.2 Temperature=80°C;100°C

Prenucleating at the greater temperature of 80°C, followed by a thermal deposition at the same temperature as above resulted in a polycrystalline deposit being obtained. This is shown in figure 6.20(a) which shows the cleaved edge of the sample. A peak layer thickness of 0.25μm is obtained although the layer is clearly not uniform. The surface of the layer (figure 6.20(b)) more clearly indicates the columnar nature with many crystallites ranging in size up to 0.25μm. In this case the masked region is still free of any deposit.

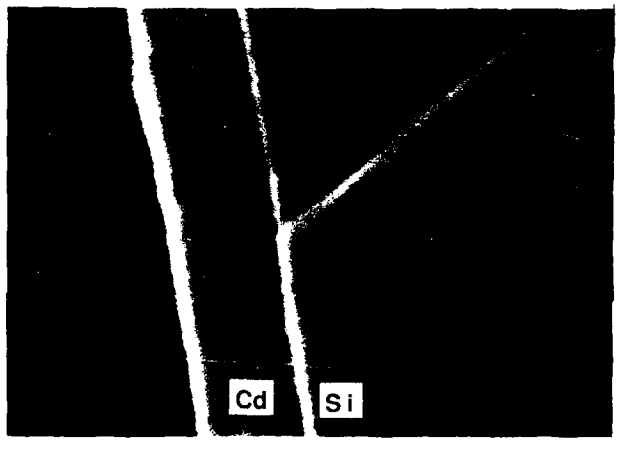

FIG. 6.19. CLEAVED EDGE OF CADMIUM DEPOSITED ON A SILICON SUBSTRATE BY PRENUCLEATING AT 40°C PRIOR TO THERMAL GROWTH AT 100°C

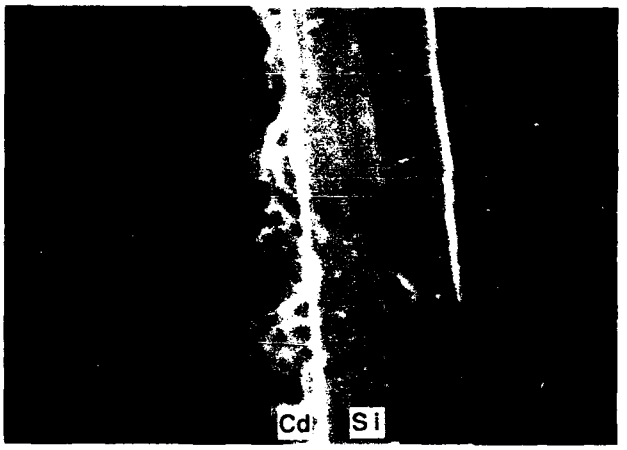

FIG. 6.20(a). CLEAVED EDGE OF CADMIUM DEPOSITED ON A SILICON SUBSTRATE BY PRENUCLEATING AT 80°C PRIOR TO THERMAL GROWTH AT 100°C.

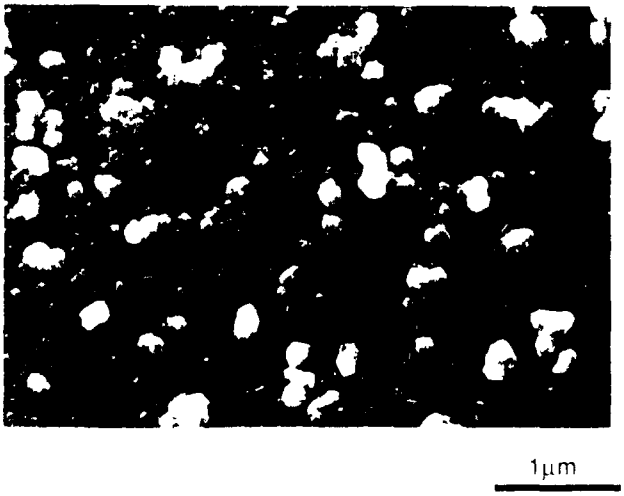

FIG. 6.20(b). SURFACE MORPHOLOGY OF CADMIUM DEPOSITED ON A SILICON SUBSTRATE BY PRENUCLEATING AT 80°C PRIOR TO THERMAL GROWTH AT 100°C.

6.4.2 GaAs substrates

6.4.2.1 T=30°C;100°C

Performing the same type of depositions onto GaAs substrates led to growth enhancement in both the low and high intensity regions of the UV. In this case the prenucleation temperature was reduced to 30°C for 30 minutes with the thermal deposition performed as before at 100°C for sixty minutes.

Deposits in the high intensity region led to a polycrystalline deposit as shown in figure 6.21 which shows a SEM micrograph of a cleaved edge. The sample has a developed columnar nature although the deposit is highly non uniform with some areas showing very little deposition. The maximum layer thickness is ~0.2μm. In the low intensity region isolated crystallites are present on the substrate.

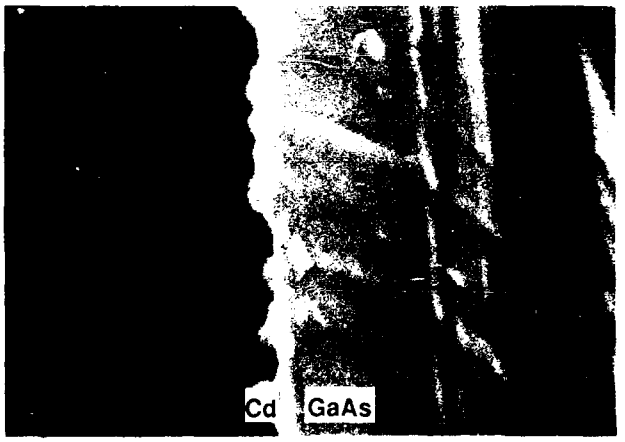

FIG. 6.21. CLEAVED EDGE OF CADMIUM DEPOSITED ON A GALLIUM ARSENIDE SUBSTRATE BY PRENUCLEATING AT 30°C PRIOR TO THERMAL GROWTH AT 100°C

6.5 Nucleation

Nucleation, both homogeneous and heterogeneous may be described by either of two models, namely the atomistic and the capillarity model.

The former model is based on terms of geometry and the atomic binding of the nucleating clusters and requires a rigorous and explicit statistical mechanical treatment. The capillarity model is based on bulk or macroscopic thermodynamic properties being assigned to the small clusters. Although this latter technique is not always as quantitatively accurate as the atomistic model the capillarity model is nevertheless useful in predicting the nucleation behaviour of deposition systems and as it is conceptually easier to understand than the atomistic model will be used in preference to the atomistic model.

6.5.1 Capillarity model

6.5.1.1 Homogeneous nucleation

The energy needed for the formation of a nucleus is given by the algebraic sum of the energy which is necessary for the formation of the surface, $\sigma.s$ and of the bulk $\Delta p.v$, where σ=specific surface energy, s the surface area of the nucleus, Δp the pressure reduction due to the condensation, v the volume of the vapour necessary for the formation of a nucleus.

$$W = \sigma.s-\Delta p.v \quad \ldots\ldots\ldots 6.1$$

For the case of spherical nuclei formation in the gas phase, i.e homogeneous nucleation,

$$W=\Delta G_0=\sigma 4\pi r^2-\Delta G_v{}^4/_3\pi r^3 \quad \ldots\ldots\ldots 6.2$$

where ΔG_0 is the Gibbs free energy of formation of a spherical cluster, ΔG_v is the Gibbs free energy difference per unit volume of liquid between supersaturated vapour of pressure p and bulk liquid of equilibrium vapour pressure, p_e, i.e.

$$\Delta G_v = kT/V \ln[p/p_e] \quad \ldots\ldots\ldots 6.3$$

This situation is depicted graphically in figure 6.22, where the surface and bulk contributions to the change in the free energy during nucleation are shown separately along with the combined free energy change as a function of the radii of the nuclei. This latter curve shows that the size of the nucleus increases due to the work carried out in the formation of the surface. This represents an unstable system, but after increasing in size

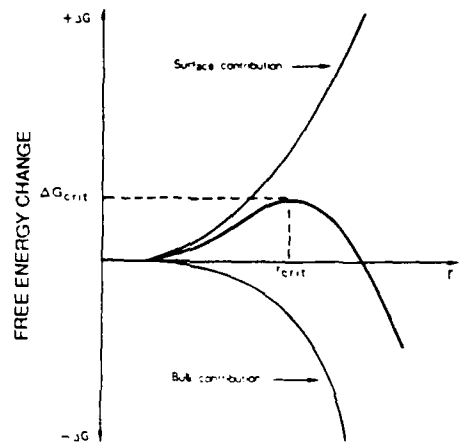

FIG 6.22. FREE ENERGY CHANGE OF NUCLEI AS A FUNCTION OF THEIR RADII. THE SURFACE AND BULK CONTRIBUTIONS ARE SHOWN SEPARATELY. ΔG_{Crit} IS THE FREE ENERGY OF FORMATION OF THE CRITICAL NUCLEUS (AFTER REF. (96)).

to a certain critical radius r_{crit}, the change in free energy decreases and becomes negative, and hence it is energetically favourable for the formation of nuclei greater than r_{crit}.

ΔG_{crit}, the free energy change leading to the formation of the critical nucleus or the activation energy necessary for nucleation, may be obtained by substition of r_{crit}, (obtained by maximisation of equation 6.2 for r) into equation 6.2. This then gives the following relation for ΔG_{crit} :-

$$\Delta G_{crit}=16\pi\sigma^3/3\Delta G_v^2 \text{ ..... } 6.4$$

Volmer[97] assumed metastable equilibrium conditions to enable the application of Boltzmann statistics in order to give the nucleation rate, i.e. he assumed that the nuclei do not grow further than their critical size but redissolve upon reaching r_{crit}.

This then gives a probability for the formation of a critical nucleus of $\Pi=Z\exp-\Delta G_{crit}/kT$, and hence the nucleation rate is Π divided by the average lifetime of the critical nucleus, τ, i.e.

$$J=z\tau^{-1}\exp-\Delta G_{crit}/kT \text{ .....} 6.5$$

A more rigorous approach used by Becker and Doering[98]whereby the steady state concentration of the nuclei under irreversible conditions led to corrective terms being applied to equation 6.5, resulted in the following expression for the nucleation rate:-

$$J = 4\pi r_{crit}^2 a_c \frac{p}{\sqrt{2\pi mkT}} n_1 \sqrt{\frac{\Delta G_{crit}}{3\pi kTi_{crit}^2}} \exp\frac{-\Delta G_{crit}}{kT} \text{ ..... } 6.6$$

where i is the number of monomers in the critical cluster, a_c the condensation coefficient and n_1 the conc. of monomers per unit volume.

6.5.1.2 Heterogeneous nucleation

Heterogeneous nucleation may also be described in similar terms and an analogous expression for the nucleation on a solid surface has been derived by Hirth and Pound[99], where they have considered the growth of critical nuclei by collisions with adsorbed monomers by diffusion over the substrate surface resulting in the following heterogeneous nucleation rate:-

$$J_{HET} = CR \exp \frac{\Delta G_{des} - \Delta G_{sd} - \Delta G^*}{kT} \quad \ldots\ldots\ldots \quad 6.7$$

where ΔG_{sd} and ΔG_{des} are the free energy of activation for the surface diffusion of adsorbed species and the free activation energy for the desorption process respectively. ΔG^* is the free energy of heterogeneous nucleation and is a function of the contact angle θ, between the nucleus and the substrate and of the substrate interfacial energies between the condensate-vapour, condensate-substrate and the substrate vapour, $\sigma_{c\text{-}v}$, $\sigma_{c\text{-}s}$, and $\sigma_{s\text{-}v}$ as shown in figure 6.23 and equals $[16\pi\sigma_{c\text{-}v}{}^3/(3\Delta G_v{}^2)][2+\cos\theta][1-\cos\theta]^2$ where $\cos\theta=[\sigma_{s\text{-}v}-\sigma_{c\text{-}s}]/\sigma_{c\text{-}v}$. The pre-exponential term of C in equation 6.7 equals

$$C = \sqrt{\frac{\Delta G^*}{3kTi^2}}\, a_o^2 \pi r^* \sin\theta\, N_o \quad \ldots\ldots\ldots \quad 6.8$$

where a_o is the jump distance of the adsorbed monomers and N_o the monomer adsorption site density.

6.5.1.3 Nucleation rate dependence on supersaturation

With regard to the preceding equations an important point is the dependence of the nucleation rate on the supersaturation as shown in figure 6.24, which illustrates that the nucleation rate increases rapidly over a small range of supersaturations. This then explains the behaviour of the cadmium depositions in which no deposition was detected at 0.6 torr partial pressure of DMCd, but a small increase to 1.3 torr resulted in the appearance of considerable growth features. In the case of the lower supersaturation we may be below the threshold value required for substantial nucleation whereas at the increased concentration of 1.3 torr we may be on the steeply rising side of the nucleation rate curve of figure 6.24.

It was seen in figure 6.3 that selective nucleation was apparent on a substrate scratch feature. This type of preferential nucleation is not unusual and occurs frequently with even defects on a more microscopic scale, e.g. point defects, substrate contamination etc. all serve to alter the interfacial free energies and induce localised nucleation at lower supersaturations.

Equation 6.7 also shows the strong dependence of nucleation behaviour on differing substrate material and that it is dependent on the relative values of the interface free energies.

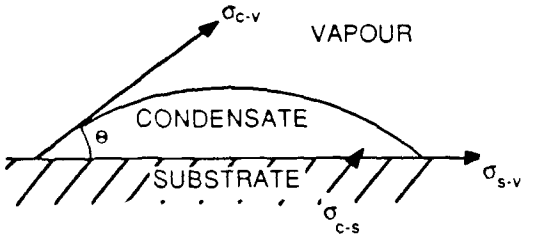

FIG. 6.23. SCHEMATIC DIAGRAM OF A HEMISPHERICAL CAP MODEL FOR HETEROGENEOUS NUCLEATION SHOWING THE INTERFACIAL FREE ENERGIES AND THE CONTACT ANGLE.

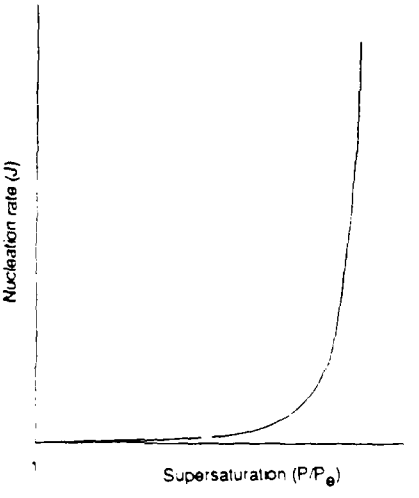

FIG 6.24. NUCLEATION RATE AS A FUNCTION OF SUPERSATURATION (AFTER REF. (96)).

6.5.1.4 Stage law for nucleation

In the case of the deposition onto the silicon substrates it was found that the nucleation proceeded in either of two morphologies. At low temperatures the deposit was amorphous in nature whereas at increased temperatures a fine polycrystalline deposit was obtained.

This behaviour is somewhat similar to that of deposition of germanium onto crystalline substrates (Kleber and Mietz[100]), where a temperature for the transition of the amorphous phase to the crystalline phase was obtained.

The amorphous phase will nucleate if the activation energy for nucleation is lower than that for the crystalline phase. This is described by the stage law which gives the condition for nucleation of the amorphous phase according to the following relation:-

$$\frac{\sigma_{cv}^3}{\rho_c^2 \ln\left[\frac{p_v}{p_e}\right]_c^2}\phi_c > \frac{\sigma_{av}^3}{\rho_a^2 \ln\left[\frac{p_v}{p_e}\right]_a^2}\phi_a \quad \ldots\ldots\ldots \quad 6.9$$

where $\phi_c = 1/[4(2+\cos\theta)(1-\cos\theta)^2]$ and ϕ_a is a similar expression for the crystalline phase and ρ is the density of the particular phase.

This is in effect an inequality based on the the critical free energy for nucleation, i.e. equation 6.4. This then implies that the specific surface energy for nucleation of the crystalline phase is greater than the amorphous phase, i.e. $\sigma_{cv} > \sigma_{av}$. Conceptually this means that the work required for the generation of an amorphous surface is less than for the crystalline and this is valid due to the absence of a rigid lattice in the former case.

At greater temperatures then, the probability of the formation of a crystalline network is increased though this may be due to several factors in addition to providing sufficient energy for greater atomic ordering. Particularly, changes in the adsorbed layers with temperature could change the wetting properties on the substrate, i.e. a change of θ of figure 6.23 resulting in a change of ϕ in equation 6.9 for the different phases. Also changes with temperature would change $(p_e)_a$ and $(p_e)_c$ due to their strong temperature dependence. The nature of the substrate itself heavily influences the microstructure of the deposit, i.e. on a crystalline substrate the overlayer will find it easier to grow with a greater degree of crystallinity than if the substrate is amorphous, due to less difficult ordered nucleation on the former. In this case the silicon substrate was not given any type of in-situ surface cleaning treatment hence the surface presenting itself as the initial growth interface would have been the amorphous oxide. Photodeposition of platinum by Braichotte et al.[58] onto carbon membranes were

similarly amorphous. Although neither of these authors investigated the effect of temperature on the microstructure of their photolytic deposits, thermal growth by an argon ion laser at higher temperatures did lead to polycrystalline growth.

6.5.1.5 Nucleation delay

ΔG, the driving force for nucleation, decreases with an increase in temperature due to increased equilibrium vapour pressures, and this causes a reduction in the growth rate at progressively higher temperatures. If the temperature is high enough this leads to no deposition as the amount of cadmium "evaporating" is comparable to that depositing. In the case of the sapphire and the silicon substrates this temperature was 100°C whereas for the GaAs substrate it reduced to 50°C and reflects the additional difficulty in depositing on this substrate.

Clearly the substrate influence is considerable and this is shown in the delay before detection of nucleation for the different substrates. For the sapphire substrates some deposit was detected after only 5 minutes deposition whereas for the silicon using comparable deposition temperatures the delay increased to 20 minutes at 80°C. In the case of the GaAs substrate this delay is increased to ~30 minutes even at the lower temperature of 30°C with no deposition evident at the growth temperatures used with the silicon substrates.

The effect of temperature on the delay in nucleation is also consistent with the change in the chemical potential with temperature; a plot of delay versus temperature for all three substrates is shown in figure 6.25. The nucleation delay for the sapphire substrates is shown not to vary considerably with temperature, over the range measured, for the initial uniform deposit on the substrate. However there is a great deal of error in this case as the formation of this initial layer has occurred very rapidly and the plotted points are essentially the delay in forming the layer rather than a nucleation delay. However the subsequent 3-D growth on this initial layer is also plotted and does show a marked increase in the time taken for nucleation at the higher temperature. This latter behaviour is then somewhat similar to the nucleation delay obtained with the silicon and GaAs substrates.

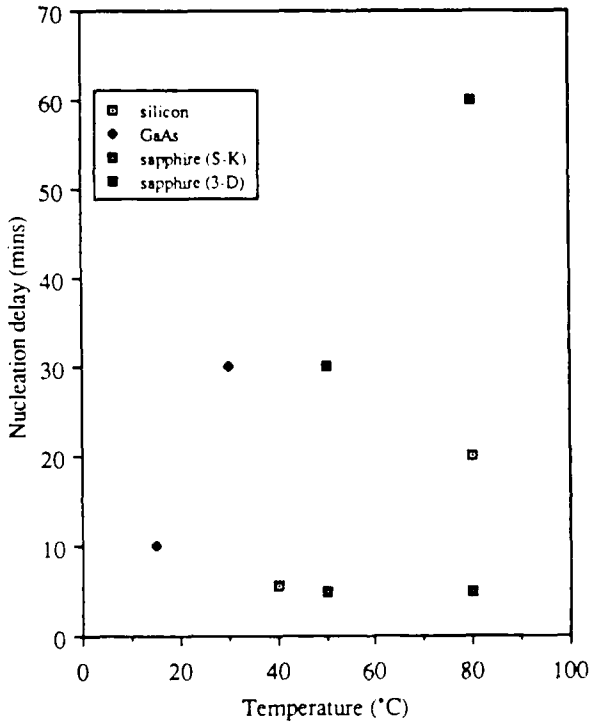

FIG 6.25. NUCLEATION DELAY AS A FUNCTION OF TEMPERATURE FOR PHOTODEPOSITION ONTO SAPPHIRE, SILICON AND GALLIUM ARSENIDE SUBSTRATES.

6.6 Diffusion

Diffusion of species over the substrate surface and where crystalline growth has occurred is clearly an important mechanism in the development of the growing deposit. This is illustrated in the early growth stages where the development of the initial nuclei into larger crystallites has occurred by coalescence of the nuclei thus leaving much of the substrate area bare.

This effect is better seen at lower temperatures and particularly for the deposition onto the GaAs substrate. In this case at relatively higher temperatures the size of the denuded region surrounding the more "formed" crystallites is greater. A reduction of temperature to 0°C still showed free regions around the crystallites but this has reduced greatly to less than 100nm from the crystallite perimeter. Hence it can be clearly seen that even at this low temperature the diffusion process is still occurring.

6.7 Effect of temperature on microstructure

Deposition onto the sapphire substrates shows two morphologies, the difference depending on the deposition temperature. At the reduced temperature of 30°C the layer is built up of small nuclei "packed" over each other whereas with only a small increase in the temperature to 50°C a more columnar but non-uniform deposit is obtained.

At the higher temperature the nucleation density will decrease and also the contribution from the adsorbed layer will be less. Therefore the preference will be for the nucleation to occur non uniformly with the subsequent growth being dominated by the cadmium generated in the vapour, resulting in growth of these randomly distributed nuclei. These effects together with the greater diffusion at the higher temperatures leads to the non uniform columnar growth obtained.

At the reduced temperature of 30°C the nucleation density is greater and also, as predicted by the atomistic model for nucleation, the critical cluster size would be expected to be lower. This coupled with the reduced diffusion at the lower temperature results in a more dense, and finer grain sized film.

6.8 Adsorption

6.8.1 *Growth assuming adsorption of DMCd*

The growth rate contribution from the adsorbed DMCd may be calculated for the temperatures and partial pressures at which deposition was carried out.

The surface reaction rate, R_s equals the product of the UV beam intensity I, the surface coverage of the adsorbed alkyl molecules θ, the cross-section for dissociating dimethylcadmium σ, and the quantum efficiency η, as follows:-

$$R_s = I\theta\sigma\eta \quad \text{.....6.10}$$

but using the expression for I as in equation 5.17 gives:-

$$R_s = I_o \exp[-\sigma pL/kT]\theta\sigma\eta \quad \text{.....6.11}$$

where θ is a function of the alkyl pressure and is described by the adsorption isotherm of figure 2.3. Then for a cross section for dissociation σ, at 254 nm, of 5E-22 cm^2, a UV path length L of 2cm, a quantum efficiency η of 1 and a beam intensity I_o of 1mWcm^{-2} (1.3E 19 photons $m^{-2}s^{-1}$), the surface growth rate may be calculated. For a temperature of 40°C and a DMCd partial pressure of 1.3 torr equation 6.11 reduces to:-

$$R_s = 4.37\ E\text{-}3\theta \quad \text{.....} \quad 6.12$$

but from the adsorption isotherm, at low pressure, the surface coverage θ, may be approximated as being directly proportional to the pressure p, for low surface coverage, hence giving a growth rate of:-

$$R_s = 3.12\ E\text{-}3 \text{ monolayers/sec}$$

which for the cadmium structure gives a value for the surface growth rate of 27Å/hr.

Alternatively, using the same vapour transport model as in chapter 5, with diffusion of cadmium through a 1cm boundary layer with unity diffusion coefficient gives rise to a growth rate of 6000 Å/hr.

The relative values of these two growth rates compared with the experimentally obtained value of 300 Å/hr show clearly that the dominant growth is occurring from the vapour and not via the adsorbed layer. However at lower temperatures the surface growth rate will increase due to the increase in surface coverage.

6.8.2 Whisker growth

Increased adsorption of the DMCd at the lower temperatures is also consistent with the whisker like growth observed for the deposition onto the GaAs at 0°C. This was not seen at greater temperatures suggesting that high supersaturations and/or deposition from the liquid like DMCd adlayers contribute to this form of growth and the latter may be somewhat analogous to a VLS type of growth mechanism with precipitation beginning from the DMCd adsorbed layers. This is supported by the growth direction of the whiskers which all lie along the substrate surface usually emanating from a pointed feature of the larger crystallites. Growth of these whiskers is never seen in any direction other than parallel to the substrate surface.

6.9 Reduced UV intensity

Nucleation in the low intensity region for the growth onto the GaAs substrate at 0°C showed a significantly less dense form of deposition. However the size of the crystallites in this reduced intensity region is larger compared with those in the adjacent higher intensity illuminated region.

This may be due to the reduced number of photons in the low intensity region resulting in less dissociation of the adsorbed DMCd and consequently leading to a smaller number of critical sized nuclei distributed over this part of the substrate. This would leave free a greater concentration of species, i.e. subcritical monomers, readily available to diffuse along the substrate and incorporate themselves at the favoured nucleation sites where the crystallites have grown from the critical sized nuclei, thus leading to greater sized crystallites compared with the high intensity region.

6.10 Prenucleation

Prenucleating the substrate provides a means of overcoming the slow growth rates encountered with purely photodeposition. In all cases of deposition using this technique the microstructure of the initial photonucleated stage was preserved.

In the case of the silicon substrate with conditions giving rise to the "amorphous-like" nucleation the additional thermal growth at 100°C resulted in a thicker but still amorphous layer. With the higher temperature nucleation, the eventual deposit was polycrystalline similar to the nucleation stage.

At this temperature, no thermal deposition was found on the bare substrate. With the GaAs a similar effect occurred whereby the deposition was thickened in the regions only where Cd was photolytically nucleated. In the low intensity region isolated crystallites of Cd were detected but in very low densities thus indicating that very little nucleation onto the substrate occurs after the photolytic stage, and that the thermal growth only deposits on the prenucleated areas.

At the relatively low temperatures employed the pyrolysis of the DMCd is inefficient, hence the equilibrium pressure of cadmium p_e, relative to the amount of cadmium liberated p_v, is too high for successful nucleation. At greater temperatures, although the dissociation of the DMCd becomes more efficient, nucleation becomes even more difficult due to the very strong temperature dependence of the equilibrium partial pressure which increases rapidly with temperature, hence reducing the probability of nucleation even further.

Photodeposition however provides a route for the initial nucleation due to its ability to operate at lower temperatures, hence keeping p_e small, and also by increasing the cadmium generated in the vapour p_v. Although the nucleation onto the substrate may be provided photolytically, low growth rates have to be tolerated, due to the need to prevent the onset of homogeneous Cd dust formation in the vapour by using low DMCd concentrations. However, thickening the layer thermally is now possible over the areas which have been nucleated photolytically, as the barrier for nucleation on the cadmium surface is less than that of the bare GaAs substrate. This is consistent with an investigation into the modification of nucleation barriers by Tsao and Ehrlich[101]. These authors have defined a figure of merit which is the product of the area of the non-nucleated region that can be maintained nucleation free and the height of film to be grown, and obtained large values for deposition of cadmium onto silica. Nucleation onto

GaAs would be more difficult due to the crystalline substrate surface and hence greater figures of merit would be expected.

Autocatalysis of the DMCd may also be an effect contributing to thermal growth over regions where a cadmium deposit is already present as this would lead to more efficient dissociation of the reactant molecules in the presence of cadmium. Flicstein et al[94] attributed the preferential decomposition of trimethylaluminium for their depositions to autocatalytic pyrolysis. However an investigation into the pyrolysis behaviour of DMCd by Czerniak and Easton[9] has shown this effect may be minimal.

6.11 Growth models

6.11.1 Stranski-Krastinov

The behaviour in the case of deposition onto sapphire substrates falls into the category of the Stranski-Krastinov growth, whereby the deposit on the substrate forms initially in a layer-by-layer manner and is then subsequently followed by the formation of three dimensional clusters on top of the initial deposit. This mode of growth can be loosely regarded as a combination of the Volmer-Weber growth model and the Frank van der Merwe or layer-by-layer growth mode.

6.11.2 Volmer-Weber

According to the Volmer-Weber model the growth occurs by the formation of three dimensional clusters on the free substrate. In this case the bare substrate has a lower interfacial free energy than the interfaces associated with the thin film, resulting in minimisation of the free energy by the formation of clusters or, in terms of interfacial energies, $\sigma_{sv} < \sigma_{cs} + \sigma_{cv}$.

6.11.3 Frank-Van Der Merwe (layer-by-layer)

This growth occurs when a film covers the substrate and thickens uniformly as the name suggests in a layer-by-layer manner. The growth may be correlated with strong interactions between the film atoms and the substrate. For the layer-by-layer growth mode the substrate vapour interfacial energy is much larger than the other terms resulting in a reversal of the free energy balance of the above interfacial energy inequality.

Clearly in the case of the cadmium depositions on the sapphire substrates the growth is occurring in Stranski-Krastinov manner. The deposit has formed initially as a very thin layer but in a continuous manner. Short period depositions always showed the presence of this film, indicating that this initial layer has nucleated very rapidly. Longer growth runs do not show any apparent increase in the layer thickness of this uniform layer but do however show the appearance of clusters of nuclei formed on top of the initial layer.

The first stage of growth here is heavily influenced by the substrate and may be attributed to the strong interaction between substrate and the deposit as in the layer-by-layer growth mode. As the initial stage proceeds the substrate interaction with the deposit reduces and a situation analogous to the Volmer-Weber growth mode is favoured whereby it is energetically more feasible for the cadmium to deposit in the form of small three dimensional clusters once the critical cluster size has been attained.

In the case of the growth onto silicon substrates the growth appears to occur in a two dimensional manner and may be likened to the layer-by-layer growth model. This is the case regardless of the microstructure of the cadmium condensate, i.e. amorphous or polycrystalline, and the layer develops by lateral growth of the nuclei into a continuous film by island coalescence. No three dimensional growth (or film thickening) is observed until the complete silicon substrate is covered uniformly with cadmium.

Growth onto the GaAs substrate shows a different behaviour from the growth onto the sapphire and silicon substrates, indicative of greater surface diffusion. Although the nucleation is more difficult on the GaAs substrates compared with the sapphire and silicon substrates, as indicated by the increase in nucleation delay, the surface diffusion of the cadmium appears to be greater. Although the early growth appears to be somewhat in accordance with the layer-by-layer growth model by virtue of the initial two dimensional island formation, the high surface mobility leads to growth of cadmium crystallites at selected growth sites. Mass transport from the two dimensional islands to these favoured nucleation sites is clearly an important mechanism in their growth and may be related to surface free energies of the island condensate and their consequent unstable nature. Growth at these selected growth centres or capture zones then develops three dimensionally at the sacrifice of the two dimensional islands present on the substrate consequently leaving much of the substrate bare of any deposit, at least until more nucleation occurs, after which the process repeats itself setting up new capture zones. This formation of clusters is then consistent with the Volmer-Weber growth model.

At reduced temperatures the diffusion process becomes less efficient and leaves less of the substrate free of any deposit. This is assisted by the more dense nucleation at the reduced temperatures, resulting in a finer grain size deposit between the larger crystallites (as discussed in section 6.7). The larger crystallites in this case are presumably earlier nucleation centres which grow preferentially until the denser nucleation occurs.

Chapter 7: Conclusions

7.1 Cadmium telluride depositions

Growth of CdTe layers can be considerably enhanced using photodeposition. However the growth rate has to be controlled carefully to prevent exceeding the critical threshold for homogeneous vapour phase nucleation to ensure crystallinity does not deteriorate.

In the growth of CdTe on GaAs substrates, several degrees of crystallinity may be obtained. These range from fine grained polycrystalline layers through columnar structures to epitaxial layers with the degree of crystallinity being dependent on homogeneous vapour phase nucleation effects and an imbalance in the alkyl ratios. Suppression of homogeneous vapour phase nucleation is essential to obtain single crystal growth and may be achieved by increasing the growth temperature or decreasing the concentrations in the vapour by reducing the UV intensity or decreasing the alkyl inlet concentrations. Additionally a cadmium alkyl rich stoichiometry has to be maintained to avoid polycrystalline growth on GaAs substrates at temperatures below 350°C.

Dislocation structure of the epitaxial layers is also improved with increasing alkyl ratio. It is possible to deposit single crystal layers which do not exhibit the usual threading dislocations penetrating into the layer by using low UV intensity at 300°C with a DMCd:DETe alkyl ratio of 1.5.

A difference in activation energy from 22kcal/mol to 9kcal/mol between the thermal growths and the photolytic growths indicates that the rate limiting steps for the deposition process differ in the two cases. This difference is consistent with the enhanced growth rates seen in the photolytic depositions.

The Langmuir-Hinshelwood surface adsorption model may be used to describe the reduction in growth rate when the DMCd partial pressure is increased. This model predicts a growth rate reduction if cadmium is adsorbed on the surface, acting as an inhibitor occupying a single surface site. It also describes the growth rate increase with DETe which appears to result from a triple site occupancy of DETe for either competitive or independent adsorption.

The preferred orientation of the polycrystalline deposits appears to be (111) although low supersaturation conditions promote (100) growth. This is also consistent with the UHV depositions in which single crystal layers grow as (111) at lower temperatures and (100) at higher temperatures.

Differing dislocation structures obtained for (111) layers grown on (100) GaAs substrates by UHV sputtering and MOVPE may be as a result of viewing through different orientations and thus may not be inconsistent with each other but allow a 3-D view of the dislocation structure to be constructed.

Layer strain is evident in the deposited layers with little extended dislocation structure, and does not agree with the theoretically calculated layer thicknesses required before misfit dislocations are generated. HRTEM of the interface and exact strain measurements would perhaps clarify the situation The latter may be carried out by cross-sectional TEM using convergent beam electron diffraction (CBED) or, more reliably, over larger areas by Rutherford back scattering (RBS) techniques.

Preliminary SIMS depth profiling of a photodeposited layer grown at 350°C shows a reduction of gallium diffusion of two orders of magnitude into the layer from the substrate compared with normal thermally deposited layers grown at 410°C. Further work could be concentrated on the diffusion into the deposited layers which exhibit minimal extended dislocations and would allow a correlation of gallium diffusion with the dislocation structure.

7.2 Cadmium depositions

The deposition parameters must be closely controlled to avoid homogeneous vapour phase nucleation. Hence high temperatures, low UV intensities and reduced partial pressure conditions are to be preferred. However, high temperatures also promote a reduction of nucleation and therefore a balance has to be achieved between obtaining sufficient heterogeneous nucleation and preventing homogeneous vapour phase nucleation.

Heterogeneous depositions onto sapphire, silicon and GaAs showed distinct differences in their growth behaviour. Deposition onto sapphire occurred as in the Stranski-Krastinov model, deposition onto the silicon in the layer-by-layer and the deposition onto GaAs as in the Volmer-Weber growth model.

A change of microstructure on sapphire substrates from a granular polycrystalline to columnar growth at higher temperatures may be due to a decrease in relative contributions from the vapour phase and adsorbed layers, a reduction in the nucleation density and increase in the critical cluster size.

The vapour phase contribution to the growth is predominant at high temperatures with the adsorbed DMCd layers becoming more important at lower temperatures. This provides a ready source of DMCd at the substrate to yield a dense coverage of nuclei on photodissociation.

Dense deposits and whisker growth parallel to the substrate surface imply considerable adsorption of DMCd onto GaAs substrates for growths at 0°C.

A high density of deposit was obtained below room temperature although preferential growth on favoured nucleation sites was apparent. The major differences between the substrates were the enhanced diffusion and greater difficulty in nucleation on the GaAs. Rapid surface diffusion promoted non-uniform growth but increasing the nucleation density by decreasing the temperature gave a uniform deposit.

Nucleation onto silicon showed two distinct topographies dependent on the deposition temperature. At reduced temperatures an amorphous layer was obtained and a slight increase resulted in polycrystalline growth. This may be due to local atomic bonding changes at the interface.

Prenucleation was successful on both Si and GaAs substrates and the topography of such deposits replicated that of the initial nucleation stage, i.e. thermal growth of a UV nucleated amorphous deposit led to an amorphous layer, etc.

The high diffusion at low temperatures and the crystalline nature of the isolated deposits on the GaAs indicate that low temperature epitaxy can be a viable prospect. Although low growth rates are a by-product of this technique the advantages of superior crystallinity far out-weigh this and in any case small dimensions are to be preferred for the next generation of 3-D device structures.

References.

(1) J.B. Mullin, S.J.C. Irvine and D.J. Ashen, J.Cryst.Growth 55,1981,92

(2) S.J.C. Irvine, J.B. Mullin and A. Royle, J.Cryst.Growth 57,1982,15

(3) D.W. Kisker, K.S. Jeffers, M.Steigerwald and T.Y. Kometani, Proc.ICMOVPE III Conference,Universal City, CA 1986

(4) W.E. Hoke and P.J. Lemonias, Appl.Phys.Lttrs. 48,1669,1986

(5) W.E. Hoke and P.J. Lemonias, Appl.Phys.Lttrs. 46,398,1985

(6) J.B. Mullin and S.J.C. Irvine, J Vac.Sci.Tech. 21,1,1982

(7) J.B. Mullin and S.J.C. Irvine, J.Vac.Sci.Tech. A4,3,1986

(8) J.B. Mullin, S.J.C. Irvine, J.Giess and A.Royle, J.Cryst.Growth 72,1985,1

(9) M.R. Czerniak and B.C. Easton , J.Cryst.Growth 68,1984,128

(10) I.B. Bhat, N.R. Taskar and S.K. Ghandhi, J.Electrochem.Soc. Jan 1987

(11) W.E. Hoke and R. Trackweski , J.Appl. Phys. 54 ,9, 1983

(12) J.L. Schmit, J.Vac.Sci.Tech., A3, 1, 1985

(13) S.J.C. Irvine and J.B. Mullin, J.Cryst.Growth 55,1981,107

(14) S.J.C. Irvine, J. Tunnicliffe and J.B. Mullin, J.Cryst.Growth 65, 1983, 479

(15) J. Tunnicliffe, S.J.C. Irvine, O.D. Dosser and J.B. Mullin, J.Cryst.Growth 68,1984,245

(16) J.Thompson, P. Mackett and L.M. Smith, Materials Lttrs. 5, 3 (1987), 72

(17) J.Thompson, P. Mackett and L.M. Smith, ACCG-7/II-IV-87 Conference abstracts, July 1987, Monterey, California.

(18) S.K. Ghandhi and I. Bhat, Appl.Phys.Lttrs. 45,6,1984

(19) N.R. Taskar, I.B. Bhat and S.K. Ghandhi, J.Cryst.Growth 77,1986,480

(20) W.E. Hoke, P.J. Lemonias and R. Traczewski, Appl.Phys.Lttrs. 44,11,1984

(21) I.Bhat, L.M.G. Sundaram, J.M. Borrego and S.K. Ghandhi, MRS 37,1985

(22) N.R. Tasker, I.B. Bhat, J.M. Borrego and S.K. Ghandhi, J.Electron.Mat. V15,3,1986

(23) S.K. Ghandhi, N.R. Tasker and I.B. Bhat, Appl.Phys.Lttrs. 47,7,1985

(24) P.Y. Lu, L.M. Williams and S.N.G. Chu, J.Vac.Sci.Tech. A4,4,1986

(25) R.D. Feldman, D.W. Kisker, R.F. Austin, K.S. Jeffers and P.M. Bridenbaugh, J.Vac.Sci.Tech. A4,4,1986

(26) P.L. Anderson, J.Vac.Sci.Tech. A4,4,1986

(27) R.L. Chou, M.S. Lin and K.S. Chou, Appl.Phys.Lttrs. 48,8,1986

(28) M.S. Lin , R.L. Chou and K.S. Chou, J.Cryst.Growth 77,1986,475

(29) H.S. Cole, H.H. Woodbury and J.F. Schetzina, J.Appl.Phys. 55,8,1984

(30) W.E. Hoke, R. Traczewski, V.G. Kreismanis, R. Korenstein and P.J. Lemonias, Appl.Phys.Lttrs. 47,3,1985

(31) J. Thompson, K.T. Woodhouse and C. Dineen, J.Cryst.Growth 77,1986,452

(32) S.J.C. Irvine, J.B. Mullin, D.J. Robbins and J.L. Glasper, J.Electrochem.Soc. 132,4,1985

(33) S.J.C. Irvine, J.B. Mullin and J. Tunnicliffe, J.Cryst.Growth 68,1984,188

(34) W.L. Ahlgren, R.H. Himoto, S. Sen and R.P. Ruth, Third International Conference on MOVPE, April 13-17,1986 Universal City,California,USA

(35) S.J.C. Irvine, J. Giess, J.B. Mullin, G.W. Blackmore and O.D. Dosser, J.Vac.Sci.Tech. B3,5,1985

(36) S.J.C. Irvine and J.B. Mullin, J.Cryst.Growth 79,1986,371

(37) B.J. Morris, Appl.Phys.Lttrs. 48,13,1986

(38) S.J.C. Irvine, J.B. Mullin, G.W. Blackmore, O.D. Dosser and H. Hill, Mat. Res. Soc. Symp. Proc. V90, 389

(39) D.W. Kisker and R.D. Feldman, Materials Lttrs. 3,1985,12

(40) D.W. Kisker and R.D. Feldman, J.Cryst.Growth 72,1985,102

(41) S.J.C. Irvine, J. Giess, J.S. Gough, G.W. Blackmore, A. Royle, J.B. Mullin, N.G. Chew and A.G. Cullis, J.Cryst.Growth 77,1986,437

(42) J.Giess, J.S. Gough, S.J.C. Irvine, G.W. Blackmore, J.B. Mullin and A. Royle, J.Cryst.Growth 72,1985,120

(43) W.L. Ahlgrehn, R.P. Ruth, J.B. James, E.A. Patten and J.L. Staudeumann, MRS. Symp.Proc. V90,1987,405

(44) S.Nishida, T. Shiimoto, A. Yamada, S. Karasawa, M. Konagai and K. Takahashi, Appl.Phys.Lttrs. 49,2,1986

(45) A. Yamada, S. Nishida, M. Konagai and K. Takahashi, Ext.abstracts of the 18th conf. on solid state devices and materials 1986, 217

(46) N. Putz, H. Heinecke, E. Veuhoffe, G. Arens, M. Heyen, H. Luth and P. Balk, J.Cryst.Growth 68,1984,194

(47) W. Roth, H. Krautle, A. Krings and H. Beneking, MRS V17,1983,193

(48) J.G. Eden, J.E. Greene, J.F. Osmundsen, D. Lubben, C.C. Abele, S. Gorbatkin and H.D. Desai, MRS V17,1983,185

(49) H. Ando, H. Inuzuka, M. Konagai and K. Takahashi, J.Appl. Phys. 58,2,1985

(50) V.M. Donnelly, D. Brasen, A. Appelbaum and M. Geva, J.Appl. Phys. 58,5,1985

(51) W.E. Johnson and L.A. Schlie, Appl.Phys.Lttrs. 40,9,1982

(52) M.R. Aylett and J. Haigh, Laser processing and diagnostics, Proc. of an int. conf, Univ. of Linz, Austria, 1984, 263

(53) J.E. Bouree, J. Flicstein, Y.I. Nissim and C. Licoppe, Ext.Abs. MRS, Beam Induced Chemical Processes,71,1986

(54) R. Solanki, P.K. Boyer, J.E. Mahan and G.J. Collins, Appl.Phys.Lttrs.38,7,1981

(55) A.E. Adams, M.L. Lloyd, S.L. Morgan, and N.G. Davis, Laser processing and diagnostics, Proc. of an int. conf, Univ of Linz,Austria,1984,269

(56) T.F. Deutsch, Laser processing and diagnostics, Proc. of an int. conf, Univ of Linz,Austria,1984,241

(57) D.J. Ehrlich, R.M. Osgood, T.F. Deutsch, IEEE J.Quant.Electronics QE 16,11,1980

(58) D. Braichotte and H. van den Bergh, Laser processing and diagnostics, Proc. of an int. conf, Univ of Linz, Austria, 1984

(59) Y. Rytz-Froidevaux, R.P. Salathe and H.H. Gilgen, MRS Boston 1982 proc. V17, 29 Laser diagnostics and photochemical processing for semiconductor devices

(60) F.A. Houle, C.R. Jones, R. Wilson and T.H. Baum,MRS Ext Abst.1984,64

(61) A.E. Adams, S. Horbaczewsi, M.L. Lloyd and K. Middleton, E-MRS Energy beam and solid interactions and transient thermal processing 1985, IV, 113

(62) M.L. Lloyd and K.G. Gibbs, MRS 29,1984,35

(63) H.H. Gilgen, Ext.Abst.of laser chem.proc. MRS 1984,54

(64) D.J. Ehrlich and R.M. Osgood, Chem.Phys.Lttrs. 79,2,1981

(65) C.J. Chen and R.M. Osgood, Chem.Phys.Lttrs. 98,4,1983

(66) D.J. Ehrlich, R.M. Osgood and T.F. Deutsch, Appl.Phys.Lttrs. 38,11,1981

(67) J.Y. Tsao and D.J. Ehrlich, Appl.Phys.Lttrs. 45,6,1984

(68) D.J. Ehrlich, R.M. Osgood and T.F. Deutsch, J.Vac.Sci.Tech. 21,1,1982

(69) G.S. Higashi and C.G. Fleming, Ext. Abs. MRS, Beam Induced Chemical Processes, 1986

(70) G.S. Higashi, G.E. Blonder, C.G. Fleming V.R. McCrary and V.M. Donnelly, J.Vac. Sci and Technol. B (in press)

(71) S.R.J. Brueck and D.J. Ehrlich, Phys. Rev. Lttrs., 48,1678,1982

(72) R.M. Osgood and H.H. Gilgen, Ann.Rev.Mater.Sci. 1985,15,549

(73) G.E. Blonder, G.S. Higashi and C.G. Fleming, Appl.Phys.Lttrs., 50,12,1987

(74) L.A. Kolodziejski, R.L. Gunshor, N. Otsuka and C. Choi, J.Vac.Sci and Tech., A4,4,1986

(75) L.A. Kolodziejski, R.L. Gunshor, N. Otsuka, X.C. Chang, S.K. Chang and A.V. Nurmikko, Appl.Phys.Lttrs. 47,8,1985

(76) H.A. Mar , N. Salansky and K.T. Chee, Appl.Phys.Lttrs. 44,9,1984

(77) R.D. Feldman, R.F. Austin, D.W. Kisker, K.S. Jeffers and P.M. Bridenbaugh, Appl.Phys.Lttrs. 48,3,1986

(78) J. Giess, J.S. Gough, S.J.C. Irvine, J.B. Mullin and G.W. Blackmore, Mat. Res. Soc. Symp. Proc. V90,153

(79) R.N. Bicknell, R.W. Yanka, N.C. Giles, J.F. Schetzina, T.J. Magee, C. Leung and H. Kawayoshi, Appl.Phys.Lttrs. 44,3,1984

(80) A.G. Cullis, N.G. Chew, J.L. Hutchison, S.J.C. Irvine and J.Giess, Microsc.Semicond. Mater. Conf. Oxford March 1985, Inst. Phys.Conf. Ser. No76, sect 1

(81) J. Petruzzello, D. Olego, S.K. Ghandhi, N.R. Taskar and I. Bhat, Appl. Phys. Lttrs. 50, 10, 1987

(82) P.D. Brown,J.E. Hails, G.J. Russell and J. Woods, Appl. Phys. Lttrs. 50,17,1987

(83) J.T. Chueng and T. Magee, J.Vac.Sci and Tech. A1,3,1983

(84) A.G. Cullis, N.G. Chew, S.J.C. Irvine and J. Giess, Inst Phys Conf. Ser.no 87: section 2 Microsc. Semicond. Mater. Conf. Oxford, 6-8 April 1987

(85) S. Wood, J. Greggi , R.F.C. Farrow, W.J. Takei, F.A. Shirland and A.J. Noreika, J.Appl.Phys. 55,12,1984

(86) Alfa Catalogue (Ventron GmbH, W. Germany,1984)

(87) Y.S. Touloukian and D.P. Dewitt, Thermal Physical Properties of Matter, TPRC Data Series, V8, IFI/Plenum, USA, 1972

(88) Oriel Corporation catalogue, 1979, USA

(89) Data sheet for Illumination Industries 3kW, Mark VI capillary lamp

(90) S.J.C. Irvine and J. Geiss, Private Comm.

(91) S.J.C. Irvine and J.B. Mullin, E-MRS Meeting,June 1987,Vol XV,223

(92) J.H. Basson and H. Booyens, Phys. Stat. Sol. (a) 80,663,1983

(93) Y.S. Touloukian, R.K. Kirby, R.E. Taylor and T.Y.R. Lee, Thermal Physical Properties of Matter, TPRC Data Series, V13, IFI/Plenum, USA, 1977

(94) K. Oe, Y. Shinoda and K. Sugiyama, Appl. Phys. Lttrs. 33,1978,962

(95) J. Flicstein, J.E. Bouree and Y.I. Nissim, E-MRS proc.XI,1986

(96) M.M. Faktor and I. Garrett, 'Growth of crystals from the vapour', Chapman and Hall, London 1974.

(97) M. Volmer, Die Kinetik der Phasenbuilding, Steinkopff, Dresden, 1939

(98) R. Becker and W. Doring, Ann.Phys. 24,5,1935

(99) J.P. Hirth and G.M. Pound,'Condensation and Evaporation', Pergamon, London (1963)

(100) W. Kleber and I. Mietz, Kristall and Technik 3,509,1968.

(101) J.Y. Tsao and D.J. Ehrlich, J.Cryst.Growth 68,1984,176

DOCUMENT CONTROL SHEET

Overall security classification of sheet ..... UNCLASSIFIED .....

(As far as possible this sheet should contain only unclassified information. If it is necessary to enter classified information, the box concerned must be marked to indicate the classification eg (R) (C) or (S))

1. DRIC Reference (if known)	2. Originator's Reference Memo 4208	3. Agency Reference	4. Report Security Classification U/C
5. Originator's Code (if known) 7784000	6. Originator (Corporate Author) Name and Location ROYAL SIGNALS AND RADAR ESTABLISHMENT ST ANDREWS ROAD, GREAT MALVERN WORCESTERSHIRE WR14 3PS		
5a. Sponsoring Agency's Code (if known)	6a. Sponsoring Agency (Contract Authority) Name and Location		

7. Title UV PHOTO ENHANCED MOCVD OF CADMIUM AND CADMIUM TELLURIDE

7a. Title in Foreign Language (in the case of translations)

7b. Presented at (for conference papers) Title, place and date of conference

8. Author 1 Surname, initials	9(a) Author 2	9(b) Authors 3,4...	10. Date	pp. ref
Haq S			1988.04	166

11. Contract Number	12. Period	13. Project	14. Other Reference

15. Distribution statement
UNLIMITED

Descriptors (or keywords)

continue on separate piece of paper

Abstract This technical memorandum comprises a thesis submitted by the author for the degree of PhD at the University of Birmingham. The research was carried out, both at the Department of Metallurgy and Materials, University of Birmingham, and at RSRE in EM2 Division. The UV photolysis of dimethylcadmium (Me_2Cd) and diethyltelluride (Et_2Te) were investigated using high pressure mercury arc lamps. Metallic Cd films were deposited onto gallium arsenide, silicon and sapphire substrates in order to investigate nucleation mechanisms and film growth models. Cadmium telluride epitaxial layers were grown onto (100) gallium arsenide substrates both with and without UV illumination. Film quality and structure have been studied using transmission electron microscopy, X-ray diffraction, scanning electron microscopy and secondary ion mass spectrometry.